JAERI-M
83-177

AN EXPERIMENTAL STUDY OF INDUCED ACTIVITY IN TYPE 316 STAINLESS STEEL BY IRRADIATION IN D-T NEUTRON FIELDS

October 1983

Yujiro IKEDA, Yasushi SEKI, Hiroshi MAEKAWA
Yukio OYAMA and Tomoo NAKAMURA

日本原子力研究所
Japan Atomic Energy Research Institute

JAERI-M レポートは，日本原子力研究所が不定期に公刊している研究報告書です。
入手の問合わせは，日本原子力研究所技術情報部情報資料課（〒319—11 茨城県那珂郡東海村）あて，お申しこしください。なお，このほかに財団法人原子力弘済会資料センター（〒319-11 茨城県那珂郡東海村日本原子力研究所内）で複写による実費領布をおこなっております。

JAERI-M reports are issued irregularly.
Inquiries about availability of the reports should be addressed to Information Section, Division of Technical Information, Japan Atomic Energy Research Institute, Tokai-mura, Naka-gun, Ibaraki-ken 319-11, Japan.

編集兼発行　日本原子力研究所
印　　刷　山田軽印刷所

JAERI-M 83-177

An Experimental Study of Induced Activity in Type 316 Stainless Steel by Irradiation in D-T Neutron Fields

Yujiro IKEDA, Yasushi SEKI, Hiroshi MAEKAWA, Yukio OYAMA and Tomoo NAKAMURA

Department of Reactor Engineering,
Tokai Research Establishment, JAERI

(Received October 5, 1983)

Experiments on induced activities in type 316 stainless steel (SUS316) have been performed in order to verify an induced activity calculation code system, THIDA, by using the FNS facility. Sample of 10 mm ϕ × 2 mm t SUS316 were irradiated in three different D-T neutron fields. One sample was positioned at 10 cm from the target with no assembly around it and the other two placed inside the Li_2O-C pseudo-spherical blanket assembly. After irradiation, spectra of gamma-rays emitted from produced activities in each sample were successively measured by using a 60 cm^3 Ge(Li) detector following the cooling times from 10 min to about one month. The gamma-ray spectra and relative doses were compared with those calculated by THIDA. All the measured and calculated total gamma-ray intensities and relative doses agreed with each other within 15 % with one exception. Though the agreements were good as a whole, there were some disagreements in the individual gamma-ray intensities. The disagreements were investigated from the viewpoints of the THIDA code system and their nuclear data library.

Keywords; Induced Activity, THIDA Code System, D-T Neutron, Irradiation, Li_2O-C Pseudo-spherical Blanket Assembly, Ge(Li) Detector, Gamma-ray, Relative Dose.

D－T中性子照射によるタイプ316ステンレス鋼中の誘導放射能の実験的研究

日本原子力研究所東海研究所原子炉工学部
池田　裕二郎・関　　泰・前川　　洋
大山　幸夫・中村　知夫

（1983年10月5日受理）

核融合炉における誘導放射能計算コードシステム，THIDAの検証を行うために，タイプ316ステンレス鋼（SUS 316）中の誘導放射能の実験をFNS加速器を用いて行った。直径10 mm，厚さ2 mmのSUS 316鋼試料を三つの異なるD－T中性子場で照射した。一つは，ターゲットから10 cmの周辺に体系の無い位置で，他の二つは，黒鉛反射体付酸化リシウム（Li_2O－C）ブランケット模擬体系中のターゲットからそれぞれ12.6 cmおよび22.6 cmの位置であった。照射後，10分から約1ケ月の冷却時間を置いて，各々の試料中に生成された放射能から放出されたγ線スペクトルを60 cm^3Ge（Li）検出器により測定した。測定したγ線スペクトルおよびそのスペクトルより求めた相対線量をTHIDAによる計算値と比較した。全γ線強度に関して，実験値と計算値は，±15％以内で一致し全体的に良い結果を示しTHIDAコードの有効性を示すことができた。しかしながら，個々のγ線強度では，差が大きいものがあり，この差について，THIDAコードシステムおよび核データの観点から検討を行った。

Contents

目　　次

1 INTRODUCTION

The radioactivity in the structural materials of a D-T fusion reactor induced by 14 MeV neutrons is very important in terms of the following; (a) gamma-ray dose estimation for personnel access after reactor shutdown, (b) decayheat after shutdown, (c) production of long-lived radioactive wastes. Calculational studies concerning the radioactivities, afterheat and transmutation have been made by many authors.[1]-[10] Recently, Jarvis carried out these calculations with simplified model of a D-T tokamak reactor for five different kind of materials which are considered to be the candidates for the structural materials,[11] and reviewed the nuclear data requirements for the reactor design.[12] A code system THIDA has been developed for the calculation of exposure dose rate around a fusion device at Japan Atomic Energy Research Institute (JAERI).[13] It has been applied in the optimization of shielding in term of personnel access[14] and in shielding design of INTOR.[15] As for experimental studies, Qaim[16]-[18] has systematically measured the cross sections for 14 MeV neutron induced reactions on the first wall and structural materials to be used in the fusion reactor.

Although there were needs for comprehensive comparison between predicted activation calculations and measurements to check the code system mentioned above, no appropriate data for activation had been available.

Therefore, as the first step, the activation in a type 316 stainless steel (SUS316) were measured by irradiation experiments using an intense 14 MeV neutron source FNS (Fusion Neutronics Source)[19] in order to verify the THIDA code system including its nuclear data library. Three D-T neutron irradiation fields were chosen to clarify the effect of the difference in the neutron fields on the induced activity. One was the direct 14 MeV neutron field without any assembly simulating a field near the first wall in an actual reactor. The others were those of different locations in a lithium oxide pseude-spherical fusion blanket assembly with graphite reflector.[20] It is thought that these locations simulate possible D-T neutron fields in the fusion reactor environment. Comparisons between the calculation and the measurements were made for the gamma-ray productions by induced activities. The objective of this report is to make clear the problems about the nuclear data (activation cross section and decay property) used in THIDA and to show explicitly the validity of this code system to apply in the nuclear design of fusion reactors.

2. EXPERIMENT

2.1 Irradiation condition

The 14 MeV neutrons were produced by bombarding a water cooled tritium-titanium metal target of 7 mg/cm^2 with 310 keV deuteron beam of about 2 mA using the FNS accelerator.[19] The sample were placed in three different well-defined neutron irradiation fields. One sample was positioned at 10 cm in front of the target. There was no structural material or assembly around the sample to avoid perturbation of the neutron field. The second and the third sample were placed in the lithium oxide (Li_2O) pseudo-spherical fusion blanket assembly with graphite (C) reflector.[20] One was located at 12.6 cm from the target in the middle of Li_2O region and the other was at 22.6 cm, just at the boundary of Li_2O and C regions. These three locations were chosen in order to simulate the D-T neutron fields in an actual fusion reactor environment. Samples were irradiated by D-T neutrons with source intensity of about 2.0×10^{11} n/sec. Irradiation times were 3 hours for the first case without any assembly and 8 hours for the other case in the Li_2O-C assembly. Total neutron yields at the target were $2.86 \pm 0.11 \times 10^{15}$ and $7.10 \pm 0.28 \times 10^{15}$. These yield were monitored by the associated alpha particle counting method.[21] Schematic arrangements of both cases are shown in Figs. 1 and 2 together with thier one-dimentional models for neutron flux calculation by ANISN.[22]

2.2 Irradiation sample

The type 316 stainless steel (SUS316) was chosen as the irradiation sample in order to examine the THIDA code system because SUS316 is considered to be one of the most promising candidates for the main structural material of fusion reactors. The size of each sample is 10 mm in diameter and 2 mm in thickness. The atomic composition and nuclear components in SUS316 are shown in Table 1. Its major feature is that it include molybdenum. In Table 2 activation reactions, product nuclei, half-life, dominant gamma-ray energies, branching ratios, weights in that size of SUS316 and natural abundance are listed.[23] From the Table 2, it can be seen that a wide variety of radioactivities are produced because of the complex

composition of SUS316. In FIg. 3, the growth curves of produced radioactivities per unit flux of 14 MeV neutron are shown. From this figure, intensities of radioactivities after an irradiation time can be roughly estimated.

2.3 Gamma-ray measurement

After each irradiation, gamma-ray spectra emitted from individual samples were obtained by using a 60 cm^3 Ge(Li) detector which has a resolution of 1.75 keV (FWHM) at 1.33 MeV, connected with a 4096 multi-channel pulse height analyzer. The measured sample position was at 5 cm from the Ge(Li) detector head. In order to obtain information on spectrum change with cooling times, several spectrum measurements were successively made during the decay in each sample. The time scheme of the irradiation, cooling time and collecting time for each case are shown in Table 3. Here, the measurement cases are named as A, B and C corresponding to samples in the direct neutron field, at 12.6 cm in Li_2O and at 22.6 cm on the boundary of Li_2O and C region, respectively. An absolute gamma-ray detection efficiency was obtained using standard sources and the efficiency curve is shown in Fig. 4.

3. EXPERIMENTAL RESULTS

In Fig. 5.1 to 5.10, gamma-ray spectra corresponding to each measurement in Table 3 are shown. In the measurement of 10 min cooling time (A-1), gamma-ray peaks from short-lived nuclei, ^{52}V(3.76 m) and ^{49}Cr(41.9 m), are clearly observed. Gamma-ray lines of ^{49}Cr are also observed in the measurement of one hour cooling time (A-2). In the spectra of A-1, A-2, A-3, B-1 and C-1, it can be seen that the contribution due to ^{56}Mn(2.579 hr) is dominant and its value comes to about 90 % of the total intensities. There are also significant contribution due to ^{57}Ni(36 hr) and ^{99}Mo(66 hr). In the measurements after about one month cooling time (A-4, B-3 and C-3), dominant gamma-rays changed to those from ^{51}Cr(27.7 d), ^{57}Co(277 d) and ^{54}Mn(312 d). Moreover, long-lived component of ^{60}Co(5.4 y) becomes clearly observable.

Measured gamma-ray spectra were analyzed by a gamma-ray spectrum analysis code BOB75[24] to obtain the gamma-ray energies and their peak areas. After the background subtraction, each gamma-ray intensity was deduced from peak areas by corrections of the detector efficiency and gamma-ray self-absorptions in the 2 mm thick SUS316 sample. The absorption coefficient is shown in Fig. 6. The self-shielding for neutrons in the SUS316 volume was not considered in the gamma-ray intensity calculation.

4. CALCULATIONAL METHOD

4.1 THIDA code system

The THIDA code system[13] has been developed in order to calculate the transmutaion, hazard potential, induced activity, dose rate and after-heat which are considered to be important for the fusion reactor design. The flow of the calculation is as follows; (1) at the first stage, calculation of neutron flux distribution during the reactor operation is carried out, (2) secondly, it calculates induced activity built up during the operation by using the obtained neutron flux and subsequently calcualtes the activities after shutdown, (3) activities are transformed to multi-group gamma-ray sources and transport calculation is done to obtain gamma-ray flux distributions, (4) in the last stage, gamma-ray dose distribution are derived from the fluxes.

4.2 Calculations

Calculations of neutron flux distributions in those experimental arrangements shown in Figs. 1 and 2 were performed by using the one-dimensional S_N code ANISN.[22] Calculational models for both irradiation configurations are shown in Figs. 1.2 and 2.2. The cross section library, GICX40,[25] was used in the calculation which has 42 neutron energy groups. In Table 5, the energy group structure is shown. In order to obtain the absolute value of induced activities, the values of the mean source neutron intensity and the irradiation times were used as the calculation input data. Gamma-ray sources at each sample positions were generated by the code, ACT4, included in the THIDA code system, using both calculated neutron flux and the activation cross section library, CROSSLIB,[26] which also included in the THIDA code system. The output format of the gamma-ray spectrum has 54 energy groups which cover a range from 30 keV to 3 MeV. The structure is shown in Table 6. Gamma-ray having energies above 3 MeV were put into the first group (2.7 to 3.0 MeV).

In this experiments aiming to verify the THIDA code system, the code ACT4 was modified a little to calculated gamma-ray intensity over collecting time. Thereafter, direct comparisons of gamma-ray intensities between the calculation and the measurement could be possible. The calculation flow is schematically shown together with the experimental procedure in Fig. 7.

5. COMPARISON OF RESULTS

Gammar-ray intensity distribution obtained from each measurement were divided into the 54 energy groups to compare with the calculated value. When there were multiple gamma-rays in one group, they were all summed up. The energy range for these comparison was restricted from 90 KeV to 3 MeV because of the low efficiency of the Ge(Li) detector below 90 keV and the energy bound of 3 MeV in the calculation. Results of both calculation and measurement are shown in Tables 7.1-7.10. In the tables, relative doses as well as gamma-ray intensities in each group are listed to estimate the contribution of the group to the total dose rate. The relative dose means the value multiplying the conversion factor by the obtained gamma-ray intensity. The conversion factor of the dose from photon is shown in Fig. 8. Experimental errors in the tables will be discussed in the later section. The values of C/E for each group are tabulated in Table 8. Gamma-ray spectra per group for each case are shown in Figs. 9.1-9.10, where names of nuclides contributing to the gorup intensity are assigned. The C/E values are also shown in Figs. 10.1-10.10 to show clearly the difference between the calculation and the measurement. Moreover, the decay curve of major product nuclei, the shape of which should be identical for the three irradiation fields, are shown in Figs. 11.1-11.7. The C/E of total gamma-ray intensities and their relative doses are summarized in Table 9. Some discussions of the resutls are made in the following subsections.

5.1 Measurements of A-1 to A-4

According to the time scheme in Table 3, a series of gamma-ray measurements were performed after 3 hours irradiation in the direct neutron field. From the Tables 7.1-7.4 and Figs. 9.1-9.4, it is seen that in all cases the 17th energy group (810-900 keV) has the largest intensity which amounts to about 50 % of the total intensity. In cases of A-1 to A-3, the major contribution to the 17th group comes from ^{56}Mn which is reasonable since its half-life is 2.579 hr and is produced mainly from ^{56}Fe, the largest constituent in the SUS316 (see Table 1). The ratios of the calculation and the measurement (C/E's) in this group are lower than 1.0 by 1-5 %. However, in the case of A-4 (after about one month), the main contributions to the group come from ^{58}Co(70.8 d) and ^{54}Mn(312 d),

and the C/E is higher than 1.0 by 9 % differing from A-1 to A-3. Detailes examination for this group showed that the experimental contribution of ^{58}Co was lower than the calculated one by 11 % whereas the ^{54}Mn higher 22 %. Gamma-ray intensities at 3.37, 2.96, 2.66, 2.52, 2.11 and 1.81 MeV, corresponding to 1, 2, 4 and 7th groups, are due to ^{56}Mn and these C/E values are lower than 1.0 by 1-25 % same as in the 17th group. This fact indicates that the actual production of ^{56}Mn exceeds the calculated value.

Other energy groups than those mentioned above with large gamma-ray intensities were 6, 8 and 12 in the case of A-1 to A-3, corresponding to the ^{57}Ni(36 hr) of which energies are 1.92, 1.76 and 1.38 MeV. The C/E's for these groups were about 0.5-0.9. This indicates that ^{57}Ni production was underestimated in the calculation. Similar discrepancy was seen at 27th energy group contributed by ^{51}Cr(27.7 d) in cases of A-2 to A-4. Rather large underestimations by calculation were seen for the 22nd group, 511 keV annihilation gamma-ray, in A-1 to A-3, but in A-4 the agreement between the calculation and the measurement was good.

On the other hand, at the 38th group contributed by ^{99}Mo(66.6 hr), the calculation overestimated by factors of 2 to 3 for all cases. And at 39 and 40th groups due to ^{57}Co(277 d), the calculation overestimated by about 40 % in case of A-4. Moreover, the calculated gamma-ray intensities of ^{49}Cr(41.9 m) were underestimated by one order of magnitude or more.

5.2 Measurements of B-1 to B-3

A disk of SUS316 was irradiated by 8 hours at 12.6 cm from the target in Li_2O-C assembly. After irradiation, three successive gamma-ray measurements, named B-1, B-2 and B-3, were carried out. In the cases of B-1, the intensity of the 17th group due mainly to ^{56}Mn was about 50 % of the total as seen in the cases of A-1 to A-3. The calculated intensity of this group underestimated the measurement by 6 % as seen in cases of A-1 to A-3. In groups of 1, 2, 4 and 7 also due to ^{56}Mn decay, the calculation underestimated by 5-25 %. On the other hand, in cases of B-2 and B-3 for rather long cooling tiems, contributions of ^{58}Co and ^{54}Mn became dominant in the 17th group and the calculation overestimated by 6-20 %. From the decay curves in Figs. 11.5 and 11.7, it is seen that the calculation overestimated ^{58}Co production whereas ^{54}Mn production was underestimated. In the case of B-1, the contributions to 6, 8 and 12th groups came mainly from ^{57}Ni decay. The calculation underestimated them by factors of 1.5 to 2 in

the same manner as seen in A-1 to A-3. As for the intensity of 27th group from ^{51}Cr decay, the calculation also underestimated by a factor of about 2 throughout the cases B-1 to B-3. About the annihilation gamma-ray at 511 keV, the calculation underestimated in the case of B-1, overestimated in the case of B-2 and agreed with the measurement in the case of B-3. Contrary to those groups mentioned above, the calculation overestimated the measurement in 38, 29 and 40th groups due mainly to ^{57}Co and ^{99}Mo decays except in the 40th of B-1 cases where the contribution from ^{57}Ni existed. Concerning the long-lived ^{60}Co, gamma-ray energies of which are 1173 and 1132 keV corresponding to 12 and 14th groups, there are underestimations by a factor of about 2 in the calculation.

5.3 Measurements of C-1 to C-3

A SUS316 disk was placed at the distance of 22.6 cm from the target just at the boundary of the Li_2O and the graphite regions. Irradiation conditions were the same as in the case of B. The most intense group is the 17th energy group, same as in the other cases. In the measurement of C-1(10 hours cooling), the contribution for the group came mainly from ^{56}Mn decay. However, the calculation overestimated by 24 % differring from the results for the cases in A-3 and B-1 with similar cooling times. Overestimations in 1, 2, 4 and 7th groups from ^{56}Mn can be also seen. In the longer cooling cases, C-2 and C-3, the calculation overestimated the intensities of the 17th group by 15-17 %. These overestimations are large in comparison with the cases of A-4, B-2 and B-3. The calculations underestimated gamma-rays in the groups 8 and 12 corresponding to ^{57}Ni, and in the 27th group corresponding to ^{51}Cr by a factor of about 2. As for the annihilation gamma-ray, the calculation also underestimated by a factor of 2 in the case of C-1. Calculations for ^{57}Co and ^{99}Mo systamatically show overestimations as in the cases of A-1, A-2, A-3, A-4 and B-1.

6. DISCUSSION

6.1 Experimental uncertainty

In this subsection, errors in experimental results for gamma-ray intensities are discussed. The gamma-ray intensities for each spectrum were obtained by the following formula,

$$I + \delta I = \frac{C \pm \delta C}{(\varepsilon \pm \delta\varepsilon)(\rho \pm \delta\rho)}$$

C : counts of gamma-ray peak

ε : absolute detection efficiency

ρ : gamma-ray self-absorption coefficient for 2 mm thick of SUS316.

In this formula, three error terms are taken into account. (1) statistical error of gamma-ray counts and uncertainty in the fitting process in the spectrum analysis, (2) errors of the absolute gamma-ray detection efficiency at the measuring position of the irradiated sample, (3) error of gamma-ray self-absorption in 2 mm thick SUS316 disk. The term of (1) is dependent on the gamma-ray counts statistics and peak shape of the spectrum. Its error varied from 0.5 % to about 50 %. The efficiency error is estimated to be about 3 % in all energy region. The absorption error was estimated to be about 1 %.

6.2 Errors related to both calculation and experiment

Gamma-ray intensities in the calculation are obtained by the following formula,

$$I = \frac{N \cdot \phi \cdot \sigma \cdot (1 - e^{-\lambda \cdot t_i}) \cdot e^{-\lambda \cdot t_c} \cdot (1 - e^{-\lambda \cdot t_m}) \cdot b}{\lambda}$$

N : numbers of isotopes in the sample

ϕ : mean neutron flux during irradiation

σ : cross section of activation

b : branching ratio of gamma-ray per disintegration

λ : decay constant

t_i : irradiation time

t_c: cooling time

t_m: collecting time,

where symbol N is represented as

$$N = \frac{w \cdot N_a \cdot a \cdot c}{A}$$

w : weight of the sample

a : natural abundance of the isotope

c : atomic mass number

N_a: Avogadro's constant.

In order to compare absolutely the experimental data with the calculational one, the same parameters as in the experiment were used as the input parameter in the calculation.

(1) The number of nucleus

In the calculations, gamma-ray intensities were produced in a unit volume (1 cm^3) and the density of SUS316 was taken from the Japan Industrial Standard(JIS). The atomic composition in the sample of SUS316 was determined by the chemical analysis and the result is shown in Table 1 with isotopic abundance. A point to be remarked is that small constituent have rather large errors which were estimated to be up to 5 %.

(2) Irradiation, cooling and collecting times

The time parameters shown in Table 3 were used as input data in the calculations. The errors for these times were estimated to be negligibley small. The irradiation time, however, is related closely to the variation of the neutron flux during the irradiation. Its error can be included in the error for the mean neutron flux derivation.

(3) Saturation factor of induced activity

In the calculation of induced activities by the THIDA code, a constant neutron flux was assumed. However, in the actual irradiation experiment, there are usually time dependent neutron flux variation caused by both the fluctuation of d^+ beam and the consumption of the tritium target. This flux variation influenced the production rate of short-lived nuclei. Especially, on an occasion that its half-life is shorter than the irradiation time, the effects of activation saturation factor become large. The correactions for the saturation factor were made for short-lived production nuclide, ^{49}Cr, ^{52}V, ^{56}Mn and ^{57}Ni. The neutron production rate was monitored throughout the irradiation. For the calculation of the saturation factor,

the monitored output was used together with each half-lives. For example, the saturation factor of $^{56}Fe(n,p)^{56}Mn$ reaction in the cases of B and C was 7 % smaller than the calculated value using the time averaged neutron flux. The erros associated with this corrections were estimated to be smaller than 1 %.

(4) Absolute neutron yield

The total source neutron yield during each irradiation was measured by the associated alpha particle counting method[21] and its time averaged value was used in the calculation. The estimated error was about 4 %.

6.3 Uncertainties in the calculation

(1) Source neutron spectrum

As a source neutron spectrum, 14 MeV mono-energetic neutron corresponding to the first group of the GICX40 library[25] which extended from 13.72 to 15.0 MeV was used in the neutron flux calculation by ANISAN.[22] However, the source neutron spectrum was significantly affected by the structural materials of the target assembly.[27],[28] It means that there was some amount of difference in neutron spectrum between the calculation and actual experimental field.

(2) Neutron group structure

The neutron energy group structure as shown in Table 5, was used in the calculation. From this table, it is seen that the groups near 14 MeV energy region have rather wide energy intervals. In general, there is prominent 14 MeV neutron peak in the D-T neutron fields where high threshold reactions often occur. The cross sections of the reactions such as (n,2n) reaction, rise steeply near the threshold energy.

Calculations for the high threshold reaction rate $^{58}Ni(n,2n)^{57}Ni$ were carried out to show the group structure effect using two cross section sets having different group structures, 42 and 135. The reaction-rate ratio (135g/42g) in the Li_2O-C assembly at 4.2 cm and 12.5 cm were 1.26 and 1.30, respectively. These ratios indicate that the value with the 42 group set is lower than that with the 135 group set by 26 % to 30 %. The calculated reaction rate with the 135 group set agrees with the measured value in the experimental error. The cross section curves are shown in Fig. 13.

In the present calculation, it was considered that the 42 group structure was too coarse to calculate accurately the high threshold reactions such as $^{58}Ni(n,2n)^{57}Ni$ and $^{52}Cr(n,2n)^{51}Cr$. There may be some amount of underestimation for these reactions in the calculation.

(3) Neutron flux calculation

At the boundary of the Li_2O and C regions where the measurements on the C cases were made, the calculated neutron flux may be somewhat different from the actual flux. Since the neutron energy spectrum changes rapidly near the boundary of regions, it is necessary to make a model accurately.

6.4 Discussions on the total gamma-ray intensity and relative dose

From Table 9, in short cooling measurements (10 min to 13.8 hr), the calculation underestimated total gamma-ray intensities by 3-9 % except in the case of C-1, where overestimation of 24 % is observed. Similar results can be seen in the C/E of relative doses. It can be said that the calculation represented the experimental data well by considering the approximation in the source neutron spectrum, the rather coarse neutron group structure and uncertainties of the activation cross section.

Concerning the overestimation in the cases of C-1, some explanations can be expected, i.e., since the irradiation position was located just at the boundary of Li_2O and graphite regions, neutron spectrum was thought to be fairly softened. The calculated neutron spectra at 12.5 and 22.5 cm from the target are shown in Fig. 14. In spite of the small abundance of ^{55}Mn in the SUS316, the contribution of $^{55}Mn(n,\gamma)^{56}Mn$ reaction producing ^{56}Mn cannot be neglected becasue of its high sensitivity to slow neutrons, especially to thermal neutrons. The reaction cross section of $^{55}Mn(n,\gamma)^{56}Mn$ and $^{56}Fe(n,p)^{56}Mn$ are shown in Figs. 15.1 and 15.2, respectively. The reaction rates of both reactions were calculated by using the cross section and the calculated neutron fluxes as shown in Fig. 14. The contributions of $^{55}Mn(n,\gamma)^{56}Mn$ to the ^{56}Mn production were 6.5 and 36 % corresponding to the positions at 12.5 and 22.5 cm in the Li_2O-C assembly. This result indicated that the $^{55}Mn(n,\gamma)^{56}Mn$ reaction had high sensitivity to the ^{56}Mn production in the deep region of the assembly. Therefore, when the calculated neutron spectrum is softer than the actual

spectrum, the calculated reaction rate of $^{55}Mn(n,\gamma)^{56}Mn$ becomes larger than the measured value. If so, the overestimation can be explained.

On the other hand, in cases of long cooling measurements (about one month), the calculations overestimated by 1 % to 16 %. The dominant long-lived nuclei in the observed spectra were ^{54}Mn, ^{58}Co, ^{51}Cr and ^{57}Co. As examined in section 5, in the most intense group, 17th, the calculation overestimated ^{54}Mn. Cobalt-58 is produced by the reaction of $^{58}Ni(n,p)^{58}Co$ and following the decay of ^{58m}Co produced by the competing reaction of $^{58}Ni(n,p)^{58m}Co$. From the decay curve of ^{58}Co with 811 keV gamma-ray shown in Fig. 11.5, the calculation overestimated by about 10 %. This could be caused by the large uncertainty of the cross section for $^{58}Ni(n,p)^{58m}Co$, of which experimental data has been limited. Manganess-54 was produced by the reactions of both $^{54}Fe(n,p)^{54}Mn$ and $^{55}Mn(n,2n)^{54}Mn$. The amount of ^{54}Fe was three times larger than that of ^{55}Mn as seen from the Table 1. The cross sections of $^{54}Fe(n,p)^{54}Mn$ and $^{55}Mn(n,2n)^{54}Mn$ are about 0.4 and 0.8 barn for 14 MeV neutron, respectively as shown in Fig. 15.2. Both reaction rates at 12.5 and 22.5 cm in the assembly were calculated by the same manner as in the ^{56}Mn production. The calculated contributions by the $^{55}Mn(n,2n)^{54}Mn$ were 25 and 19 % of the total ^{55}Mn production at 12.5 and 22.5 cm in the assembly, respectively. These values were considered to be large to neglect the contribution. Since the threshold energy of $^{55}Mn(n,2n)^{54}Mn$ is above 10 MeV, its reaction rate strongly depends on the neutron group structure. From these considerations, the underestimation of ^{54}Mn by 25-33 % can be possible.

The influence of the group structure was also seen in the production of ^{51}Cr which was mainly produced by the reaction of $^{52}Cr(n,2n)^{51}Cr$, having threshold energy of about 12 MeV. Not only the group structure effect, but also its cross section uncertainty have to be taken into consideration for the underestimation by a factor of 2.

There were some overestimations in the calculation of ^{57}Co. Cobalt-57 was produced by the two reactions of $^{58}Ni[(n,d)+(n,np)]^{57}Co$ and following the decay of ^{57}Ni produced by $^{58}Ni(n,2n)^{57}Ni$. The overestimation may be casued by the uncertainty of the cross sections for $^{58}Ni[(n,d)+(n,np)]$ - ^{57}Co shown Fig. 15.2.

The variation of C/E for the total gamma-ray intensity and its relative dose versus cooling time are illustrated in Figs. 12.1 and 12.2, respectively. From these figures, it is clearly seen that in the cases

of short cooling time, the calculation underestimated except in the C-1 case and slight overestimations are observed in the cases of long cooling time. It can be pointed out that the overestimation becomes smaller as cooling time becomes longer.

7. CONCLUDING REMARKS

Through present irradiation experiments for SUS316 in three different neutron fields and following consective gamma-ray measurement, the THIDA code system was examined and its validity was verified. Several points to remark were deduced by comparisons between the calculation and the measurement. They are summarized in the following;

(i) The calculational results of the total gamma-ray intensities as well as their relative doses agreed with the measured ones within 15 % except in the case of C-1.

(ii) In short cooling time cases(less than one day), the dominant contributed gamma-ray was due to ^{56}Mn. Their intensities were more than 90 % of the totals. There were slight underestimations in the calculations. In the cases of long cooling time (more than 8 days), dominant gamma-rays come from ^{58}Co and ^{54}Mn. The calculation overestimated by several percents, but it can be said that the agreements are good.

(iii) In the case of C-1, the C/E was rather different from other cases. It might be considered as following; the irradiation position of the sample was located just at the boundary of the Li_2O and C regions. As the neutron spectrum at this position could have been more harder than the calculated one, the overestimation of ^{56}Mn in the calculation may be caused by the reaction of ^{55}Mn(n,γ)^{56}Mn.

(v) The fact that the calculation underestimated activities produced by high threshold reactions indicated that the 42 neutron group structure was too coarse for the calculation in the D-T neutron fields which have prominent 14 MeV peak.

Jarvis pointed out in Ref.(12) that uncertainities of a factor of one to two in the activation calculation should be acceptable in this stage of nuclear design of the fusion reactor. For the future design of a commercial fusion power reactor, however, the economical incentive demands strongly to provide more precise estimation. The accuracies suggested in Ref.(12) of 25 % for activation and 10 % for both transmutation and gas production provide realistic goal. As regards the above considerations, there were surprisingly good agreements between calculation

and experiment. The validity of the THIDA code system is demonstrated so far as SUS316 is concerned and it can be used successfully in the nuclear design on the fusion reactors. Further investigations will be needed to confirm the validity of the THIDA code system concerning more long-lived activities in SUS316 and activities in different materials. Of course, efforts are also needed for measurement and evaluation of nuclear data, i.e., activation cross sections, decay properties and so on.

ACKNOWLEDGEMENT

The authors would like to express their sincere thanks to Messers J. Kusano, C. Kustukake and S. Tanaka for the operation of the FNS accelerator. They would like to acknowledge the modification and execution of the THIDA code system by Mr. H. Kawasaki of Century Research Center Corporation Ltd..

and experiment. The validity of the THIDA code system is demonstrated so far as SUS316 is concerned and it can be used successfully in the nuclear design on the fusion reactors. Further investigations will be needed to confirm the validity of the THIDA code system concerning more long-lived activities in SUS316 and activities in different materials. Of course, efforts are also needed for measurement and evaluation of nuclear data, i.e., activation cross sections, decay properties and so on.

ACKNOWLEDGEMENT

The authors would like to express their sincere thanks to Messers J. Kusano, C. Kustukake and S. Tanaka for the operation of the FNS accelerator. They would like to acknowledge the modification and execution of the THIDA code system by Mr. H. Kawasaki of Century Research Center Corporation Ltd..

REFERENCES

(1) Blow S.: "Some Features of The Behaviour of Structural Materials in a Possible Fusion Reactor Blanket", AERE-R 6845 (1971)

(2) Vogelsang W.F., et al.: Nucl. Technol., 22, 379 (1974)

(3) Dudziak D.J. and Krakowaski R.A.: Nucl. Technol., 25, 32 (1975)

(4) Conn R.W., Sung T.Y. and Abdou M.A.; Nucl. Tehcnol., 26, 391 (1975)

(5) Williams M.L., Santoro R.T. and Gabliel T.A.; Nucl. Technol., 29, 384 (1976)

(6) Vogelsang W.F.; "Radioactivity and Associated Problems in Thermonuclear Reactors", UWFDM-178 (1976)

(7) Odenthal H.J., Dänner W. and Gorenflo H.: "AKTV", IPP-4/154 (1977)

(8) Gruber J.; "Evalution of The Activity Levels in Fusion Reactor Blankets", HMI-B202 (1977)

(9) Jung J.: "Theory and Use of The Radioactivity Code, RACC", ANL/FPP/TM-122 (1979)

(10) Jung J. and Abdou M.A.: Trans. Am. Nucl. Soc. 34, 645 (1980)

(11) Jarvis O.N.: "Transmutation and Activation of Fusion Reactor Wall and Structural Materials", AERE-R, 9298 (1979)

(12) Jarivs O.N.: "Nuclear Data Requriements for Transmutation and Activation of Reactor Wall and Structural Materials", IAEA-TECDOC-223 (Proc. of the Advisory Group Meeting) AG-159/A3, Vienna, (1978)

(13) Iida H. and Igarashi M.: "THIDA Code System for Calculation of the Exposure Dose Rate Around a Fusion Device", JAERI-M 8019 (1978) (in Japanese)

(14) Seki Y., Iida H. and Kawasaki H.: J. Nucl. Sci. Technol., 19 (1) 11(1982)

(15) "INTOR, International Tokamak Reactor, Phase One Report", International Atomic Energy Agency, Vienna (1982)

(16) Qaim S.M., Wölfle R., and Stöcklin G.: "Nuclear Data for Fusion Reactors", Proc. Symp. (Fast Neutron Interactions and the Problems of High Current Neutron Generators), Debrecen, Aug. 1975, Atomki Közlemenyeb, 335 (1976)

(17) Qaim S.M. and Stöcklin G.: "Measurement and Systematics of Cross Sections for Common and Low-yield 14 MeV Neutron Induced Nuclear Reactions on FR-material and Transmuted Species", Proc. 8th Symp. (Fusion Technology), Noordwijkerhout, June 1974, EUR 5182e, 989 (1974)

(18) Qaim S.M. and Molla N.I.: "Nuclear Data Measurements for FR-wall and Structural Materials", Proc. 9th Symp. (Fusion Technology), Garmish-Parlenkichen, June 1976, EUR 5602, 584 (1976)

(19) Nakamura T., et al.: "Integral Experiments on Lithium Oxide Spherical Assembly with Graphite Reflector and on Duct Streaming", Proc. 3rd IAEA Technical Committee Meeting and Workshop on Fusion Reactor Design and Technology, Tokyo, Oct. 5-16 (1981)

(20) Maekawa H., et al.: J. Nucl. Sci. Tehcnol., 16, 377 (1979)

(21) Maekawa H., et al.: to be published in JAERI-M report

(22) Engle, Jr W.W.: "A Useres Manual for ANISN, a One-dimensional Discrete Ordinates Code with Anisotropic Scattering", K-1693, Union Carbide Corp. (1976)

(23) Lederer C.M. and Shirley V.S. (edited): "Table of Isotopes", Seventh Edition, John Wiley and Sons, Inc., New York (1978)

(24) Baba H.: "Usage of the BOB7-Series Programs for the Analysis of Ge(Li) Gamma-ray Spectra", JAERI-M 7017, (1977)

(25) Seki Y. and Iida H.: "Coupled 42-Group Neutron and 21-Group Gamma-ray Cross Section Sets for Fusion Reactor Calculations", JAERI-M 8818, (1980)

(26) Seki Y., Iida H. and Kawasaki H.: "Graphical Representation of Transmutation and Decay Chain Data, Transmutation Cross Section and Delayed Gamma-Ray Emission Data", JAERI 1280 (1982)

(27) Seki Y., et al.: "Monte Carlo Calculations of the Source Characteristics of the FNS Water Cooled Type Tretium Target", J. Nucl. Sci. Technol., 20, 686 (1983)

(28) Ikeda Y., et al.: to be published in JAERI-M report

Table 1 Nuclear composition of SUS316 stainless steel sample used in this experiment

element	weight (%)*	nuclide	abundance	total weight ratio
Mn	1.24±0.07	^{55}Mn	1.0	0.0124
Fe	66.82±0.14	^{54}Fe	0.0584	0.0375
		^{56}Fe	0.918	0.6152
		^{57}Fe	0.0215	0.0147
		^{58}Fe	0.0029	0.0020
Ni	12.36±0.05	^{58}Ni	0.683	0.0834
		^{60}Ni	0.261	0.0330
		^{61}Ni	0.0113	0.0015
		^{62}Ni	0.0359	0.0046
		^{64}Ni	0.0091	0.0012
Cr	16.65±0.38	^{50}Cr	0.0435	0.0069
		^{52}Cr	0.8379	0.1395
		^{53}Cr	0.0950	0.0161
		^{54}Cr	0.0236	0.0041
Mo	2.24±0.02	^{92}Mo	0.148	0.0032
		^{94}Mo	0.093	0.0020
		^{95}Mo	0.159	0.0036
		^{96}Mo	0.167	0.0037
		^{97}Mo	0.096	0.0022
		^{98}Mo	0.241	0.0055
		^{100}Mo	0.0096	0.0023

* determined by chemical analysis

Table 2 Activation reactions in SUS316 with associated nuclear data

reaction	half life	*weight (mg)	**Eγ (keV)	branching	abundance
$^{50}Cr(n,\gamma)^{51}Cr$	27.7 d	9.078	320.11	0.102	4.35 %
$^{50}Cr(n,2n)^{49}Cr$	41.9 m	9.078	152.93 90.64	0.29 0.51	4.35 %
$^{52}Cr(n,2n)^{51}Cr$	27.7 d	174.86	320.11	0.102	83.79 %
$^{52}Cr(n,p)^{52}V$	3.76 m	174.86	1434.06	1.00	83.79 %
$^{53}Cr(n,p)^{53}V$	1.6 m	19.825	1006.0	0.90	9.5 %
$^{53}Cr(n,np)^{52}V$	3.76 m	19.825	1434.06	1.00	9.5 %
$^{54}Cr(n,\alpha)^{51}Ti$	5.8 m	4.925	320.11	0.934	2.36 %
$^{55}Mn(n,2n)^{54}Mn$	312.2 d	15.542	834.83	1.00	100 %
$^{55}Mn(n,\gamma)^{56}Mn$	2.579 h	15.542	846.75	0.9888	100 %
$^{55}Mn(n,\alpha)^{52}V$	3.76 m	15.542	1434.06	1.00	100 %
$^{54}Fe(n,2n)^{53}Fe$	8.51 m	48.911	377.9	0.42	5.84 %
$^{54}Fe(n,p)^{54}Mn$	312.2 d	48.911	834.83	1.00	5.84 %
$^{54}Fe(n,\alpha)^{51}Cr$	27.7 d	48.911	320.11	0.102	5.84 %
$^{56}Fe(n,p)^{56}Mn$	2.579 h	768.84	846.75	0.9888	91.8 %
$^{57}Fe(n,p)^{57}Mn$	1.6 m	18.174	122.	0.103	2.15 %
$^{57}Fe(n,np)^{56}Mn$	2.579 h	18.174	846.75	0.9888	2.15 %

* weight in the 10 ϕ x 2 t(m/m) SUS316 disk

** dominant gamma-rays emitted from product nuclei

Table 2 continue 1

reaction	half life	*weight (mg)	**Eγ (keV)	branching	abundance
$^{58}Fe(n,\gamma)^{59}Fe$	44.6 d	2.429	1099.2	0.565	0.29 %
$^{58}Ni(n,2n)^{57}Ni$	36.0 h	105.81	1372.59	0.776	68.3 %
$^{58}Ni(n,p)^{58}Co$	70.8 d	105.81	810.76	1.00	68.3 %
$^{58}Ni(n,p)^{58m}Co$	9.2 h	105.81	24.89	1.0	68.3 %
$^{58}Ni(n,p)^{58}Co$	70.8 d	105.81	810.76	1.0	68.3 %
$^{58}Ni(n,d)^{57}Co$	271 d	105.81	122.06	0.856	68.3 %
$^{58}Ni(n,np)^{57}Co$	271 d	105.81	122.06	0.856	68.3 %
$^{60}Ni(n,p)^{60}Co$	5.27 y	40.527	1332.47	1.00	26.1 %
$^{60}Ni(n,p)^{60m}Co$	10.5 m	40.527	58.6	0.988	26.1 %
$^{61}Ni(n,p)^{61}Co$	1.65 h	1.936	67.1	0.86	1.13 %
$^{61}Ni(n,np)^{60}Co$	5.27 y	1.936	1332.47	1.00	1.13 %
$^{61}Ni(n,np)^{60m}Co$	10.5 m	1.936	58.6	0.998	1.13 %
$^{62}Ni(n,p)^{62}Co$	13.9 m	5.670	1173.0	0.826	3.59 %
$^{62}Ni(n,p)^{62m}Co$	1.50 m	5.670	1173.0	0.979	3.59 %
$^{62}Ni(n,\alpha)^{59}Fe$	44.6 d	5.670	1099.2	0.565	3.59 %
$^{62}Ni(n,np)^{61}Co$	1.64 h	5.670	67.1	0.998	3.59 %
$^{64}Ni(n,\gamma)^{65}Ni$	2.52 h	1.797	1481.8	0.235	0.91 %
$^{64}Ni(n,\alpha)^{51}Fe$	6.0 m	1.797	1205.1	0.436	0.91 %

* weight in the 10 Ø x 2 t(m/m) SUS316 disk

** dominant gamma-rays emitted from product nuclei

Table 2 continue 2

reaction	half life	*weight (mg)	**Eγ (keV)	branching	abundance
$^{92}Mo(n,\gamma)^{93m}Mo$	6.95 h	4.155	684.67 1477.1	0.9968 0.9908	14.8 %
$^{92}Mo(n,2n)^{91}Mo$	15.49 m	4.155	1637.73	0.0032	14.8 %
$^{92}Mo(n,p)^{92m}Nb$	10.15 d	4.155	934.51	0.992	14.8 %
$^{92}Mo(n,\alpha)^{89}Zr$	78.4 h	4.155	909.2	0.9901	14.8 %
$^{92}Mo(n,\alpha)^{89m}Zr$	4.18 m	4.155	587.8	0.895	14.8 %
$^{92}Mo(n,np)^{91m}Nb$	62 d	4.155	1205	0.034	14.8 %
$^{94}Mo(n,2n)^{93m}Mo$	6.95 h	2.611	684.67 1477.1	0.9968 0.9908	9.3 %
$^{94}Mo(n,p)^{94m}Nb$	6.26 m	2.611	41	0.00074	9.3 %
$^{95}Mo(n,p)^{95}Nb$	35.0 d	4.464	765.78	0.9982	15.9 %
$^{95}Mo(n,p)^{95m}Nb$	87 h	4.464	204.12	1.00	15.9 %
$^{96}Mo(n,p)^{96}Nb$	23.35 h	4.689	778.22 568.86	0.968 0.552	16.7 %
$^{96}Mo(n,np)^{95}Nb$	35.0 d	4.689	765.78	0.9982	16.7 %
$^{97}Mo(n,p)^{97}Nb$	72.1 m	2.695	65.792	0.982	9.6 %
$^{97}Mo(n,p)^{97m}Nb$	1.0	2.695	757	0.979	9.6 %
$^{97}Mo(n,np)^{96}Nb$	23.35 h	2.695	778.22 568.86	0.968 0.552	9.6 %
$^{98}Mo(n,\gamma)^{99}Mo$	66.02 h	6.766	739.4	0.126	24.1 %
$^{98}Mo(n,p)^{98}Nb$	51.5 m	6.766	787.36 722.6	0.932 0.736	24.1 %

* weight in the 10 ϕ x 2 t(m/m) SUS316 disk

** dominant gamma-ray emitted from product nuclei

Table 2 continue 3

reaction	Half Life	*weight (mg)	**Eγ (keV)	branching	abundance
$^{98}Mo(n,\alpha)^{95}Zr$	64.0 d	6.766	756.7 724,2	0.546 0.431	24.1 %
$^{98}Mo(n,np)^{97}Nb$	72.1 m	6.766	657.92	0.982	24.1 %
$^{100}Mo(n,\gamma)^{101}Mo$	14.6 m	2.695	191.81	0.196	9.6 %
$^{100}Mo(n,2n)^{99}Mo$	66.02 h	2.695	739.4	0.126	9.6 %
$^{100}Mo(n,\alpha)^{97}Zr$	16.9 h	2.695	743.36	0.928	9.6 %

* weight in the 10 ø x 2 t(m/m) SUS316 disk

** dominant gamma-rays emitted from product nuclei

Table 3 Time table of cooling and collecting for gamma-ray measurements

names of measurements	cooling time	collecting time (sec)
A-1	10 min	1,000
A-2	1 hr	3,000
A-3	6.9 hr	30,000
A-4	30.1 d	486,638
B-1	13.8 hr	5,049
B-2	13.6 d	33,529
B-3	35.7 d	441,439
C-1	10.5 hr	10,000
C-2	8.0 d	492,310
C-3	28.8 d	595,386

cases of A : irradiated at the distance of 10 cm from the target without any assembly

cases of B and C : irradiated in the Li_2O-C assembly at distances of 12.6 and 22.6 cm from the target, respectively

Table 4 Measured gamma-ray energy(E_γ) and intensity(I_γ)

A-1

E_γ(keV)	I_γ	Error(%)
3369	1.949×10^5	19.2
2960	3.574×10^5	13.3
2657	6.728×10^5	10.8
2523	9.856×10^5	7.8
2113	1.270×10^7	3.5
1920	5.925×10^4	25.6
1810	2.378×10^7	3.2
1434	1.638×10^6	5.2
1378	4.590×10^5	8.3
1239	6.818×10^4	19.5
1173	1.153×10^5	14.6
1165	4.91×10^4	21.4
847	8.657×10^7	3.0
672	5.893×10^4	15.5
511	3.606×10^6	4.0
378	1.340×10^5	11.8
320	6.741×10^4	14.9
153	1.53×10^5	7.8
141	3.963×10^4	14.4
127	6.374×10^4	11.7
122	3.796×10^4	15.0
91	2.362×10^5	7.8

A-2

E_γ(keV)	I_γ	Error(%)
3369	3.396×10^5	14.7
2960	7.285×10^5	9.6
2657	1.602×10^6	6.5
2523	2.068×10^6	5.8
2113	2.849×10^7	3.2
1920	1.519×10^5	16.2
1810	5.330×10^7	3.1
1759	1.378×10^5	16.3
1635	1.941×10^5	13.6
1378	1.333×10^6	5.5
1267	1.014×10^5	16.7
1239	2.363×10^5	11.0
847	1.957×10^8	3.0
810	2.508×10^5	8.7
778	1.177×10^5	12.1
739	8.243×10^4	14.0
658	2.490×10^5	20.8
511	4.684×10^6	3.8
320	1.128×10^5	11.7
153	1.390×10^5	8.2
141	1.215×10^5	8.5
136	5.199×10^4	12.7
127	1.984×10^5	7.0
122	8.501×10^4	10.2
91	3.205×10^5	6.9

Table 4 cont. 1

A-3

Eγ(keV)	Iγ	Error(%)
3369	3.719×10^5	8.0
2960	6.743×10^5	6.1
2757	2.57×10^4	39
2732	1.699×10^4	58
2657	1.351×10^6	4.5
2599	3.860×10^4	38
2523	1.888×10^6	4.2
2283	8.054×10^4	24
2113	2.677×10^7	3.1
1920	1.490×10^6	5.5
1810	4.974×10^7	3.0
1758	6.399×10^5	12.7
1378	8.654×10^6	3.3
1260	1.894×10^5	12.0
1201	1.342×10^5	13.7
1091	1.460×10^6	5.2
1038	1.306×10^5	19.8
935	1.975×10^5	10.2
910	1.375×10^5	23.8
847	1.795×10^8	3.0
835	4.007×10^5	9.4
810	1.990×10^6	4.5
778	4.532×10^5	13.0
739	5.132×10^5	14.3
511	1.197×10^7	3.1
320	1.468×10^6	4.7
181	2.713×10^5	12.3
141	2.584×10^6	3.2
136	9.680×10^4	19.6
127	1.587×10^6	3.4
122	1.031×10^6	3.5

A-4

Eγ(keV)	Iγ	Error(%)
1674	1.81×10^5	19.6
1332	2.28×10^5	19.0
1292	1.20×10^5	25.2
1173	2.24×10^5	21.8
1099	1.980×10^5	24.1
935	2.96×10^5	14.1
863	2.59×10^5	17.4
835	9.079×10^6	3.1
810	2.823×10^7	3.0
766	2.02×10^5	22.3
511	1.035×10^7	3.1
320	1.130×10^7	3.0
136	1.876×10^6	3.6
122	1.622×10^7	3.0

Table 4 cont. 2

B-1

Eγ(keV)	Iγ	Error(%)
3369	2.390×10^4	26
2960	2.267×10^4	26
2658	5.945×10^4	15
2523	9.322×10^4	12
2113	1.171×10^6	6.8
1919	1.988×10^5	14.2
1810	2.118×10^6	5.1
1757	1.176×10^5	17.6
1378	1.362×10^6	5.4
935	3.152×10^4	25
847	7.838×10^6	3.3
835	1.721×10^5	10.5
810	7.471×10^5	5.6
778	1.039×10^5	12.9
739	1.738×10^5	9.9
511	1.553×10^6	4.0
320	3.082×10^5	5.4
181	8.972×10^4	7.2
141	1.006×10^6	3.6
137	2.986×10^4	22
127	2.432×10^5	4.8
122	2.100×10^5	5.2

B-2

Eγ(keV)	Iγ	Error(%)
1674	1.782×10^4	33
1378	2.908×10^4	26
1332	2.412×10^4	42
1291	2.222×10^4	32
1173	2.236×10^4	37
1099	1.830×10^4	33
935	6.634×10^4	17.3
864	3.425×10^4	23
835	9.006×10^5	5.3
810	4.254×10^6	3.6
765	8.118×10^3	62
739	3.908×10^4	20
511	1.394×10^6	4.1
320	1.215×10^6	3.8
181	1.005×10^4	48
141	1.954×10^5	4.2
137	1.378×10^5	5.9
122	1.157×10^6	3.5

Table 4 cont. 3

B-3

Eγ(keV)	Iγ	Error(%)
1674	3.012×10^5	11.0
1332	4.200×10^5	8.5
1291	3.067×10^5	9.7
1173	5.144×10^5	7.4
1099	2.806×10^5	9.4
935	2.530×10^5	9.2
865	4.368×10^5	7.0
834	1.200×10^7	3.1
810	4.942×10^7	3.0
765	2.224×10^5	9.0
511	1.618×10^7	3.1
320	9.821×10^6	3.1
136	1.999×10^6	3.3
122	1.656×10^7	3.0

C-1

Eγ(keV)	Iγ	Error(%)
3369	1.37×10^4	30
2960	2.71×10^4	25
2658	4.73×10^4	22
2523	7.92×10^4	15.3
2113	1.129×10^6	4.4
1919	5.43×10^4	25
1810	2.201×10^6	3.7
1757	4.07×10^4	29
1377	3.99×10^5	6.9
935	3.39×10^4	24
910	6.19×10^4	21
847	7.863×10^6	3.1
834	6.52×10^4	25
810	3.33×10^5	6.4
778	7.13×10^4	21
739	1.57×10^5	11.6
685	1.30×10^5	16.3
511	8.10×10^5	4.2
320	1.02×10^5	13.0
181	9.83×10^4	11.9
141	1.011×10^6	3.4
136	7.00×10^3	23
127	7.94×10^4	7.3
122	5.93×10^4	8.4

Table 4 cont. 4

C-2

Eγ(keV)	Iγ	Error(%)
1674	1.18×10^5	25.6
1332	5.01×10^5	10.1
1291	2.27×10^5	19.6
1174	4.30×10^5	12.7
1099	2.43×10^5	19.8
935	4.34×10^5	11.1
862	2.23×10^5	19.4
835	2.921×10^5	3.6
810	1.685×10^7	3.1
778	2.45×10^5	20.6
739	6.34×10^5	8.1
511	7.201×10^6	3.1
320	3.533×10^6	3.2
181	2.42×10^5	12.8
141	4.878×10^6	3.2
136	3.49×10^5	3.4
122	3.045×10^6	3.2

C-3

Eγ(keV)	Iγ	Error(%)
1332	5.03×10^5	10.6
1291	1.24×10^5	22.0
1173	4.83×10^5	12.3
1099	1.58×10^5	31.3
935	1.75×10^5	25.8
863	1.09×10^5	20.1
834	3.426×10^6	3.55
810	1.674×10^7	3.06
511	7.487×10^6	3.13
320	2.533×10^6	3.91
141	4.30×10^4	5.41
136	4.35×10^5	7.71
122	3.544×10^6	3.20

Table 5 The 42-group neutron energy group structure adopted in the CROSSLIB and GICX40 libraries

Group	Energy Limits	Mid-Point Energy
1	15.000 - 13.720 MeV	14.360 MeV
2	13.720 - 12.549	13.135
3	12.549 - 11.478	12.014
4	11.478 - 10.500	10.989
5	10.500 - 9.314	9.907
6	9.314 - 8.261	8.788
7	8.261 - 7.328	7.795
8	7.328 - 6.500	6.914
9	6.500 - 5.757	6.129
10	5.757 - 5.099	5.428
11	5.099 - 4.516	4.808
12	4.516 - 4.000	4.258
13	4.000 - 3.162	3.681
14	3.162 - 2.500	2.831
15	2.500 - 1.871	2.186
16	1.871 - 1.400	1.636
17	1.400 - 1.058	1.229
18	1.058 - 0.800	0.929
19	0.800 - 0.566	0.683
20	0.566 - 0.400	0.483
21	0.400 - 0.283	0.342
22	0.283 - 0.200	0.242
23	0.200 - 0.141	0.171
24	0.141 - 0.100	0.121
25	100.0 - 46.5 keV	73.2 keV
26	46.5 - 21.5	34.0
27	21.5 - 10.0	15.75
28	10.0 - 4.65	7.325
29	4.65 - 2.15	3.40
30	2.15 - 1.00	1.575
31	1.00 - 0.465	0.733
32	0.465 - 0.215	0.340
33	0.215 - 0.100	0.158
34	100.0 - 46.5 eV	73.2 eV
35	46.5 - 21.5	34.0
36	21.5 - 10.0	15.75
37	10.0 - 4.65	7.325
38	4.65 - 2.15	3.40
39	2.15 - 1.00	1.58
40	1.00 - 0.465	0.733
41	0.465 - 0.215	0.340
42	0.215 - 0.001	0.108

Table 6 Gamma-ray Energy Group Structure

Group	Energy Limits (eV) upper			lower	
1	0.300	E+07	-	0.270	E+07
2	0.270	E+07	-	0.250	E+07
3	0.250	E+07	-	0.230	E+07
4	0.230	E+07	-	0.210	E+07
5	0.210	E+07	-	0.200	E+07
6	0.200	E+07	-	0.190	E+07
7	0.190	E+07	-	0.180	E+07
8	0.180	E+07	-	0.170	E+07
9	0.170	E+07	-	0.160	E+07
10	0.160	E+07	-	0.150	E+07
11	0.150	E+07	-	0.140	E+07
12	0.140	E+07	-	0.130	E+07
13	0.130	E+07	-	0.120	E+07
14	0.120	E+07	-	0.110	E+07
15	0.110	E+07	-	0.100	E+07
16	0.100	E+07	-	0.900	E+06
17	0.900	E+06	-	0.810	E+06
18	0.810	E+06	-	0.730	E+06
19	0.730	E+06	-	0.660	E+06
20	0.660	E+06	-	0.600	E+06
21	0.600	E+06	-	0.550	E+06
22	0.550	E+06	-	0.500	E+06
23	0.500	E+06	-	0.450	E+06
24	0.450	E+06	-	0.400	E+06
25	0.400	E+06	-	0.360	E+06
26	0.360	E+06	-	0.330	E+06
27	0.330	E+06	-	0.300	E+06
28	0.300	E+06	-	0.270	E+06
29	0.270	E+06	-	0.250	E+06
30	0.250	E+06	-	0.230	E+06
31	0.230	E+06	-	0.210	E+06
32	0.210	E+06	-	0.200	E+06
33	0.200	E+06	-	0.190	E+06
34	0.190	E+06	-	0.180	E+06
35	0.180	E+06	-	0.170	E+06
36	0.170	E+06	-	0.160	E+06
37	0.160	E+06	-	0.150	E+06
38	0.150	E+06	-	0.140	E+06
39	0.140	E+06	-	0.130	E+06
40	0.130	E+06	-	0.120	E+06
41	0.120	E+06	-	0.110	E+06
42	0.110	E+06	-	0.100	E+06
43	0.100	E+06	-	0.900	E+05
44	0.900	E+05	-	0.810	E+05
45	0.810	E+05	-	0.730	E+05
46	0.730	E+05	-	0.660	E+05
47	0.660	E+05	-	0.600	E+05
48	0.600	E+05	-	0.550	E+05
49	0.550	E+05	-	0.500	E+05
50	0.500	E+05	-	0.450	E+05
51	0.450	E+05	-	0.400	E+05
52	0.400	E+05	-	0.360	E+05
53	0.360	E+05	-	0.330	E+05
54	0.330	E+05	-	0.300	E+05

Table 7.1 Comparison of gamma ray intensity (Iγ) and relative dose for A-1 case

group No.	Calculation		Experiment	
	Iγ	dose	Iγ (% error)	dose
1	4.18×10^5	5.55×10^1	5.523×10^5 (15.4)	7.33×10^1
2	1.42×10^6	1.93×10^2	1.658×10^6 (9.0)	2.26×10^2
4	1.24×10^7	1.43×10^3	1.270×10^7 (3.5)	1.46×10^3
5	1.86×10^4	2.0	———	
6	4.23×10^4	4.3	5.93×10^4 (25.6)	6.1
7	2.351×10^7	2.285×10^3	2.378×10^7 (3.2)	2.311×10^3
8	3.33×10^4	3.1	———	
11	2.10×10^6	1.60×10^2	1.638×10^6 (5.2)	1.25×10^2
12	2.77×10^5	1.97×10^1	4.59×10^5 (8.3)	3.27×10^1
13	9.04×10^4	5.9	6.82×10^4 (19.5)	4.4
14	1.70×10^5	1.03×10^3	1.64×10^5 (16.7)	9.9
16	3.34×10^4	1.7	———	
17	8.533×10^7	$3.820 \quad 10^1$	8.657×10^7 (3.0)	3.876×10^3
18	7.52×10^4	3.0	———	
19	3.06×10^4	1.1	5.89×10^4 (15.5)	2.1
20	1.74×10^5	5.6	———	
22	1.12×10^6	2.96×10^1	3.606×10^6 (4.0)	9.54×10^1
25	2.14×10^4	0.4	1.34×10^5 (11.8)	2.4
27	1.86×10^5	2.7	6.74×10^4 (14.9)	1.0
37	1.60×10^4	0.1	1.53×10^5 (7.8)	0.9
38	1.54×10^5	0.8	3.96×10^4 (14.4)	0.2
40	9.11×10^4	0.4	1.02×10^5 (12.9)	0.4
43	2.77×10^4	0.1	2.362×10^5 (7.8)	0.7
Total	1.277×10^8	8.034×10^3	1.320×10^8 (3.2)	8.228×10^3

The term of Iγ means the intergrated numbers of emitted gamma-rays during the collecting time

Table 7.2 Comparison of gamma ray intensity (Iγ) and relative dose for A-2 case

group No.	Calculation Iγ	Calculation dose	Experiment Iγ (% error)	Experiment dose
1	9.16×10^5	1.22×10^2	1.058×10^6 (10.0)	1.404×10^2
2	3.17×10^6	4.32×10^2	3.67×10^6 (6.0)	4.996×10^2
4	2.76×10^7	3.183×10^3	2.85×10^7 (3.2)	3.286×10^3
5	2.67×10^3	0.3	———	———
6	1.42×10^5	1.46×10^1	1.52×10^5 (16.2)	1.55×10^1
7	5.243×10^7	5.095×10^3	5.330×10^7 (3.1)	5.180×10^3
8	7.26×10^4	6.7	1.378×10^5 (16.3)	1.27×10^1
9	1.82×10^3	0.2	1.94×10^5 (13.6)	1.68×10^1
12	7.46×10^5	5.31×10^1	1.33×10^6 (5.5)	9.47×10^2
13	2.01×10^5	1.32×10^1	3.38×10^5 (16.7)	2.23×10^1
14	3.19×10^4	1.9	———	———
15	2.22×10^4	1.2	———	———
16	4.93×10^4	2.5	———	———
17	1.903×10^8	8.521×10^3	1.9596×10^8 (3.0)	8.73×10^3
18	1.83×10^5	7.3	2.00×10^5 (12.5)	8.0
19	3.31×10^4	1.2	———	———
20	2.80×10^5	9.1	2.49×10^5 (20.8)	8.1
21	2.02×10^4	0.6	———	———
22	9.79×10^5	2.59×10^1	4.684×10^6 (3.8)	1.240×10^2
27	1.08×10^5	1.6	1.13×10^5 (11.7)	1.65
34	2.81×10^4	0.2	———	———
37	5.99×10^3	0.04	1.39×10^5 (8.2)	0.8
38	4.85×10^5	2.6	1.22×10^5 (8.5)	0.65
39	1.90×10^4	0.1	5.20×10^4 (12.7)	0.25
40	2.69×10^5	1.2	2.83×10^5 (8.3)	1.2
43	1.01×10^4	0.03	3.21×10^5 (6.9)	1.0
total	2.7815×10^8	1.755×10^4	2.9080×10^8 (3.1)	1.904×10^4

The term of Iγ means the integrated numbers of emitted gamma-rays during the collecting time

Table 7.3 Comparison of gamma ray intensity (Iγ) and relative dose for A-3 case

group No.	Calculation		Experiment	
	Iγ	dose	Iγ (% error)	dose
1	8.20×10^5	1.09×10^2	1.09×10^6 (7.5)	1.46×10^2
2	2.83×10^6	3.85×10^2	3.28×10^6 (4.7)	4.46×10^2
4	2.48×10^7	2.860×10^3	2.685×10^7 (3.1)	3.096×10^3
6	1.13×10^6	1.16×10^2	1.49×10^6 (5.5)	1.52×10^2
7	4.70×10^7	4.57×10^2	4.974×10^7 (3.0)	4.834×10^3
8	5.52×10^5	5.08×10^1	6.40×10^5 (12.7)	5.89×10^1
9	1.20×10^4	1.0	———	———
11	1.29×10^4	1.0	———	———
12	6.00×10^6	4.27×10^2	8.65×10^6 (3.3)	6.16×10^2
13	2.31×10^5	1.52×10^1	3.24×10^5 (12.7)	2.14×10^1
14	1.78×10^4	1.1	———	———
15	1.33×10^6	7.35×10^1	1.59×10^6 (6.4)	8.79×10^1
16	3.03×10^5	1.51×10^1	3.35×10^5 (15.8)	1.67×10^1
17	1.73×10^8	7.75×10^3	1.819×10^8 (3.0)	8.144×10^3
18	1.09×10^6	4.37×10^1	9.66×10^5 (13.7)	3.88×10^1
19	3.25×10^4	1.2	———	———
20	1.14×10^5	3.7	———	———
21	1.44×10^5	4.2	———	———
22	6.88×10^6	1.82×10^1	1.197×10^7 (3.1)	3.17×10^2
23	8.73×10^4	2.1	———	———
25	6.04×10^4	1.1	———	———
27	9.99×10^5	1.46×10^1	1.47×10^6 (4.7)	2.15×10^1
34	2.45×10^5	1.8	2.71×10^5 (12.3)	2.0
38	5.03×10^6	2.71×10^1	2.59×10^6 (3.2)	1.39×10^1
39	1.84×10^5	0.9	9.68×10^4 (2.0)	0.47
40	2.41×10^6	1.06×10^1	2.62×10^6 (3.4)	1.15×10^1
Total	2.754×10^8	1.666×10^4	2.959×10^8 (3.1)	1.796×10^4

The term of Iγ means the integrated numbers of emitted gamma-rays during the collecting time

Table 7.4 Comparison of gamma ray intensity (Iγ) and relative dose for A-4 case

group No.	Calculation		Experiment	
	Iγ	dose	Iγ (% error)	dose
9	1.79×10^5	1.55×10^1	1.81×10^5 (19.6)	1.57×10^1
12	2.11×10^5	1.50×10^1	2.28×10^5 (19.0)	1.62×10^1
13	7.29×10^4	4.8	1.20×10^5 (25.2)	7.9
14	2.10×10^5	1.27×10^1	2.24×10^5 (21.8)	1.36×10^1
15	8.95×10^4	4.9	1.98×10^5 (24.1)	1.09×10^1
16	1.33×10^5	6.6	2.96×10^5 (14.0)	1.48×10^1
17	4.079×10^7	1.826×10^3	3.757×10^7 (3.1)	1.682×10^3
18	2.33×10^5	9.3	2.02×10^5 (22.3)	8.1
19	5.40×10^4	1.9	——	
22	9.95×10^6	2.63×10^2	1.035×10^7 (3.1)	2.74×10^2
27	7.45×10^6	1.09×10^2	1.130×10^7 (3.0)	1.65×10^2
38	2.76×10^4	0.1	——	
39	2.92×10^6	1.42×10^1	1.88×10^6 (3.6)	9.2
40	2.24×10^7	9.86×10^1	1.622×10^7 (3.)	7.14×10^1
Total	8.474×10^7	2.383×10^3	7.877×10^7 (3.1)	2.289×10^3

The term of Iγ means the integrated numbers of emitted gamma-rays during the collecting time

Table 7.5 Comparison of gamma ray intensity(Iγ) and relative dose for B-1 case

group No.	Calculation		Experiment	
	Iγ	dose	Iγ (% error)	dose
1	3.51×10^{4}	4.7	4.66×10^{4} (26)	6.18
2	1.21×10^{5}	1.65×10^{1}	1.53×10^{5} (13)	2.08×10^{1}
4	1.06×10^{6}	1.22×10^{2}	1.17×10^{5} (6.8)	1.35×10^{2}
6	1.36×10^{5}	1.39×10^{1}	1.99×10^{5} (14.2)	2.04×10^{1}
7	2.01×10^{6}	1.95×10^{2}	2.12×10^{6} (5.1)	2.06×10^{2}
8	6.63×10^{4}	6.1	1.18×10^{5} (17.6)	1.09×10^{1}
9	4.45×10^{3}	0.4	———	———
11	1.43×10^{4}	1.1	———	———
12	7.21×10^{5}	5.13×10^{1}	1.36×10^{6} (5.4)	9.68×10^{1}
13	1.72×10^{4}	1.1	———	———
14	4.46×10^{3}	0.3	———	———
15	2.13×10^{4}	1.18	———	———
16	5.04×10^{4}	2.5	3.15×10^{4} (25)	1.57
17	8.22×10^{6}	3.68×10^{2}	8.757×10^{6} (3.5)	3.92×10^{2}
18	2.70×10^{5}	1.08×10^{1}	2.78×10^{5} (10.5)	1.16
19	1.60×10^{4}	0.6	———	———
20	1.18×10^{4}	0.4	———	———
21	2.09×10^{4}	0.6	———	———
22	9.93×10^{5}	2.63×10^{1}	1.553×10^{6} (4.0)	4.11×10^{1}
23	1.26×10^{4}	0.3	———	———
25	1.82×10^{4}	0.3	———	———
27	1.39×10^{5}	2.0	3.08×10^{5} (5.4)	4.50
29	7.11×10^{3}	0.1	———	———
34	7.81×10^{4}	0.58	8.97×10^{4} (7.2)	0.67
38	1.63×10^{6}	8.74	1.01×10^{6} (3.6)	5.42
39	3.03×10^{4}	0.15	2.99×10^{4} (22)	0.15
40	3.52×10^{5}	1.55	4.53×10^{5} (5.0)	1.99
Total	1.605×10^{7}	8.37×10^{2}	1.768×10^{7} (4.0)	9.45×10^{2}

The term of Iγ means the integrated numbers of emitted gamma-rays during the collecting time

Table 7.6 Comparison of gamma ray intensity(Iγ) and relative dose for B-2 case

group No.	Calculation Iγ	Calculation dose	Experiment Iγ (% error)	Experiment dose
9	2.92×10^4	2.5	1.78×10^4 (33)	1.5
12	3.03×10^4	2.2	5.32×10^4 (33)	3.8
13	1.26×10^4	0.8	2.22×10^4 (32)	1.5
14	1.94×10^4	1.2	2.24×10^4 (37)	1.4
15	1.60×10^4	0.9	1.830×10^4 (33)	1.0
16	4.05×10^4	2.0	6.634×10^4 (17.3)	3.3
17	6.198×10^6	2.77×10^2	5.189×10^6 (3.7)	2.32×10^2
18	7.26×10^4	2.9	4.72×10^4 (27)	1.9
22	1.635×10^6	4.33×10^1	1.394×10^6 (4.1)	3.69×10^1
27	6.629×10^5	9.7	1.215×10^6 (3.8)	1.77×10^1
34	1.88×10^4	0.1	1.01×10^4 (48)	0.1
38	3.94×10^5	2.1	1.95×10^5 (4.2)	1.0
39	1.95×10^5	1.0	1.38×10^5 (5.9)	0.7
40	1.523×10^6	6.7	1.157×10^6 (3.5)	5.1
Total	1.085×10^7	3.524×10^2	9.546×10^6 (4.0)	3.079×10^2

The term of Iγ means the integrated numbers of emitted gamma-rays during the collecting time

Table 7.7 Comparison of gamma ray intensity(Iγ) and ralative dose for B-3 case

group No.	Calculation Iγ	Calculation dose	Experiment Iγ (% error)	Experiment dose
9	3.02×10^5	2.62×10^1	3.01×10^5 (11.0)	2.61×10^1
12	2.54×10^5	1.81×10^1	4.20×10^5 (8.5)	2.99×10^1
13	1.14×10^5	7.51	3.08×10^5 (9.7)	2.03×10^1
14	2.54×10^5	1.54×10^1	5.14×10^5 (7.4)	3.12×10^1
15	1.44×10^5	8.0	2.81×10^5 (9.4)	1.55×10^1
16	6.00×10^4	3.0	2.53×10^5 (9.2)	1.26×10^1
17	6.59×10^7	2.950×10^3	6.19×10^7 (3.1)	2.771×10^3
18	1.99×10^5	8.0	2.22×10^5 (9.0)	8.91×10^0
19	4.61×10^4	1.7	———	
22	1.68×10^7	4.45×10^2	1.62×10^7 (3.1)	4.29×10^2
27	4.74×10^6	6.92×10^1	9.82×10^6 (3.1)	1.43×10^2
39	2.46×10^6	1.20×10^1	2.00×10^6 (3.3)	9.75×10^0
40	1.88×10^7	8.27×10^1	1.66×10^7 (3.0)	7.30×10^1
Total	1.100×10^8	3.65×10^3	1.088×10^8 (3.1)	3.570×10^3

The term of Iγ means the integrated numbers of emitted gamma-rays during the collecting time

Table 7.8 Comparison of gamma ray intensity (I_γ) and relative dose for C-1 case

group No.	Calculation I_γ	Calculation dose	Experiment I_γ (% error)	Experiment dose
1	4.72×10^4	6.3	4.08×10^4 (27)	5.4
2	1.63×10^5	2.22×10^1	1.27×10^5 (17.7)	1.73×10^1
4	1.42×10^6	1.637×10^2	1.129×10^6 (4.4)	1.302×10^2
6	4.58×10^4	4.7	5.43×10^4 (25)	5.6
7	2.70×10^6	2.630×10^2	2.201×10^6 (3.7)	2.139×10^2
8	2.25×10^4	2.1	4.07×10^4 (29)	3.7
11	3.60×10^4	2.8	———	———
12	2.43×10^5	1.73×10^1	3.99×10^5 (6.9)	2.84×10^1
13	1.76×10^4	1.2	———	———
14	8.55×10^3	0.5	———	———
16	2.10×10^4	1.0	9.58×10^4 (22)	4.8
17	1.025×10^7	4.589×10^2	8.261×10^6 (3.2)	3.698×10^2
18	3.33×10^5	1.34×10^1	2.28×10^5 (14.6)	9.1
19	2.65×10^4	1.0	1.30×10^5 (16.3)	4.7
22	3.74×10^5	9.9	8.10×10^5 (4.2)	2.14×10^1
27	5.13×10^4	0.7	1.02×10^5 (13.0)	1.5
34	1.15×10^5	0.9	9.83×10^4 (11.9)	0.7
38	2.38×10^6	1.28×10^1	1.011×10^6 (3.4)	5.4
39	1.12×10^4	0.1	7.00×10^3 (23)	———
40	1.26×10^5	0.6	1.39×10^5 (7.8)	0.6
Total	1.839×10^7	9.831×10^2	1.487×10^7 (3.4)	8.225×10^2

The term of I_γ means the integrated numbers of emitted gamma-rays during the collecting time

Table 7.9 Comparison of gamma ray intensity(Iγ) and ralative dose for C-2 case

group No.	Calculation Iγ	Calculation dose	Experiment Iγ (% error)	Experiment dose
6	2.49×10^{4}	2.5	———	———
9	1.12×10^{5}	9.7	1.18×10^{5} (26)	1.02×10^{1}
12	1.94×10^{5}	1.38×10^{1}	5.01×10^{5} (10.1)	3.57×10^{1}
13	1.96×10^{5}	1.29×10^{1}	2.27×10^{5} (19.6)	1.50×10^{1}
14	6.28×10^{4}	3.8	4.30×10^{5} (12.7)	2.61×10^{1}
15	2.53×10^{5}	1.40×10^{1}	2.43×10^{5} (19.8)	1.34×10^{1}
16	1.69×10^{5}	8.4	4.34×10^{5} (11.1)	2.17×10^{1}
17	2.336×10^{7}	1.046×10^{3}	1.999×10^{7} (3.2)	8.95×10^{2}
18	1.29×10^{6}	5.17×10^{1}	8.79×10^{5} (11.6)	3.53×10^{1}
22	$6.344\ 10^{6}$	1.68×10^{2}	7.20×10^{6} (3.1)	1.91×10^{2}
27	1.95×10^{6}	2.85×10^{1}	3.53×10^{6} (3.2)	5.15×10^{1}
34	4.54×10^{5}	3.4	2.42×10^{5} (12.8)	1.8
38	9.53×10^{6}	5.11×10^{1}	4.88×10^{6} (3.2)	2.62×10^{1}
39	5.47×10^{5}	2.7	3.49×10^{5} (3.4)	1.7
40	4.212×10^{6}	1.85×10^{1}	3.05×10^{6} (3.2)	1.34×10^{1}
Total	4.870×10^{7}	1.435×10^{3}	4.207×10^{7} (3.2)	1.338×10^{3}

The term of Iγ means the integrated numbers of emitted gamma-rays during the collecting time

Table 7.10 Comparison of gamma ray intensity(Iγ) and ralative dose for C-3 case

group No.	Calculation Iγ	Calculation dose	Experiment Iγ (% error)	Experiment dose
9	1.09×10^{5}	9.5	———	———
12	7.53×10^{4}	5.4	5.03×10^{5} (10.6)	3.58×10^{1}
13	1.69×10^{5}	1.11×10^{1}	1.24×10^{5} (22.0)	8.2
14	7.53×10^{4}	4.6	4.83×10^{5} (12.3)	2.93×10^{1}
15	2.19×10^{5}	1.21×10^{1}	1.58×10^{5} (31)	8.7
16	2.00×10^{4}	1.0	1.75×10^{5} (26)	8.7
17	2.337×10^{7}	1.046×10^{3}	2.208×10^{7} (3.1)	9.08×10^{2}
22	6.07×10^{6}	1.61×10^{2}	$7.487\ 10^{6}$ (3.1)	1.98×10^{2}
27	1.38×10^{6}	2.01×10^{1}	2.53×10^{6} (3.9)	3.69×10^{1}
38	5.82×10^{4}	0.3	4.30×10^{4} (5.4)	0.2
39	6.26×10^{5}	3.1	4.35×10^{5} (7.7)	2.1
40	4.80×10^{6}	2.11×10^{1}	3.54×10^{6} (3.2)	1.56×10^{1}
Total	3.697×10^{6}	1.295×10^{3}	3.576×10^{7} (3.1)	1.251×10^{3}

The term of Iγ means the integrated numbers of emitted gamma-raya during teh collecting time

Table 8 C/E of gamma-ray intensity for individual group

g No.	ID. name (cooling time) / main nuclei(Eγ in keV)	A-1 10 min	A-2 1 hr	A-3 6.93 hr	A-4 30 day	B-1 13.8 h	B-2 13.6 d	B-3 36 d	C-1 10.5 hr	C-2 8 day	C-3 29 d
1	^{56}Mn(3369.6, 2959.8)	0.76 ± 0.12	0.87 ± 0.09	0.75±0.06		0.75±0.20			1.16±0.31		
2	^{56}Mn(2658, 2523)	0.86 ± 0.08	0.86 ± 0.05	0.86±0.04		0.79±0.10			1.28±0.23		
4	^{56}Mn(2113)	0.98 ± 0.03	0.97 ± 0.03	0.92±0.03		0.91±0.06			1.26±0.06		
6	^{57}Ni(1919)	0.71 ± 0.18	0.93 ± 0.15	0.76±0.04		0.68±0.10			0.84±0.21		
7	^{56}Mn(1810)	0.99 ± 0.03	0.98 ± 0.03	0.94±0.03		0.95±0.05			1.23±0.05		
8	^{57}Ni(1758)		0.57 0.09	0.86±0.11		0.56±0.10			0.55±0.16		
9	^{58}Co(1674)				0.99±0.19		1.64±0.54	1.00±0.11		0.95±0.25	
11	^{52}V(1434)	1.28 ± 0.07									
12	^{57}Ni(1377) ^{60}Co(1332)	0.60 ± 0.05	0.56 ± 0.03	0.69±0.02	0.93±0.18	0.53±0.03	0.57±0.19	0.60±0.05	0.61±0.04	0.39±0.04	0.15±0.02
13	^{59}Fe(1291)	1.33 ± 0.26	0.59 ± 1.0	0.71±0.09	0.61±0.15		0.57±0.18	0.37±0.04		0.86±0.17	1.36±0.30
14	^{60}Co(1173)	1.04 ± 0.17			0.94±0.20		0.86±0.32	0.49±0.04		0.15±0.02	0.16±0.02
15	^{59}Fe(1099)			0.84±0.05	0.45±0.11		0.87±0.29	0.51±0.05		1.04±0.21	1.39±0.43
16	^{92}Nb + ^{89}Zr (935, 910)			0.90±0.14	0.45±0.06	1.60±0.4	0.61±0.11	0.24±0.02	0.22±0.05	0.39±0.04	0.11±0.03
17	^{56}Mn(847) ^{54}Mn(835) ^{58}Co(810)	0.99 ± 0.03	0.97 ± 0.03	0.95±0.03	1.09±0.03	0.94±0.03	1.19±0.04	1.06±0.03	1.24±0.04	1.17±0.04	1.15±0.04
18	^{99}Mo(778, 739) ^{95}Nb(765)		0.92 ± 0.11	1.13±0.15	1.15±0.26	0.97±0.10	1.54±0.42	0.90±0.08	1.46±0.21	1.47±0.17	
19		0.52 ± 0.08							0.20±0.03		
20			1.12 ± 0.23								
22	AN(511)	0.31 ± 0.01	0.21 ± 0.01	0.57±0.02	0.96±0.03	0.64±0.03	1.17±0.05	1.04±0.03	0.46±0.02	0.88±0.03	0.81±0.03
25		1.60 ± 0.19									
27	^{51}Cr(320)	2.76 ± 0.41	0.96 ± 0.11	0.68±0.03	0.66±0.02	0.45±0.02	0.55±0.02	0.48±0.01	0.50±0.07	0.55±0.02	0.55±0.02
34	^{99}Mo(181)			0.90±0.11		0.87±0.06	1.86±0.89		1.17±0.14	1.88±0.24	
37	^{49}Cr(153)	0.105±0.008	0.0043±0.004								
38	^{99}Mo(141)	3.89 ± 0.54	3.99 ± 0.34	1.94±0.06		1.61±0.06	2.02±0.08		2.35±0.08	1.95±0.06	1.35±0.07
39	^{57}Co(136)		0.37 ± 0.05	1.90±0.38	1.55±0.06	1.01±0.22	1.41±0.08	1.23±0.04	1.6 ±0.37	1.57±0.53	1.44±0.11
40	^{57}Co(122) ^{57}Ni(127)	0.89 ± 0.12	0,95 ± 0.08	0,92±0.03	1.38±0.04	0.78±0.04	1.32±0.05	1.13±0.03	0.91±0.07	1.38±0.04	1.35±0.04
43	^{49}Cr(91)	0.117±0.009	0.031±0.002								

Table 9 C/E of total gamma-ray intensity and relative dose

measurement case	cooling time	gamma-ray intensity	relative dose
A-1	10 m	0.967 ± 0.031	0.977 ± 0.031
A-2	1 h	0.956 ± 0.030	0.922 ± 0.029
A-3	6.9 h	0.931 ± 0.029	0.928 ± 0.029
A-4	30.1 d	1.076 ± 0.033	1.041 ± 0.032
B-1	13.8 h	0.908 ± 0.036	0.886 ± 0.035
B-2	13.6 d	1.137 ± 0.045	1.145 ± 0.046
B-3	35.7 d	1.011 ± 0.031	1.022 ± 0.032
C-1	10.5 h	1.236 ± 0.042	1.195 ± 0.041
C-2	8.0 d	1.158 ± 0.037	1.072 ± 0.034
C-3	28.8 d	1.034 ± 0.032	1.035 ± 0.032

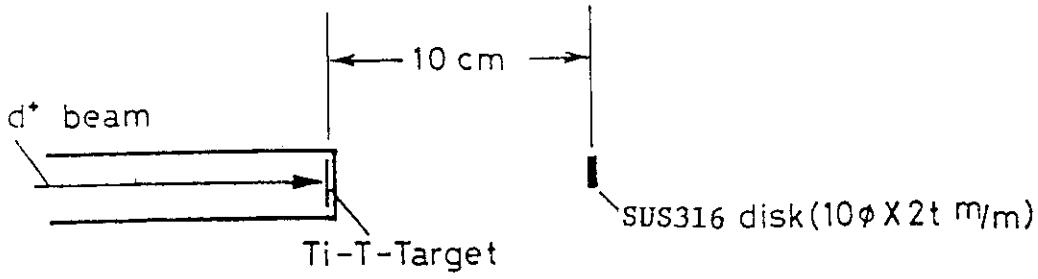

Fig. 1.1 Irradiation arrangement in case of A without any assembly around SUS316 sample

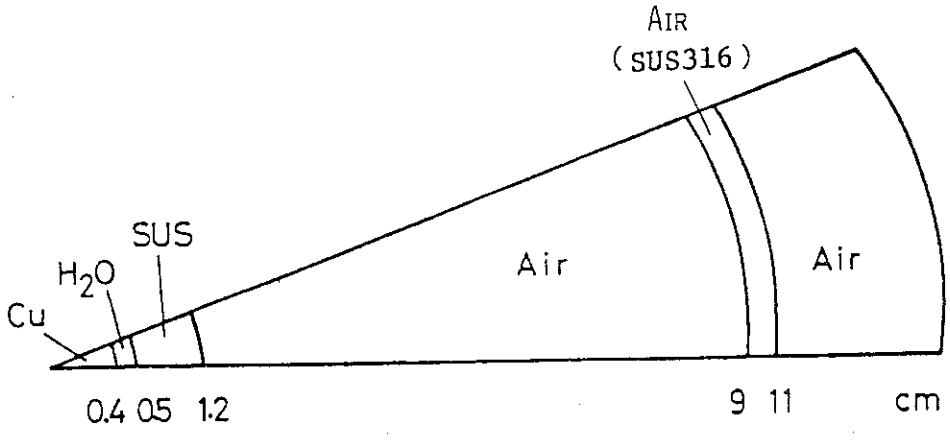

Fig. 1.2 Calculational model of case A by ANISN
The SUS316 is placed at 9-10 cm only in the activation calculation. It is excluded in the neutron transport calculation.

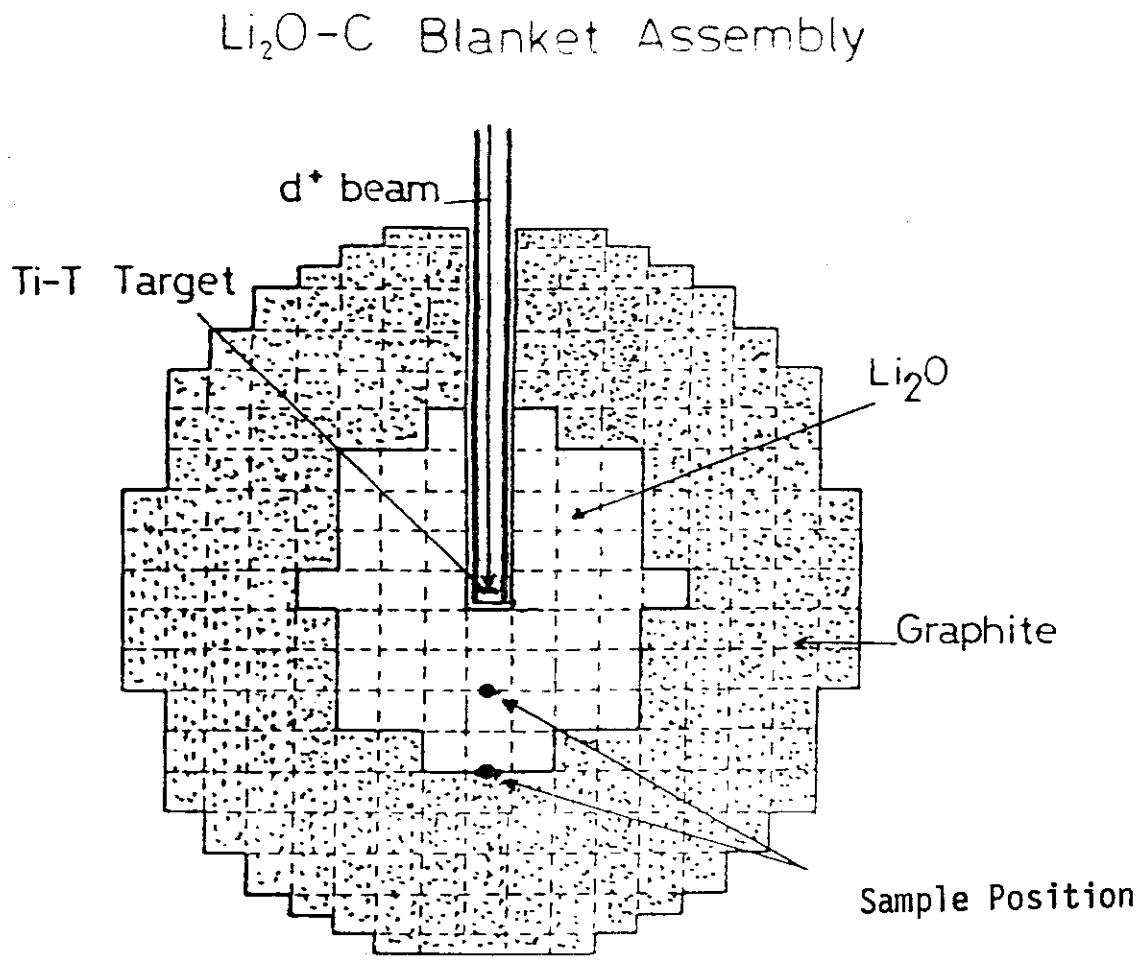

Fig. 2.1 Sectional veiw of Li_2O-C blanket assembly and sample positions

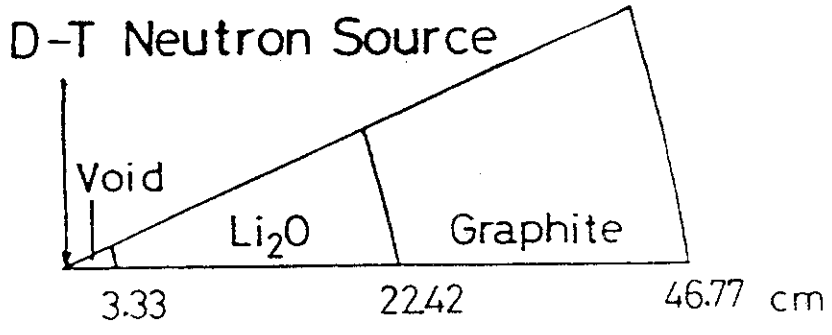

Fig. 2.2 Calculational model of Li_2O-C assembly by ANISN

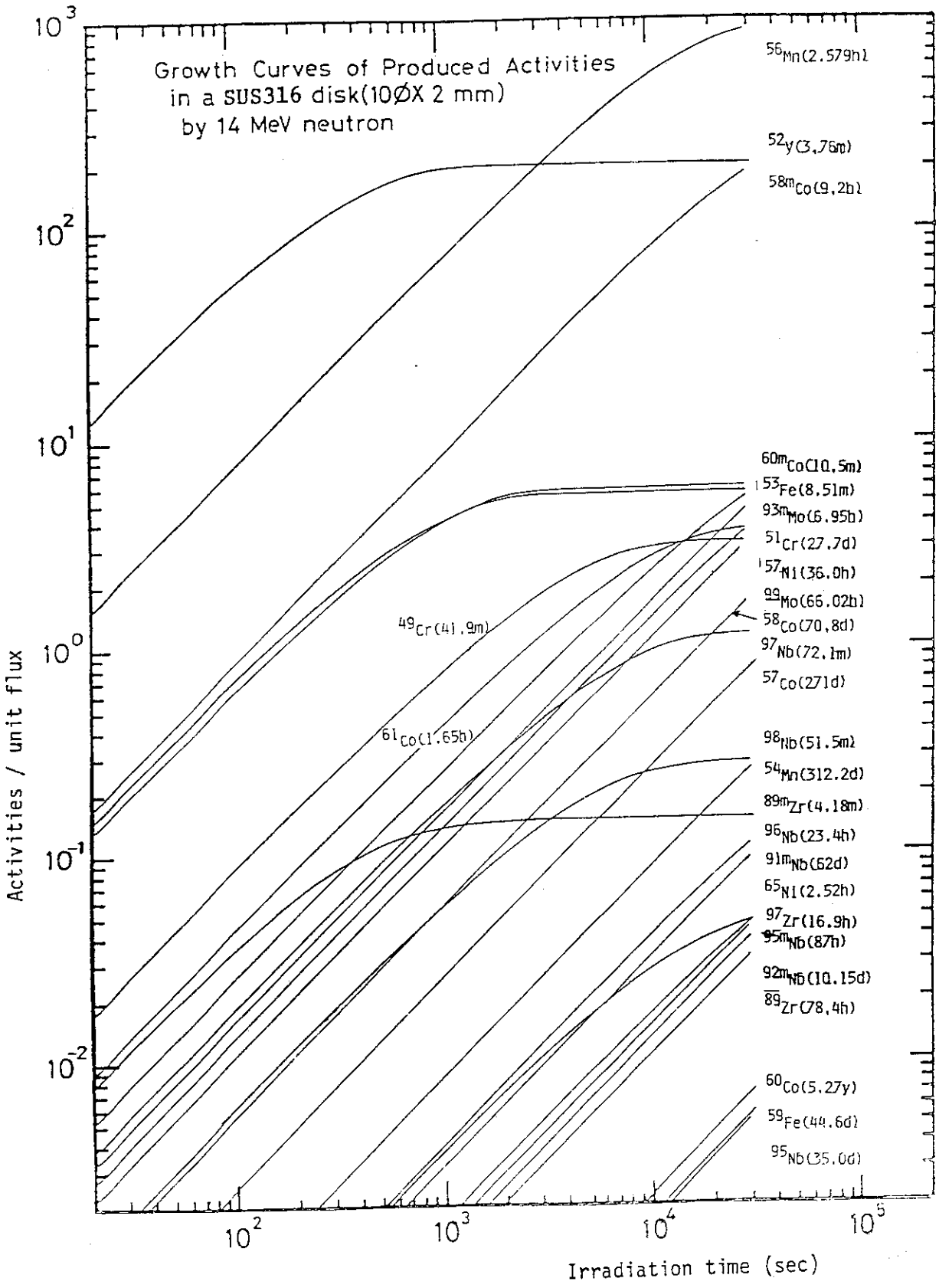

Fig. 3 Growth curves of activities in a SUS316 disk (10 mm in diameter and 2 mm in thickness) produced by 14 MeV neutron irradiation

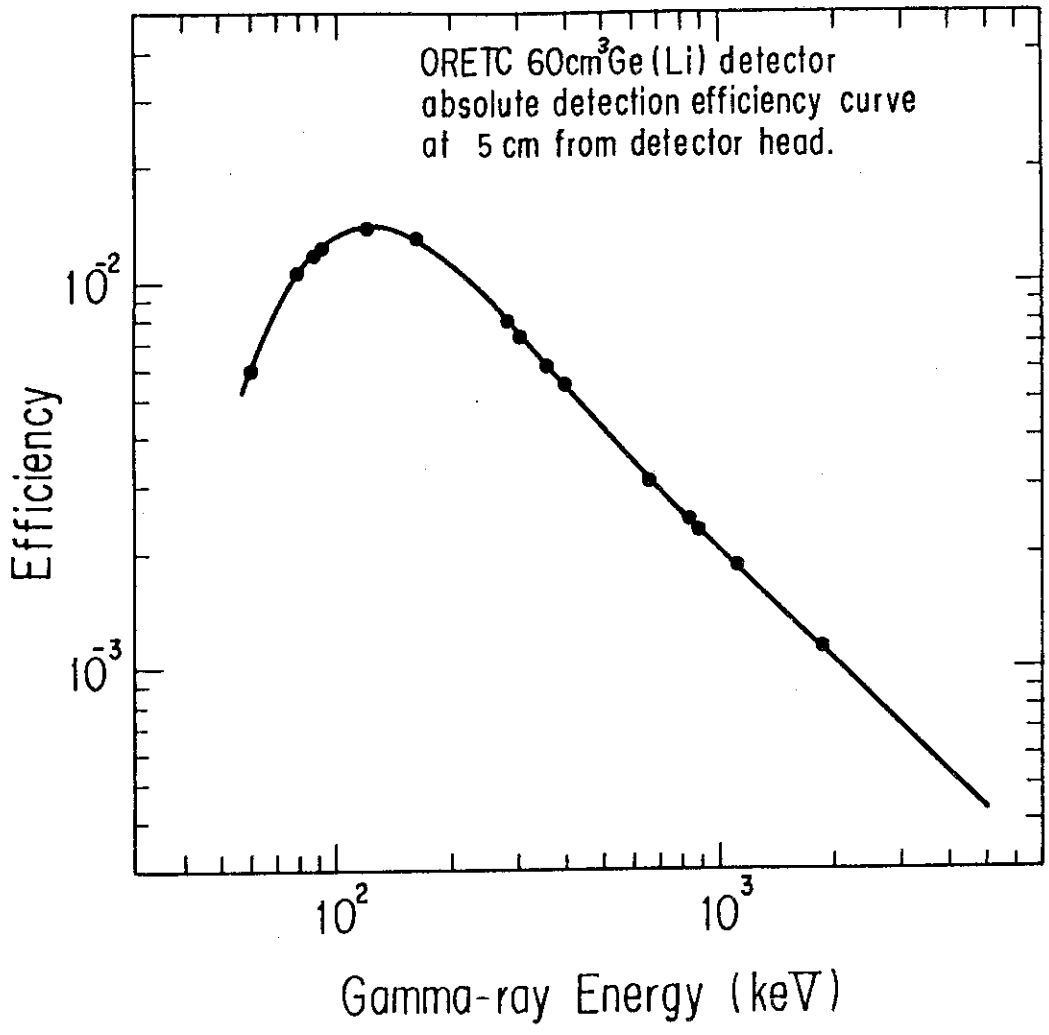

Fig. 4 Absolute Gamma-ray detection efficiency curve of 60 cm^3 Ge(Li) detector at 5 cm from the detector head.

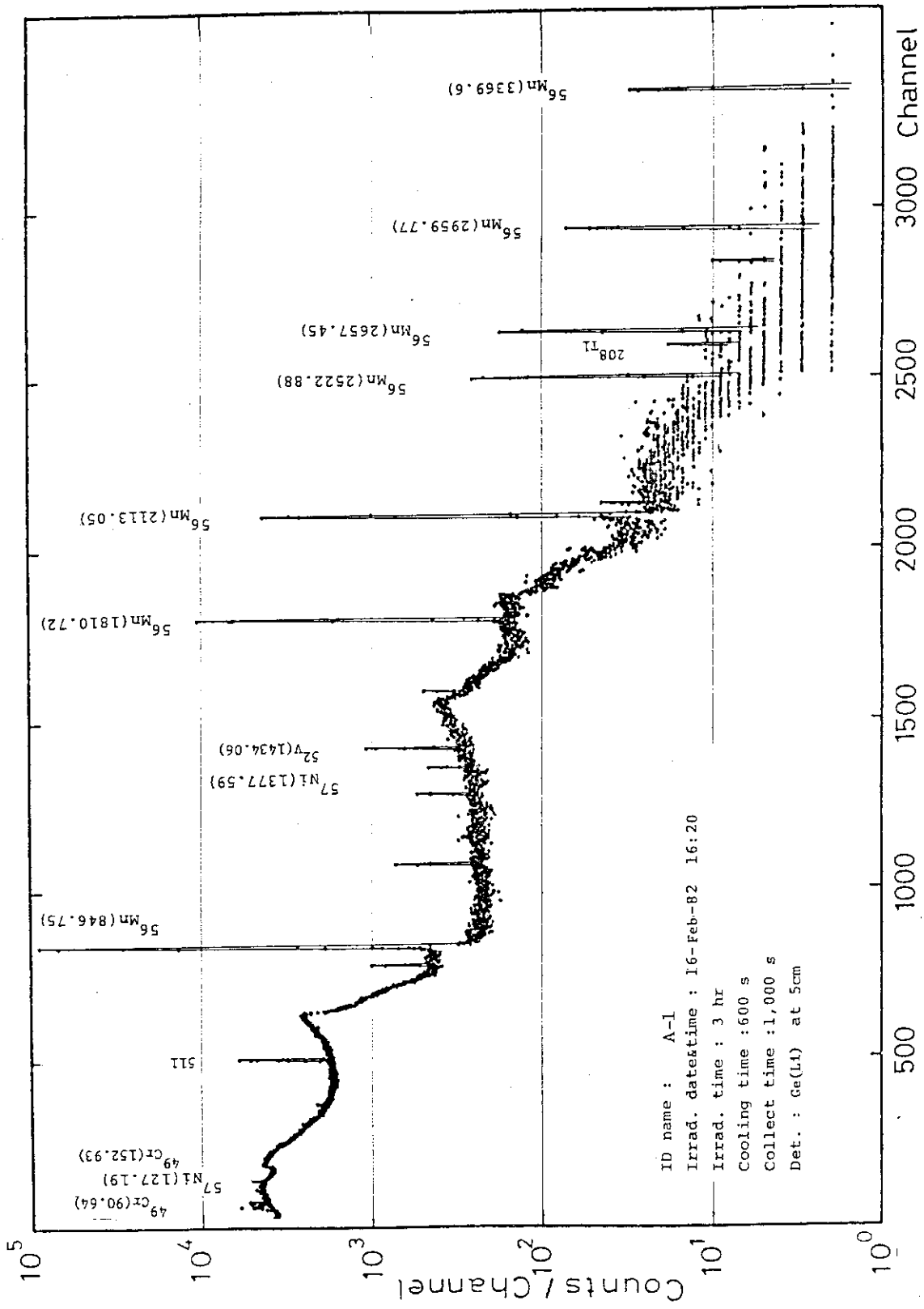

Fig. 5.1 Gamma-ray spectrum in A-1 measurement

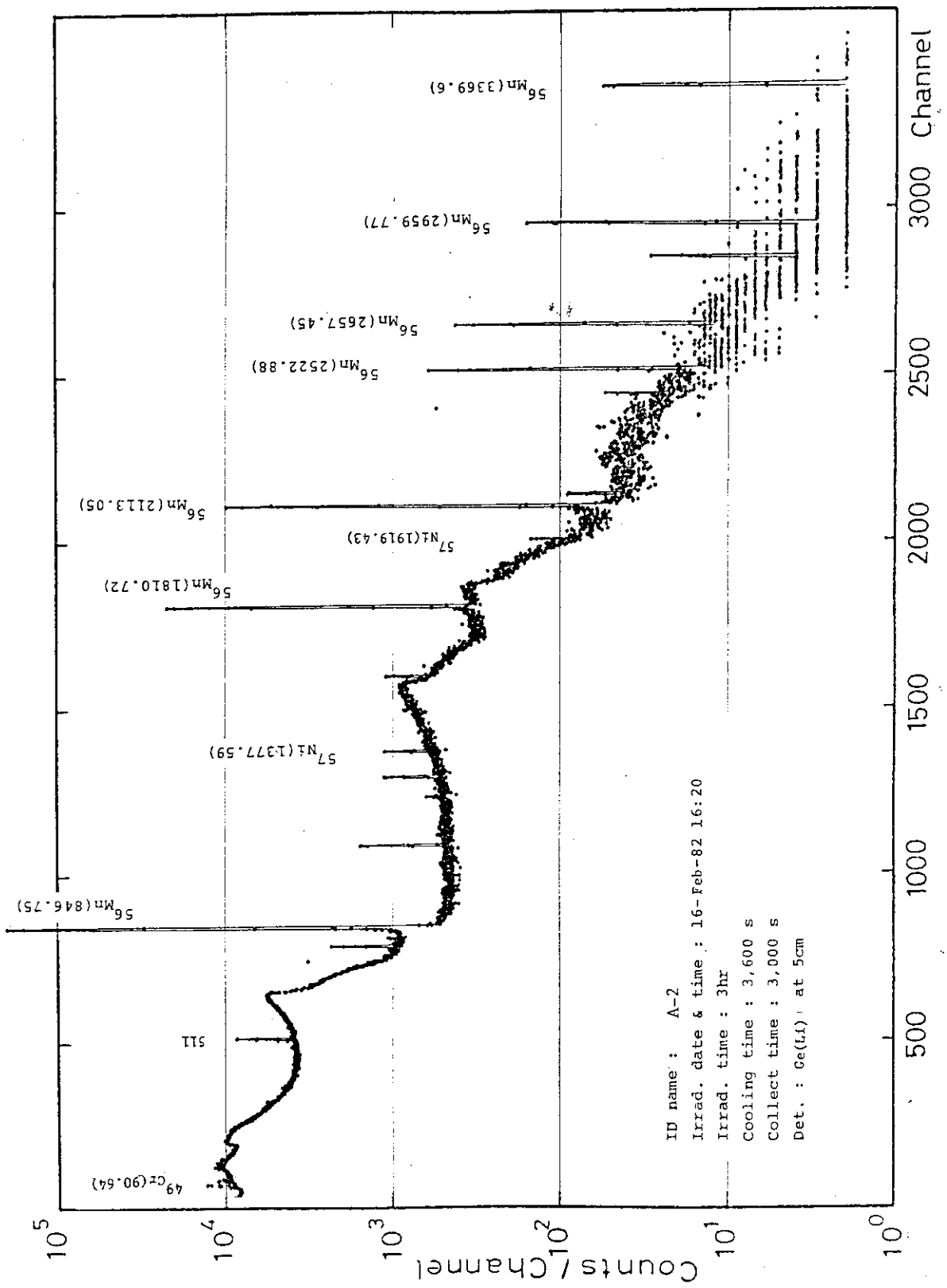

Fig. 5.2 Gamma-ray spectrum in A-2 measurement

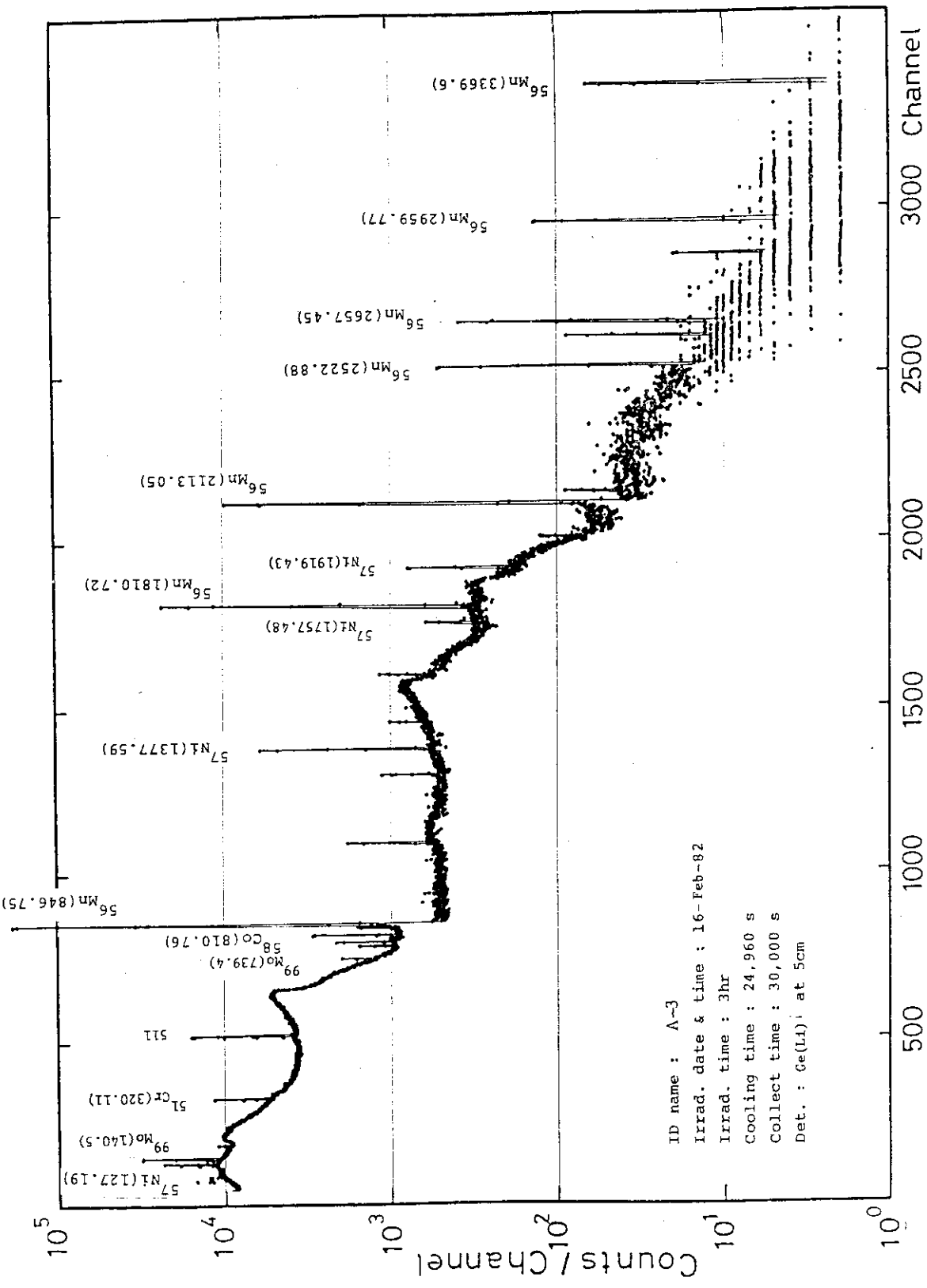

Fig. 5.3 Gamma-ray spectrum in A-3 measurement

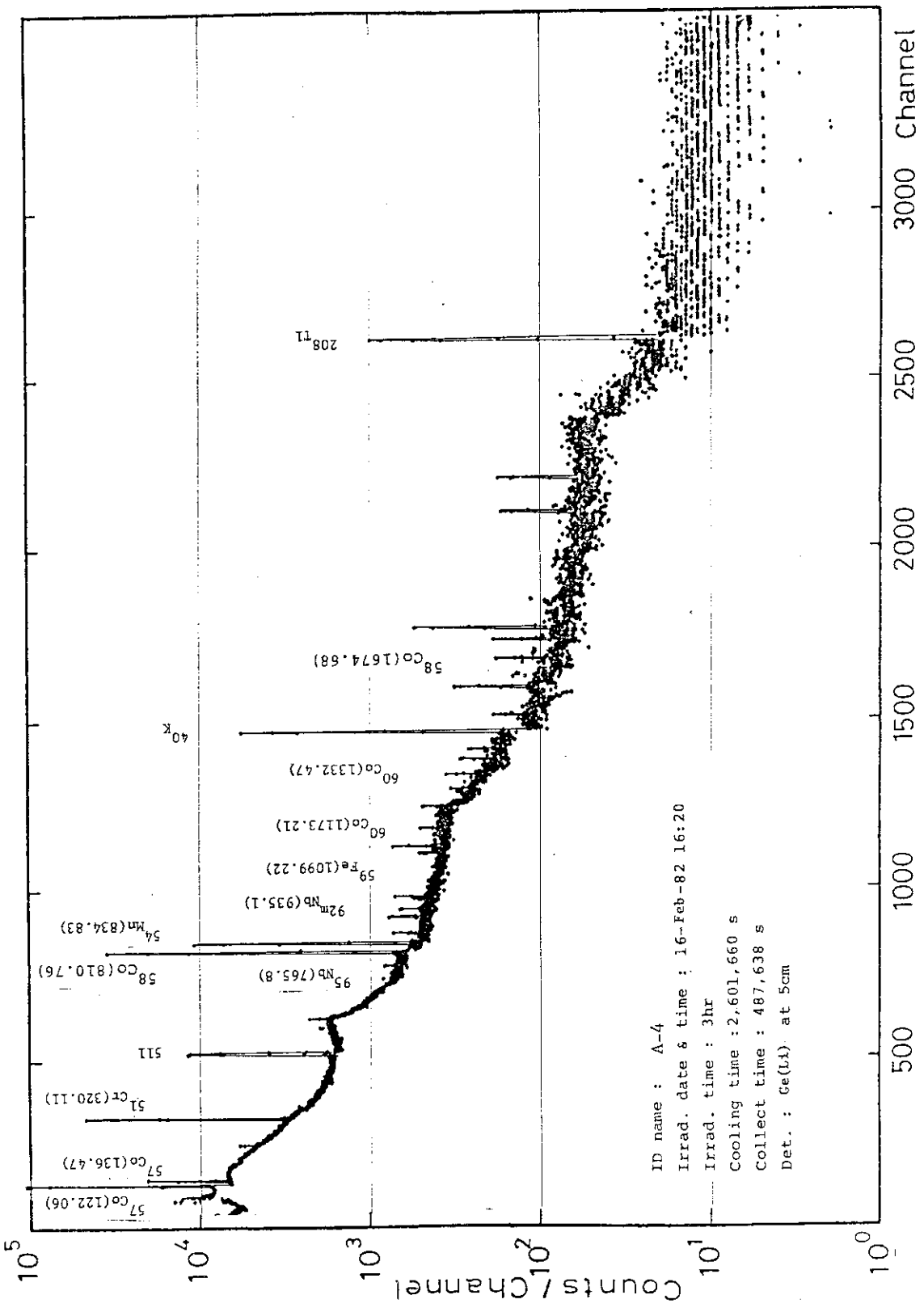

Fig. 5.4 Gamma-ray spectrum in A-4 measurement

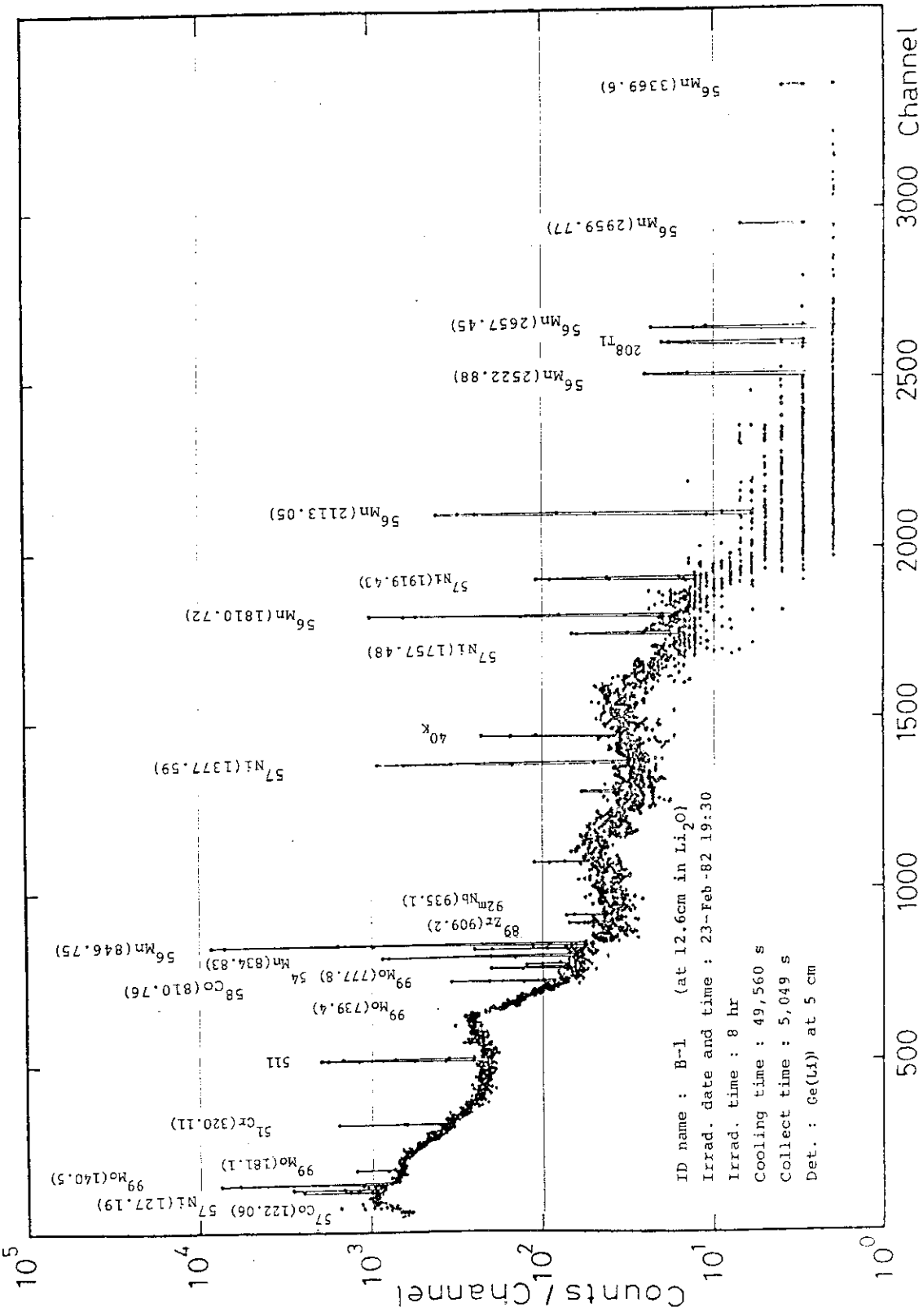

Fig. 5.5 Gamma-ray spectrum in B-1 measurement

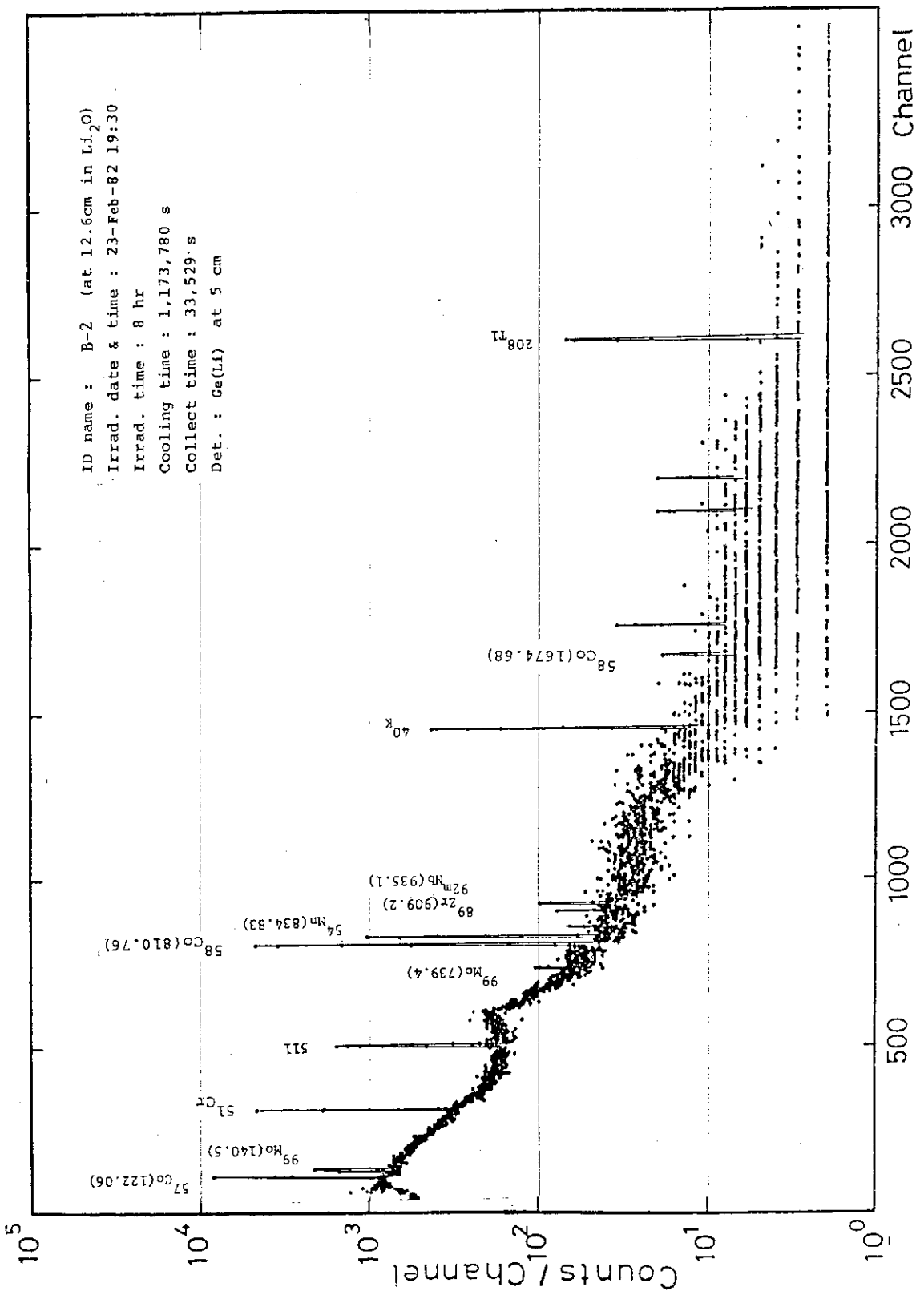

Fig. 5.6 Gamma-ray spectrum in B-2 measurement

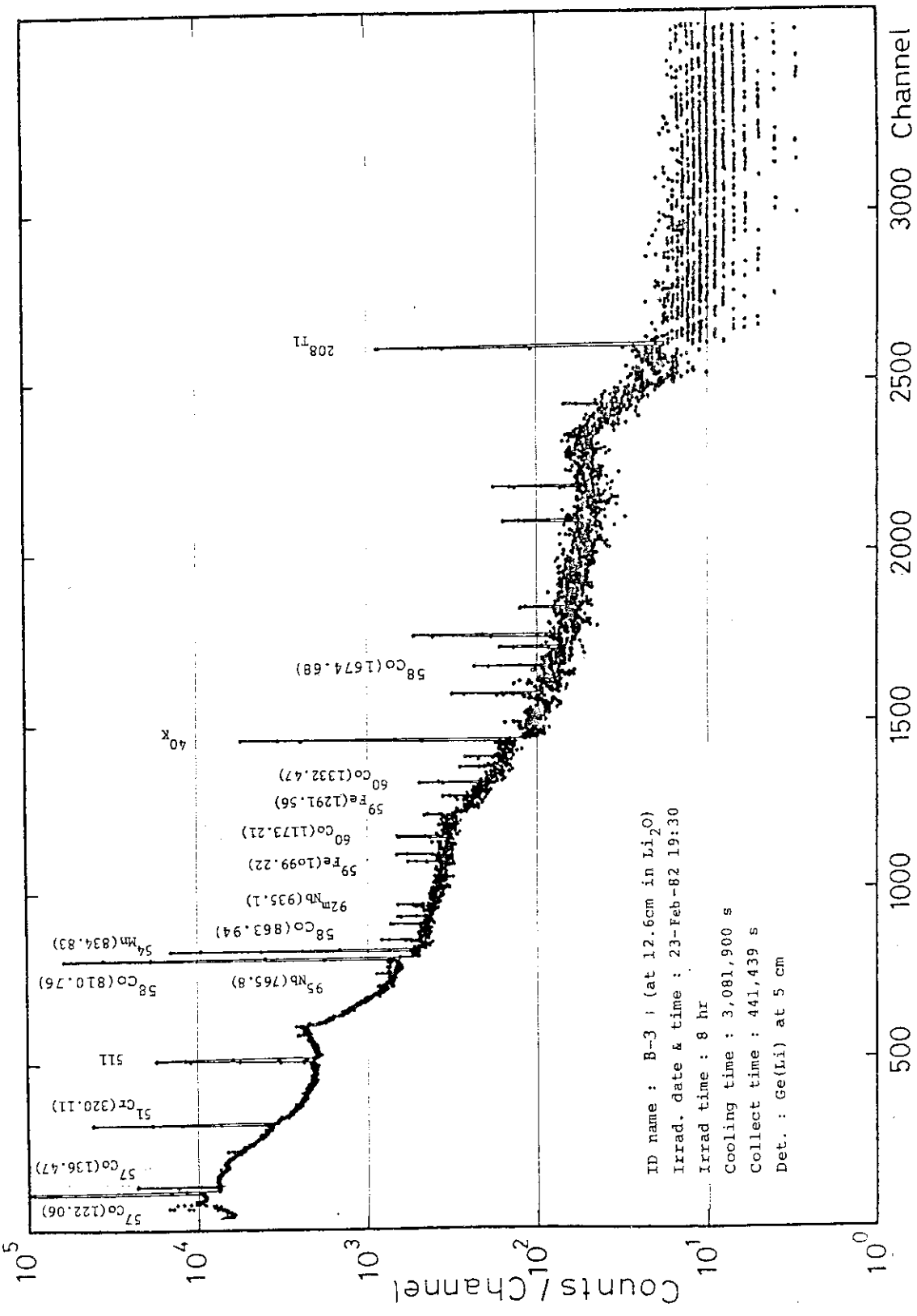

Fig. 5.7 Gamma-ray spectrum in B-3 measurement

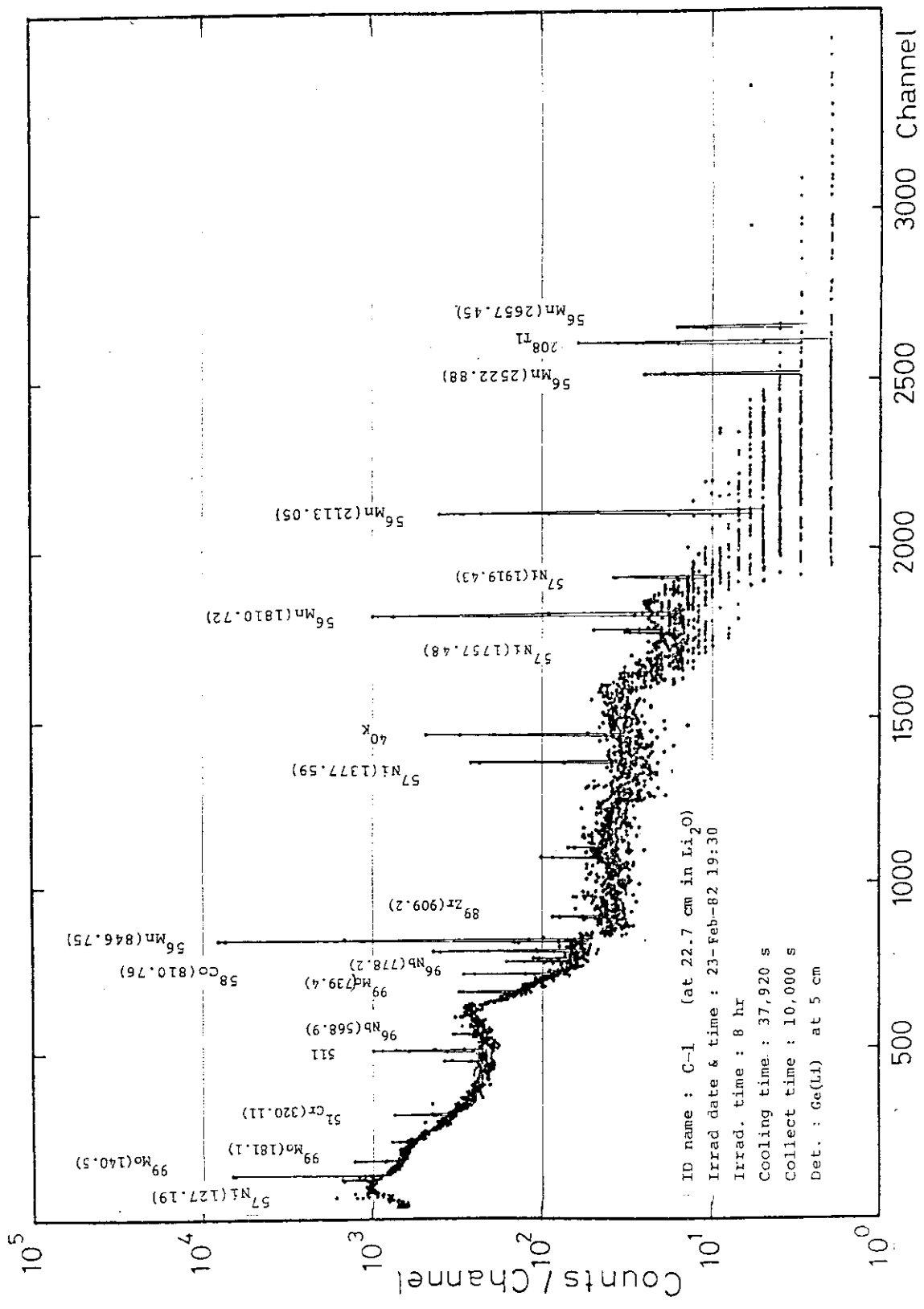

Fig. 5.8 Gamma-ray spectrum in C-1 measurement

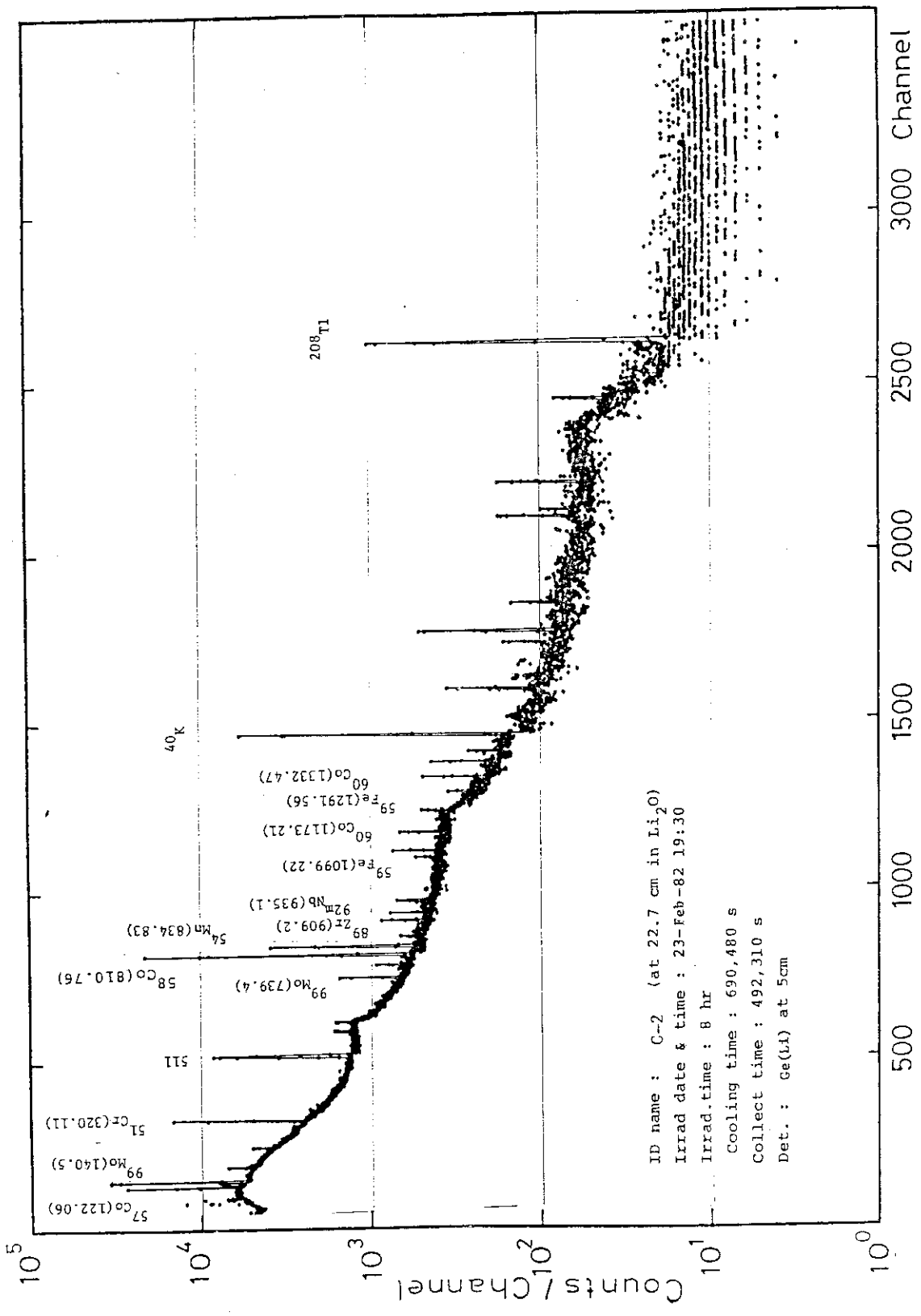

Fig. 5.9 Gamma-ray spectrum in C-2 measurement

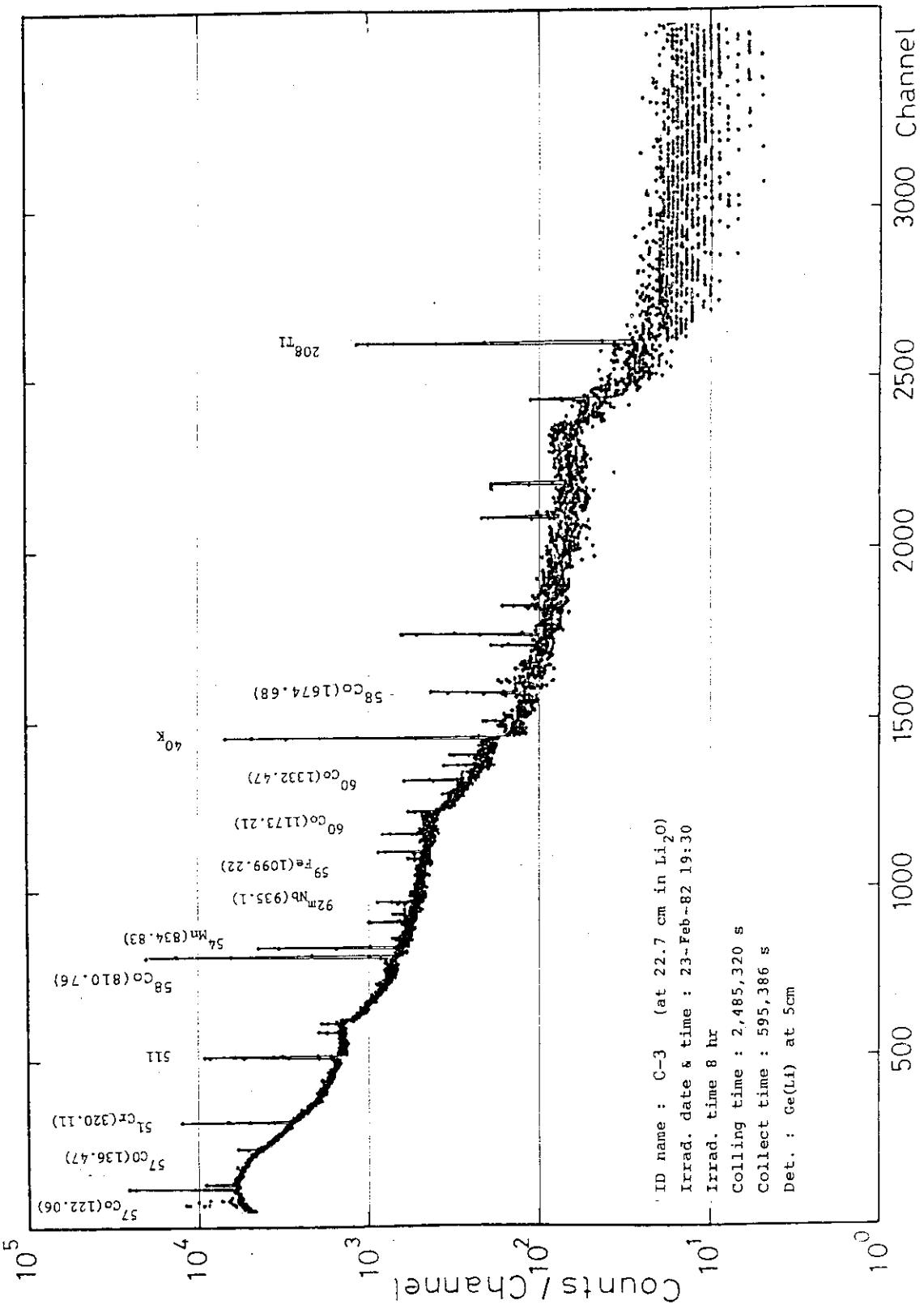

Fig. 5.10 Gamma-ray spectrum in C-3 measurement

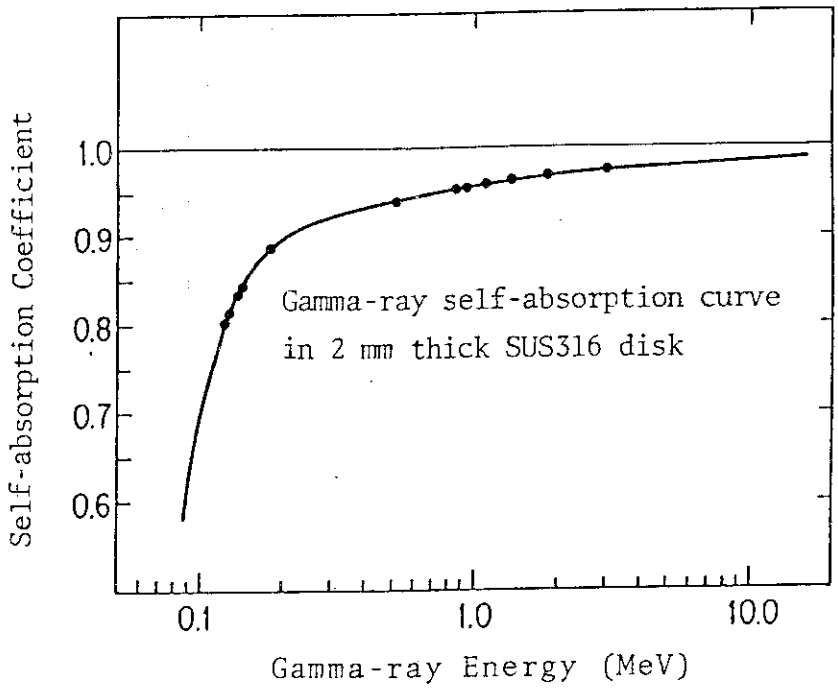

Fig. 6 Gamma-ray self-absorption curve in 2 mm thick SUS316

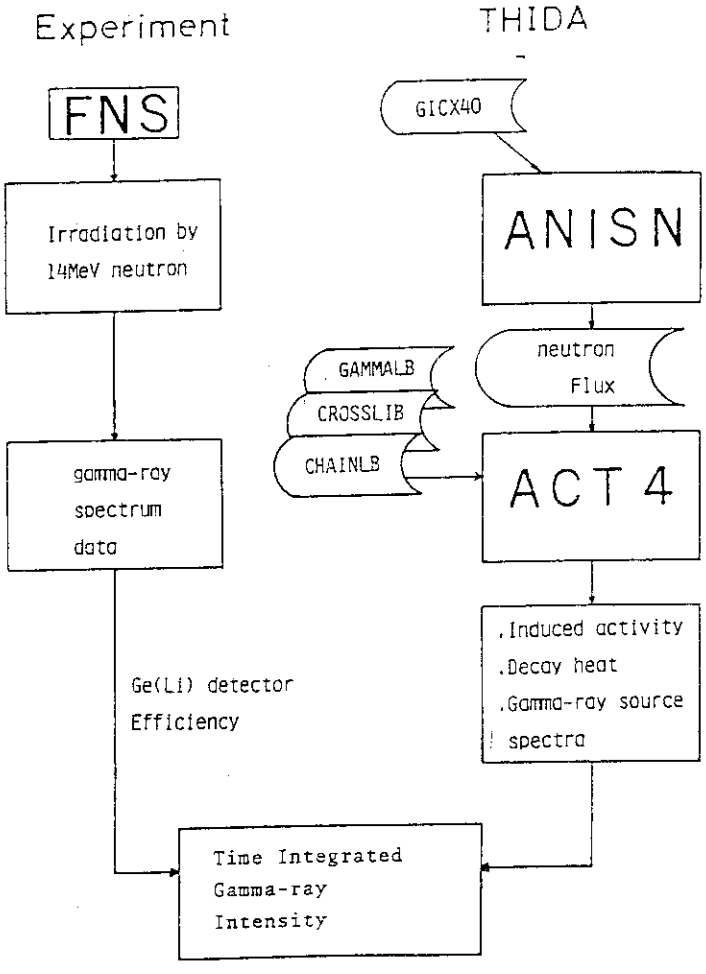

Fig. 7 Flow of Calculation and experiment for comparison

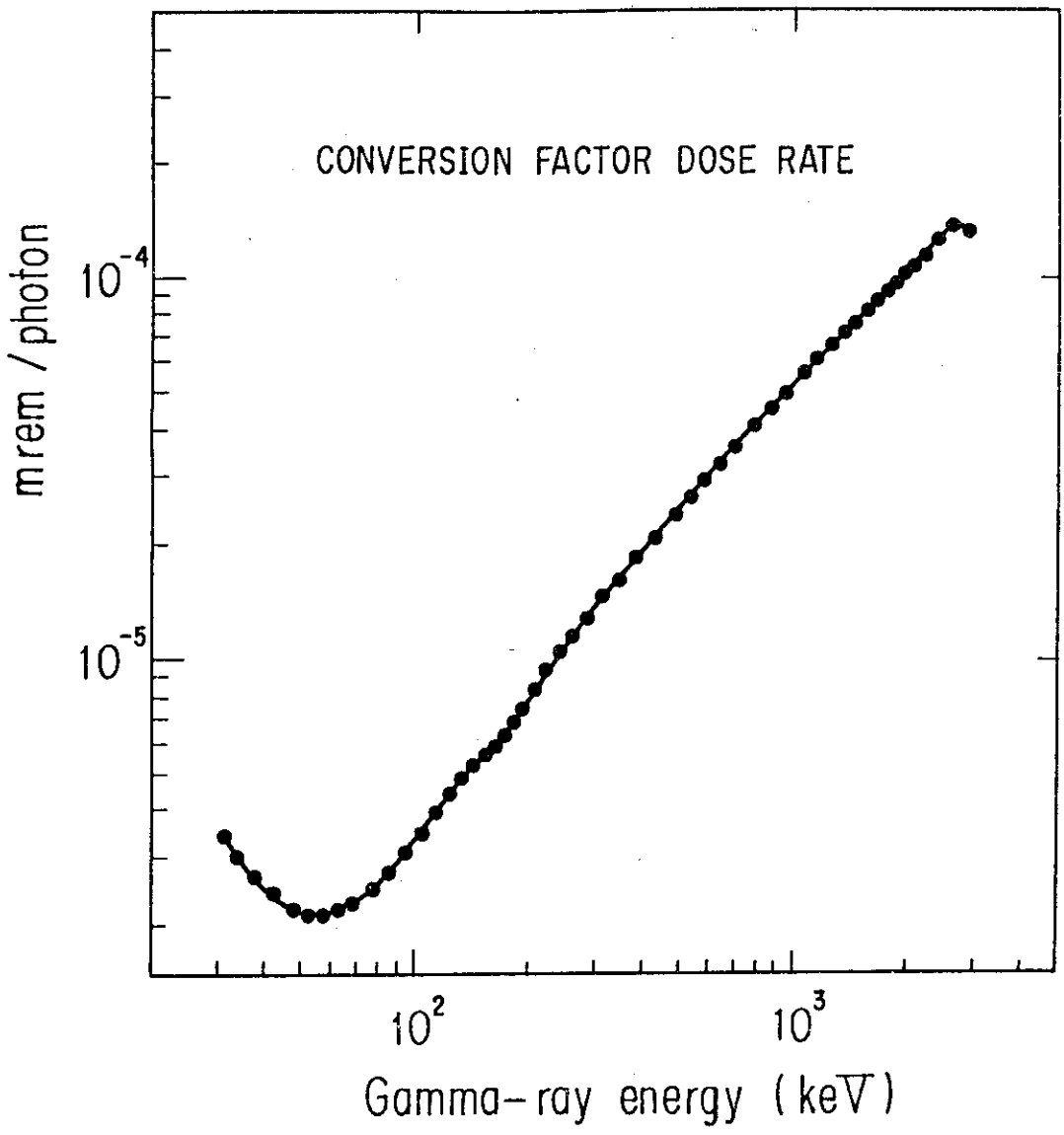

Fig. 8 Conversion factor of photon to dose rate

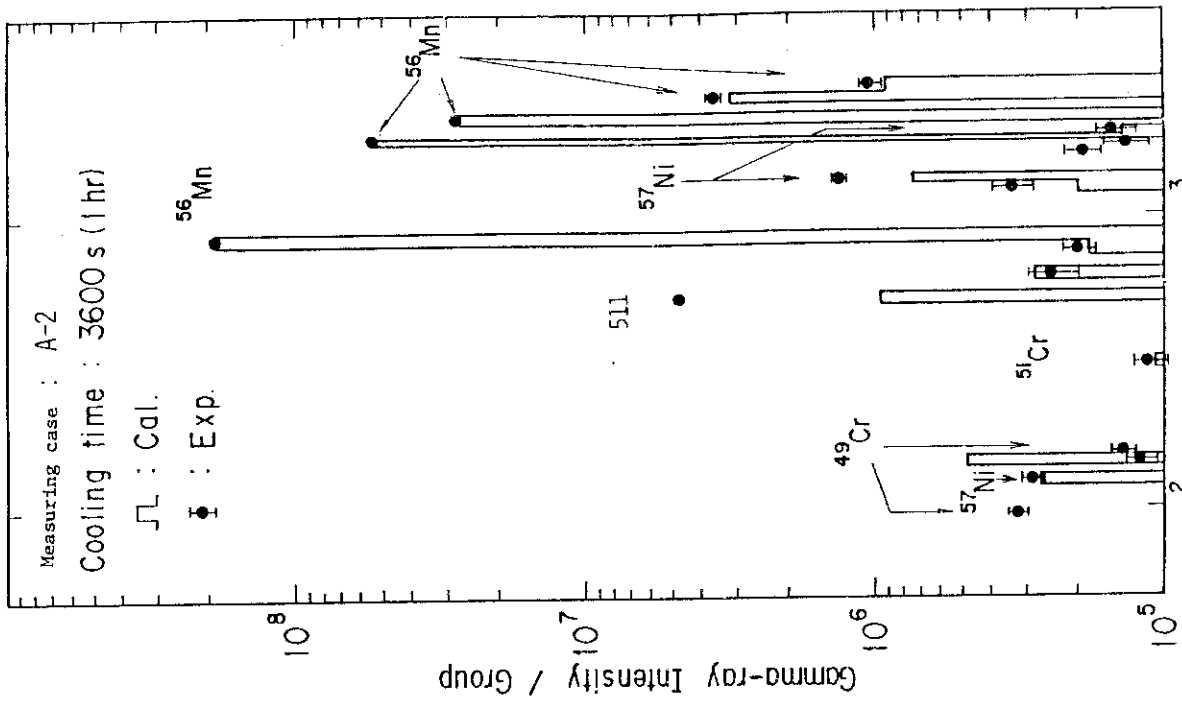

Fig. 9.2 Comparison of gamma-ray spectrum of A-2 case between calcula-tion and measurement

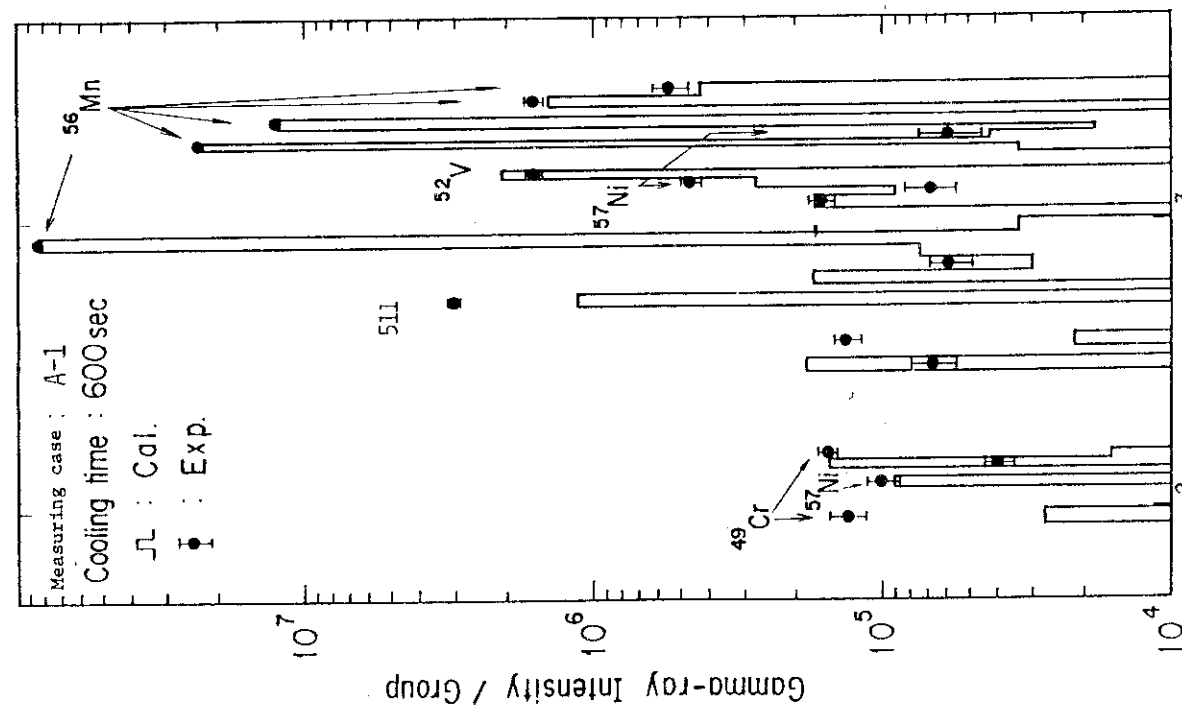

Fig. 9.1 Comparison of gamma-ray spectrum of A-1 case between calcula-tion and measurement

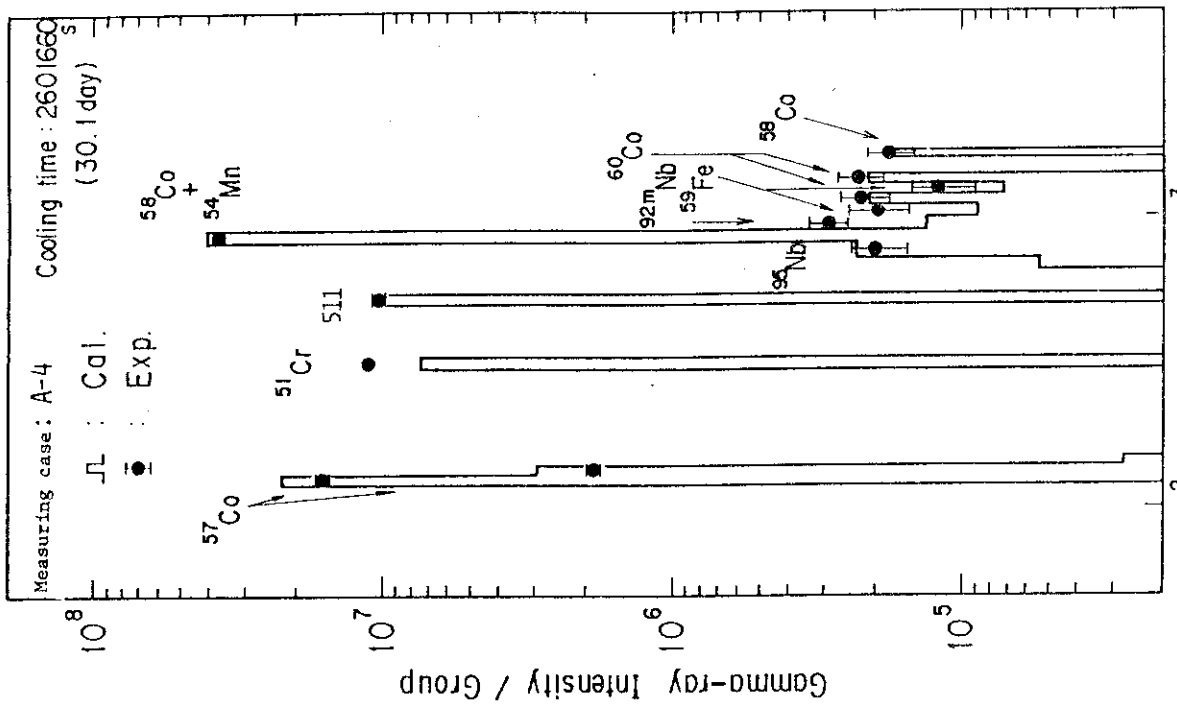

Fig. 9.4 Comparison of Gamma-ray spectrum of A-4 case between calcula-tion and measurement

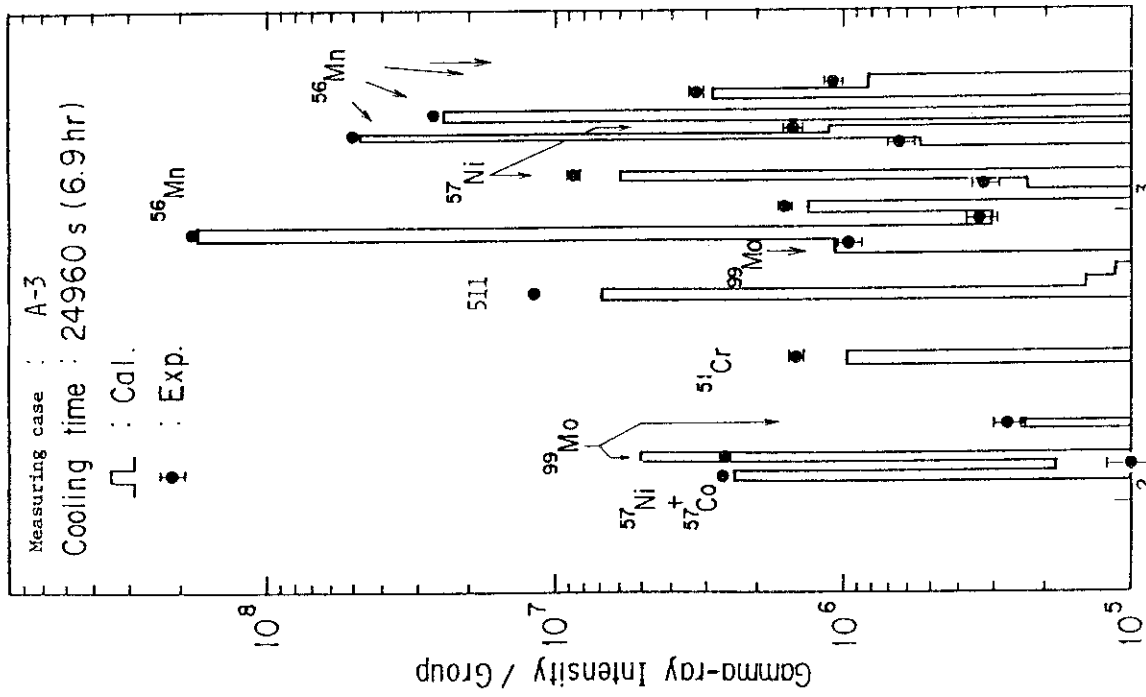

Fig. 9.3 Comparison of Gamma-ray spectrum of A-3 case between calcula-tion and measurement

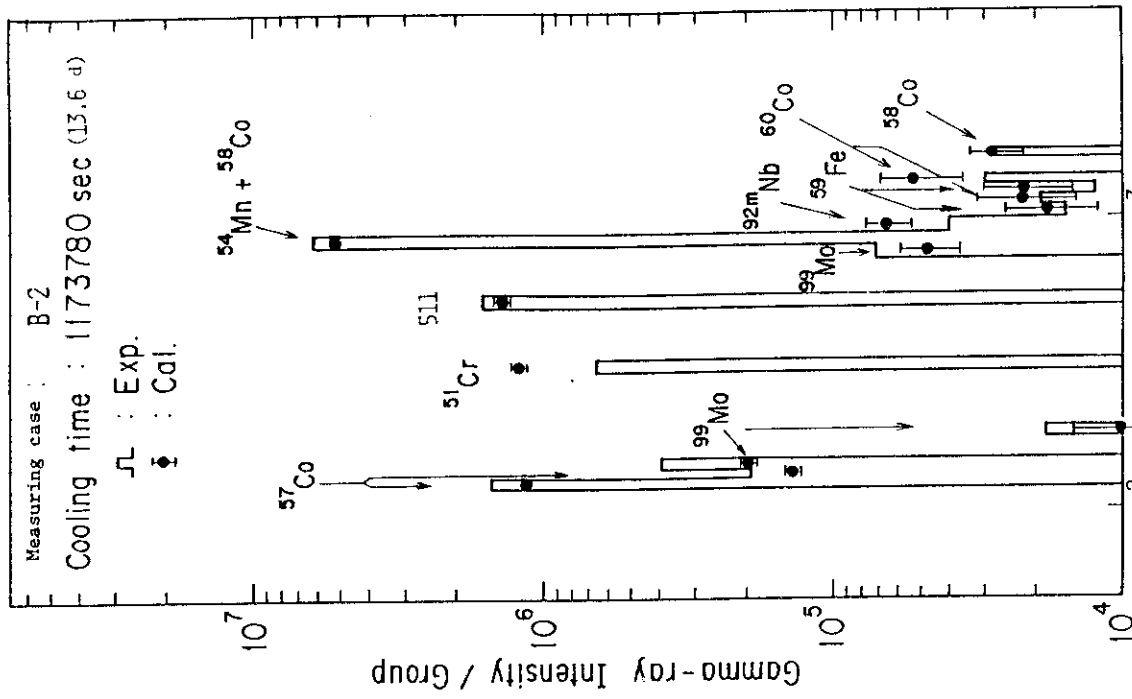

Fig. 9.6 Comparison of Gamma-ray spectrum of B-2 case between calcula-tion and measurement

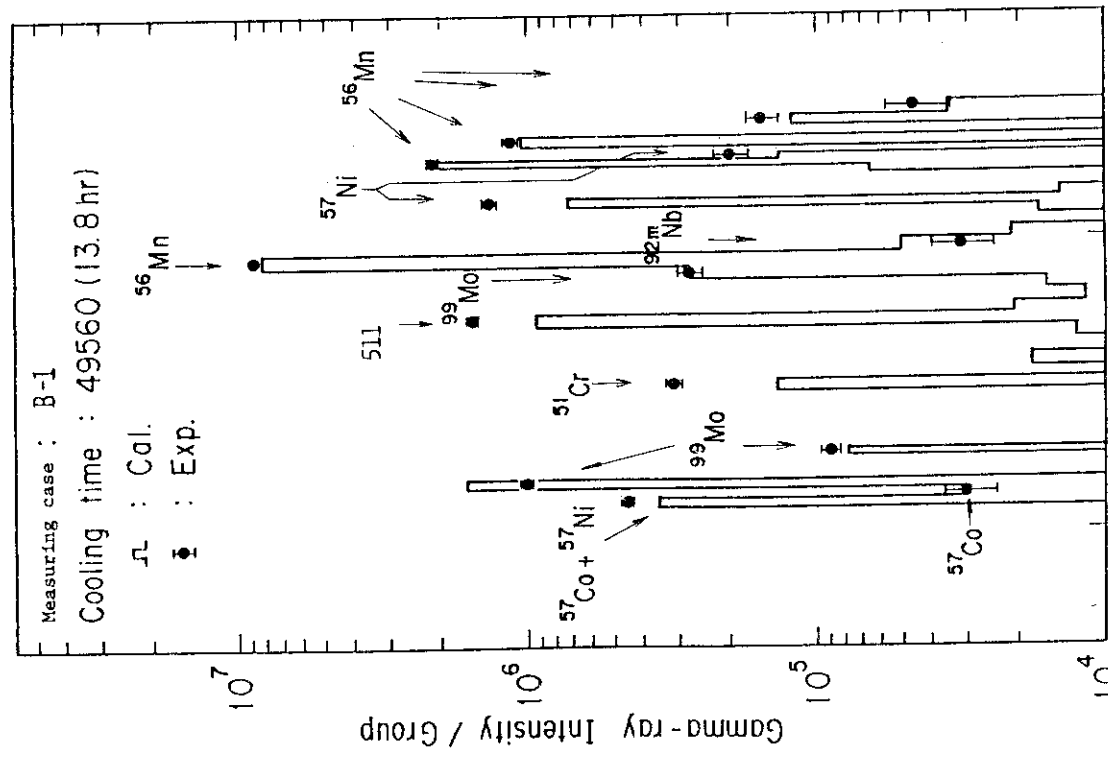

Fig. 9.5 Comparison of Gamma-ray spectrum of B-1 case between calcula-tion and measurement

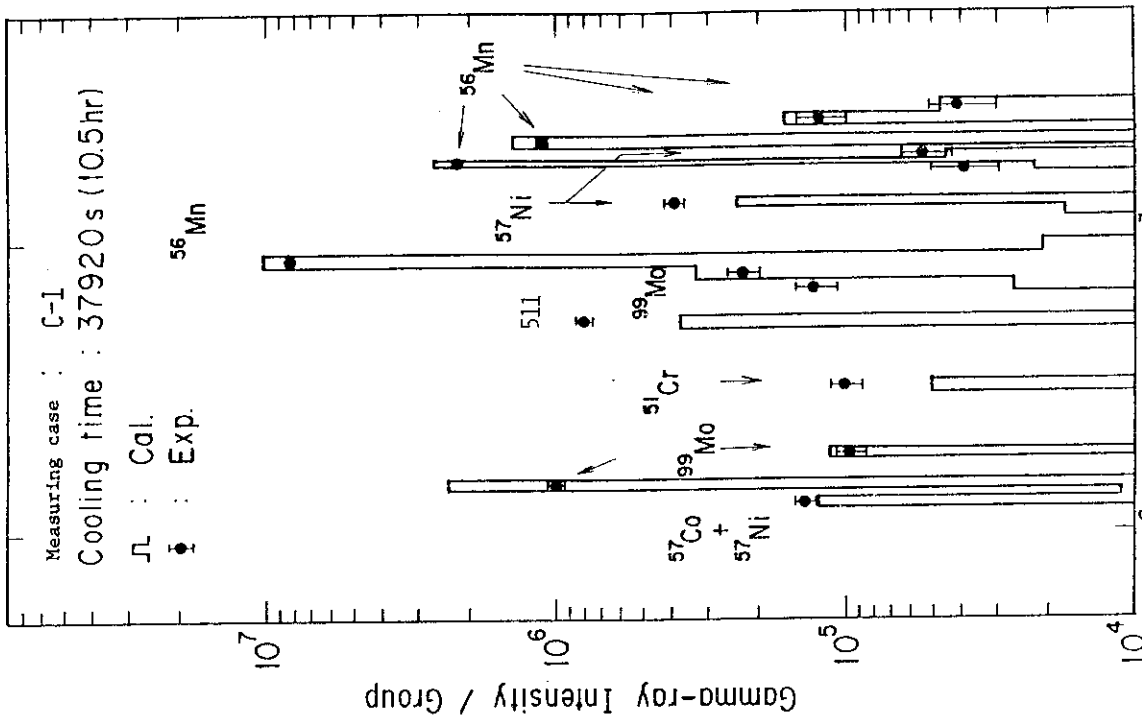

Fig. 9.8 Comparison of Gamma-ray spectrum of C-1 case between calcula-tion and measurement

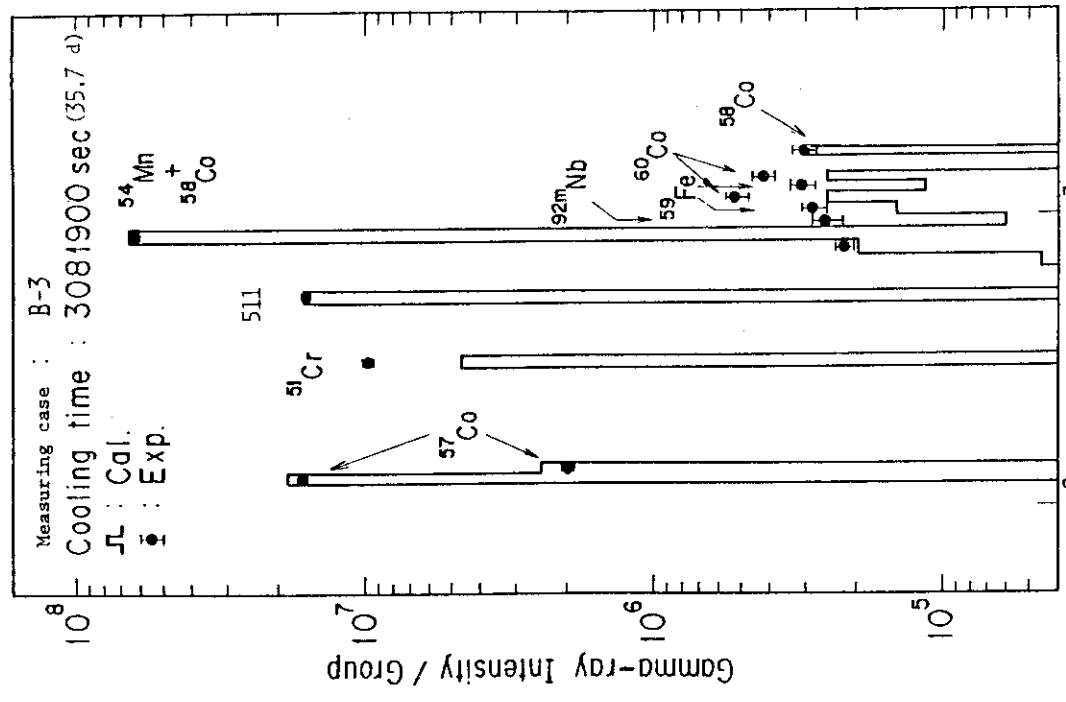

Fig. 9.7 Comparison of Gamma-ray spectrum of B-3 case between calcula-tion and measurement

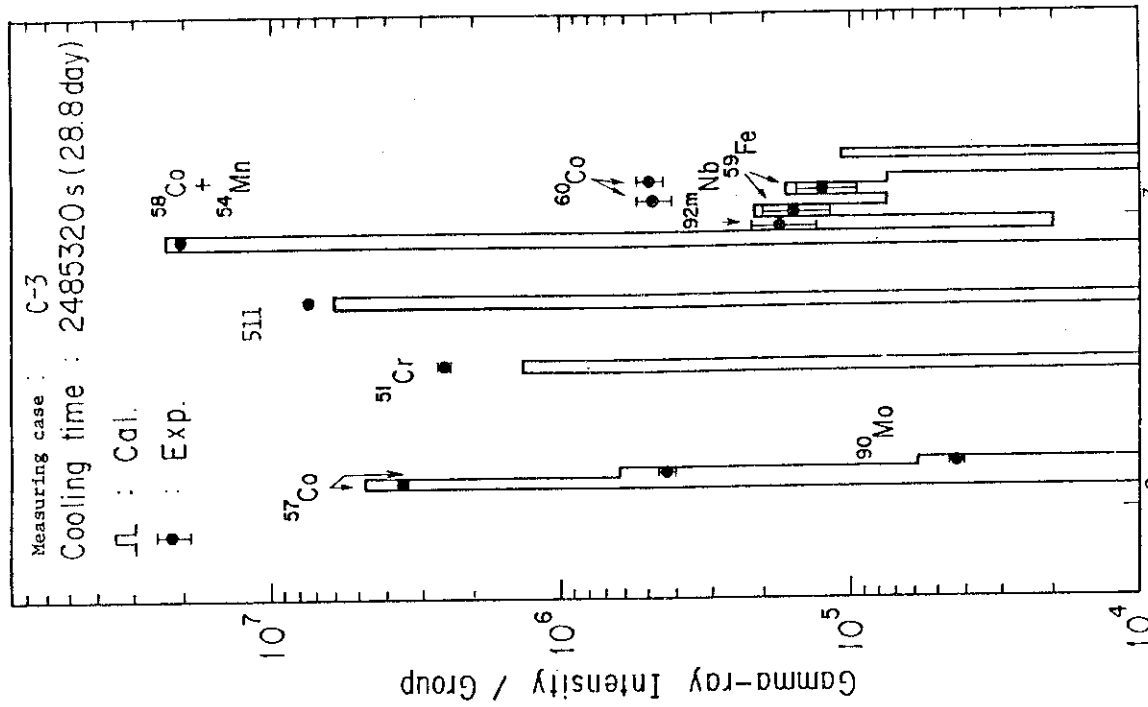

Fig. 9.10 Comparison of Gamma-ray spectrum of C-3 case between calcula-tion and measurement

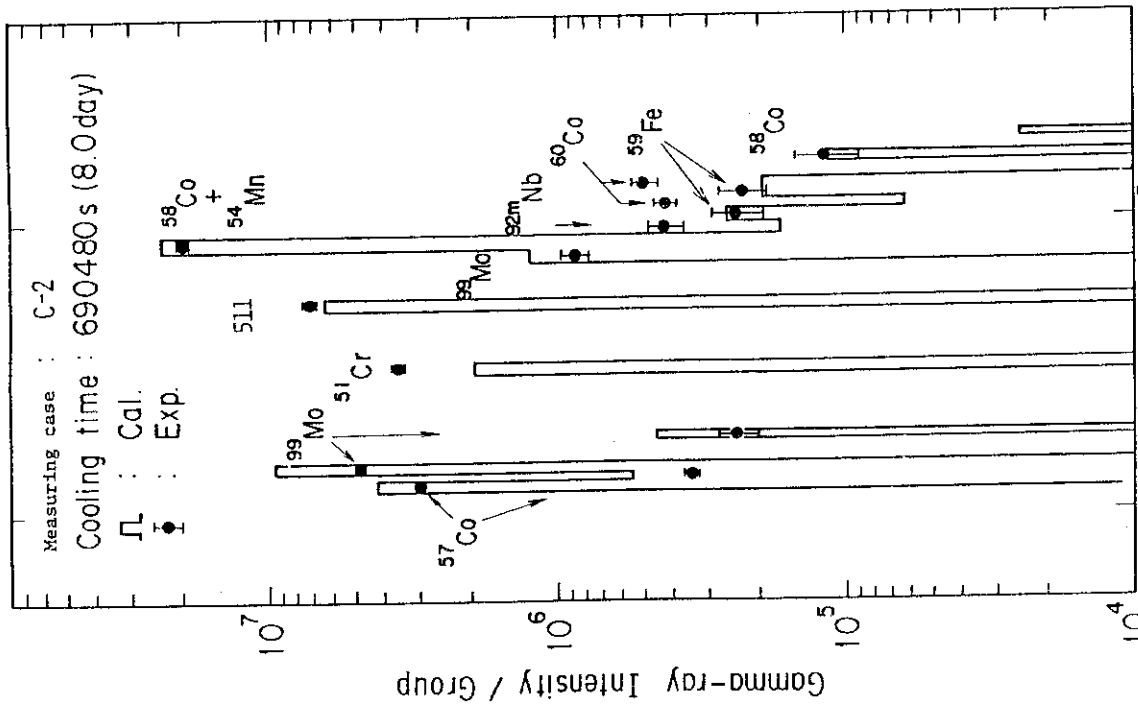

Fig. 9.9 Comparison of Gamma-ray spectrum of C-2 case between calcula-tion and measurement

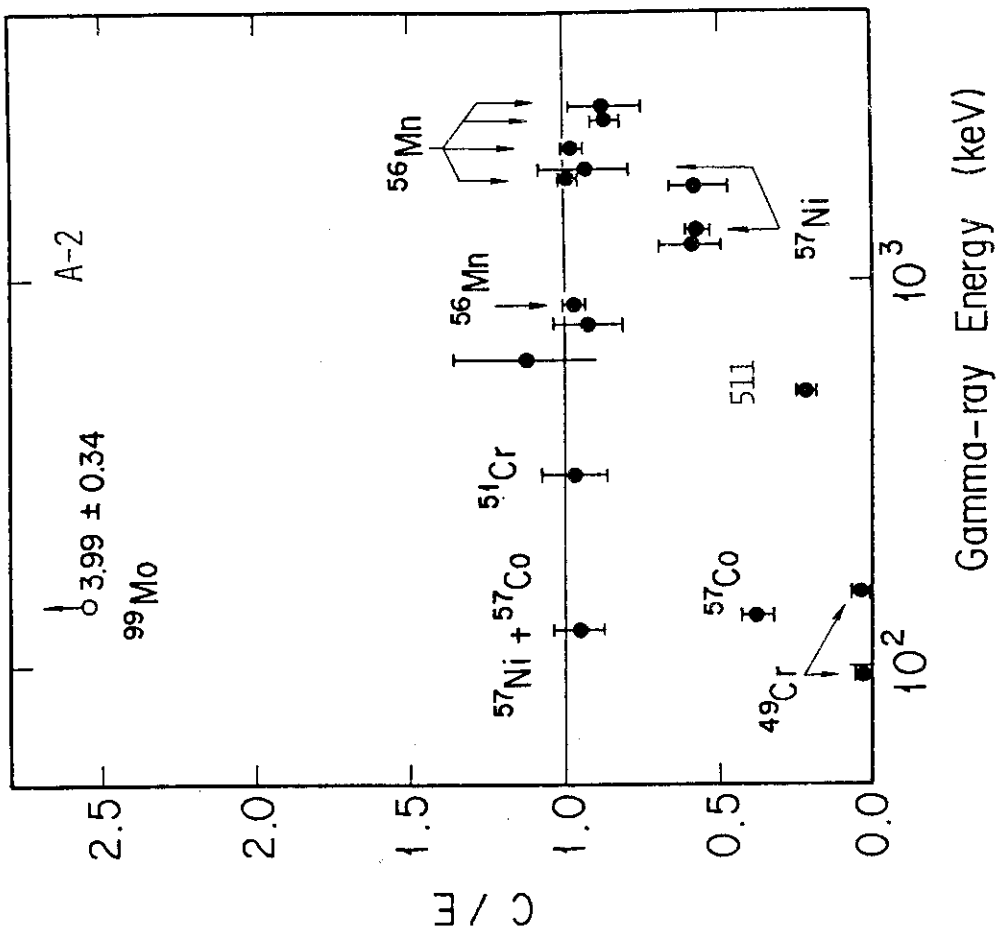

Fig. 10.2 C/E of gamma-ray intensity in A-2 case

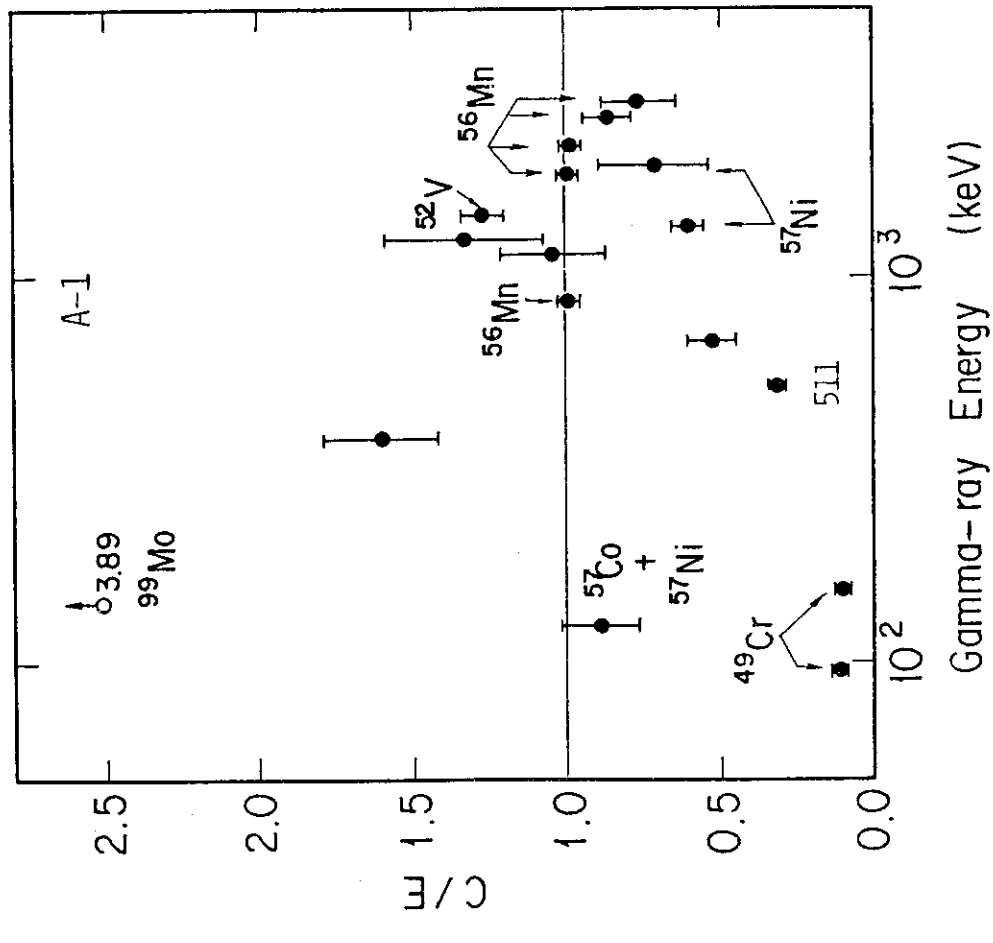

Fig. 10.1 C/E of gamma-ray intensity in A-1 case

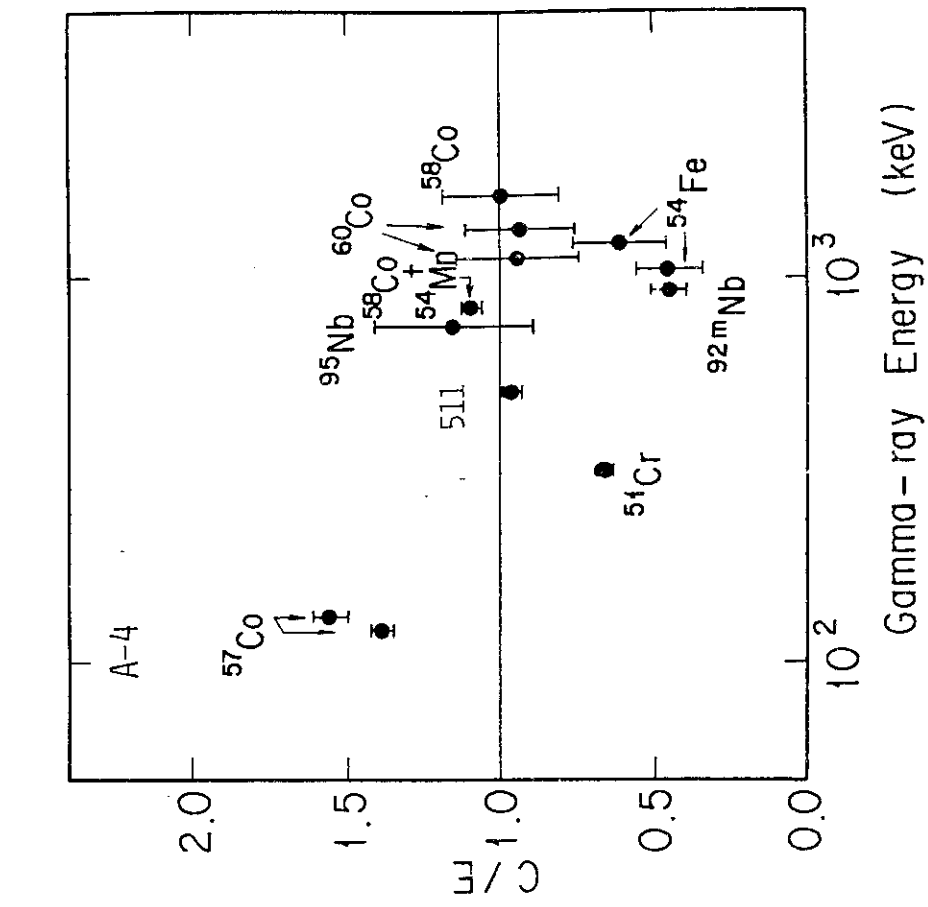

Fig. 10.4 C/E of gamma-ray intensity in A-4 case

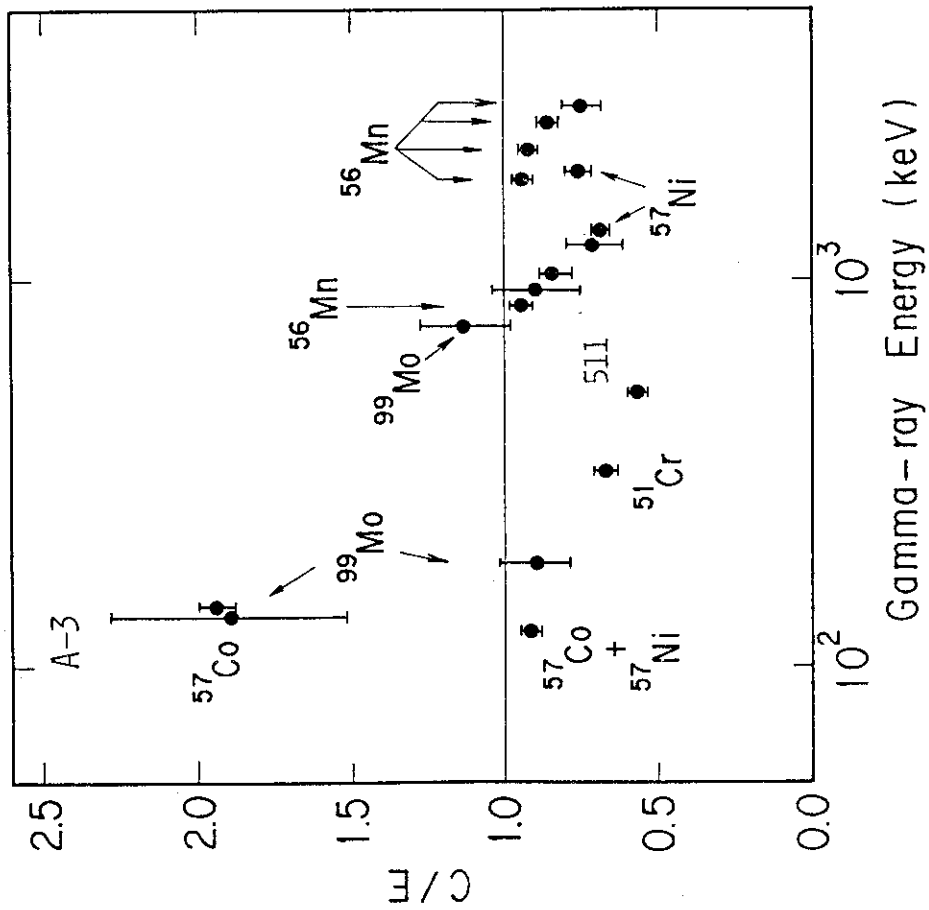

Fig. 10.3 C/E of gamma-ray intensity in A-3 case

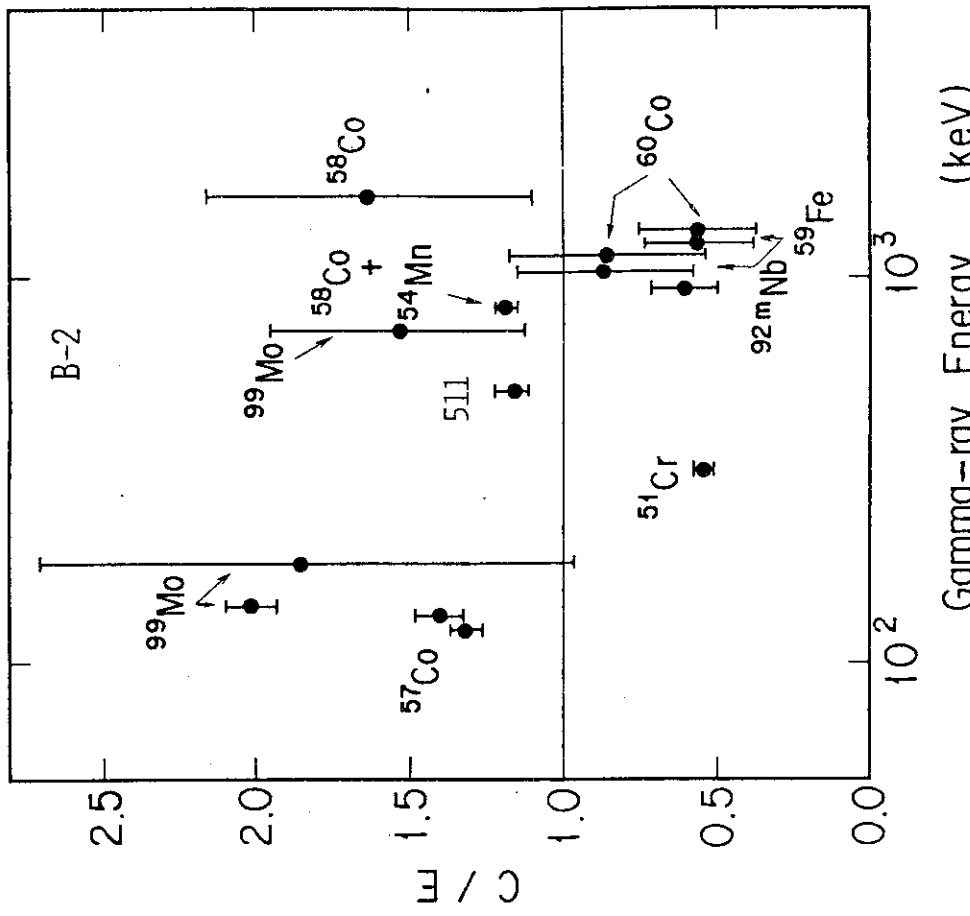

Fig. 10.6 C/E of gamma-ray intensity in B-2 case

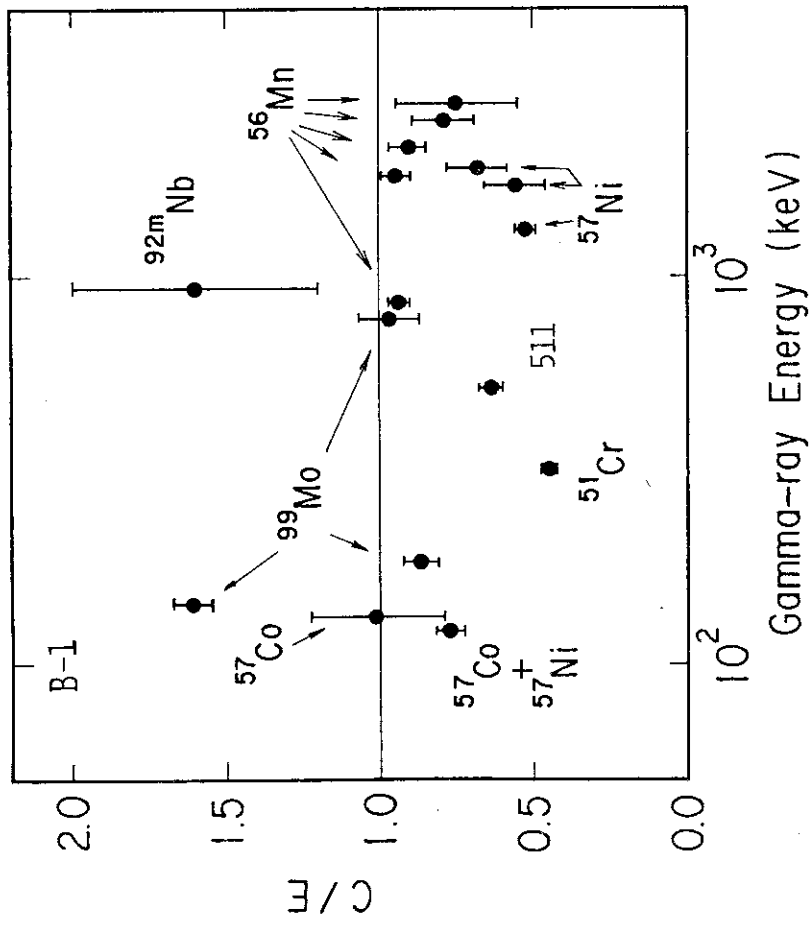

Fig. 10.5 C/E of gamma-ray intensity in B-1 case

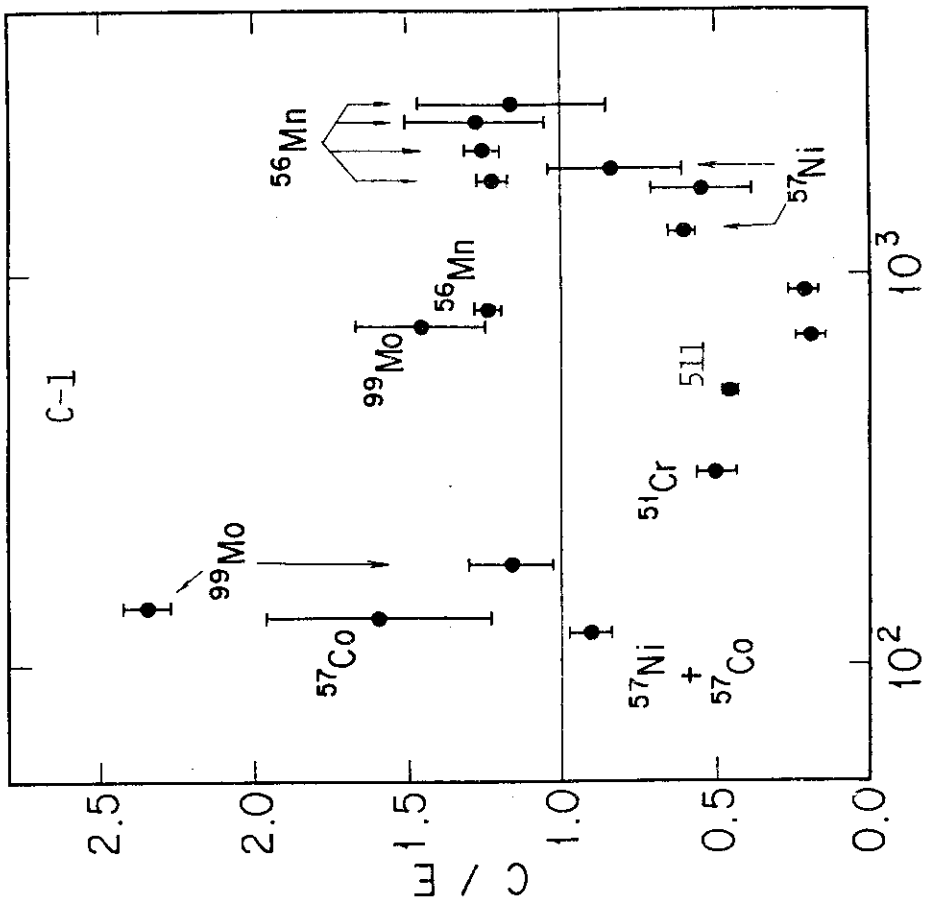

Fig. 10.8 C/E of gamma-ray intensity in C-1 case

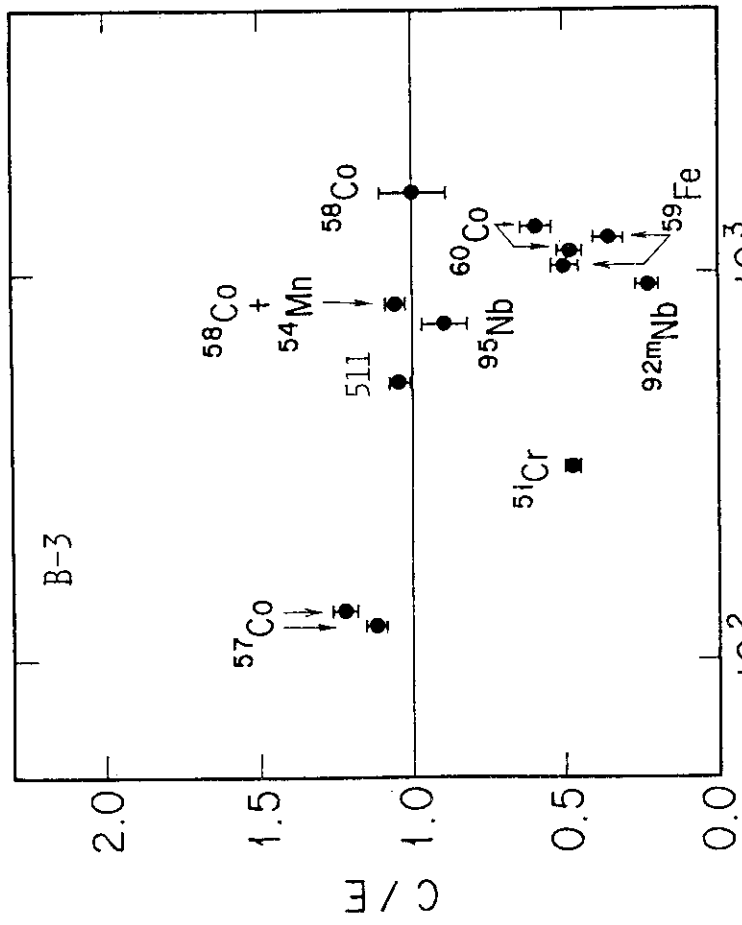

Fig. 10.7 C/E of gamma-ray intensity in B-3 case

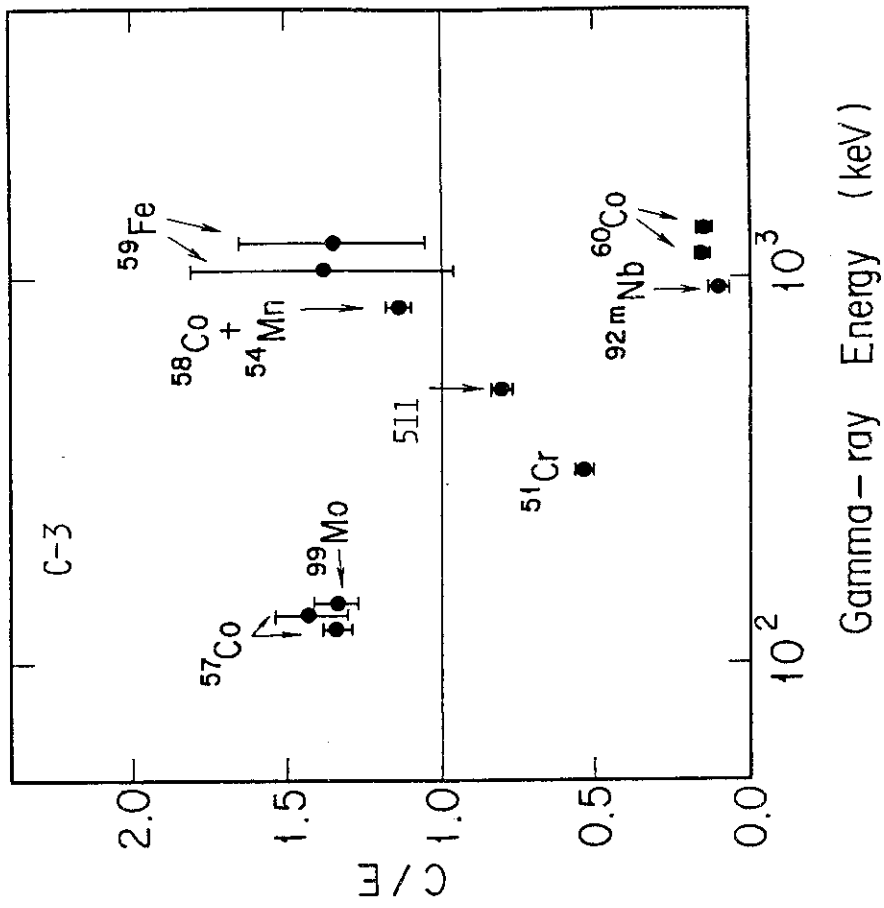

Fig. 10.10 C/E of gamma-ray intensity in C-3 case

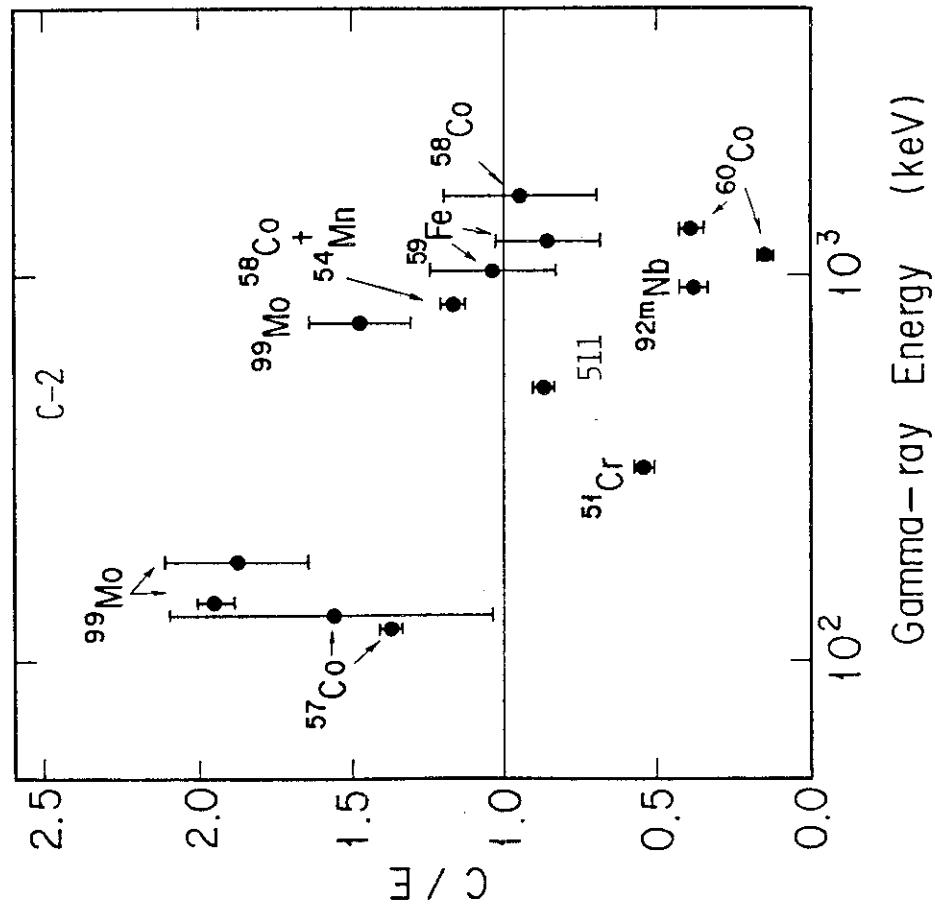

Fig. 10.9 C/E of gamma-ray intensity in C-2 case

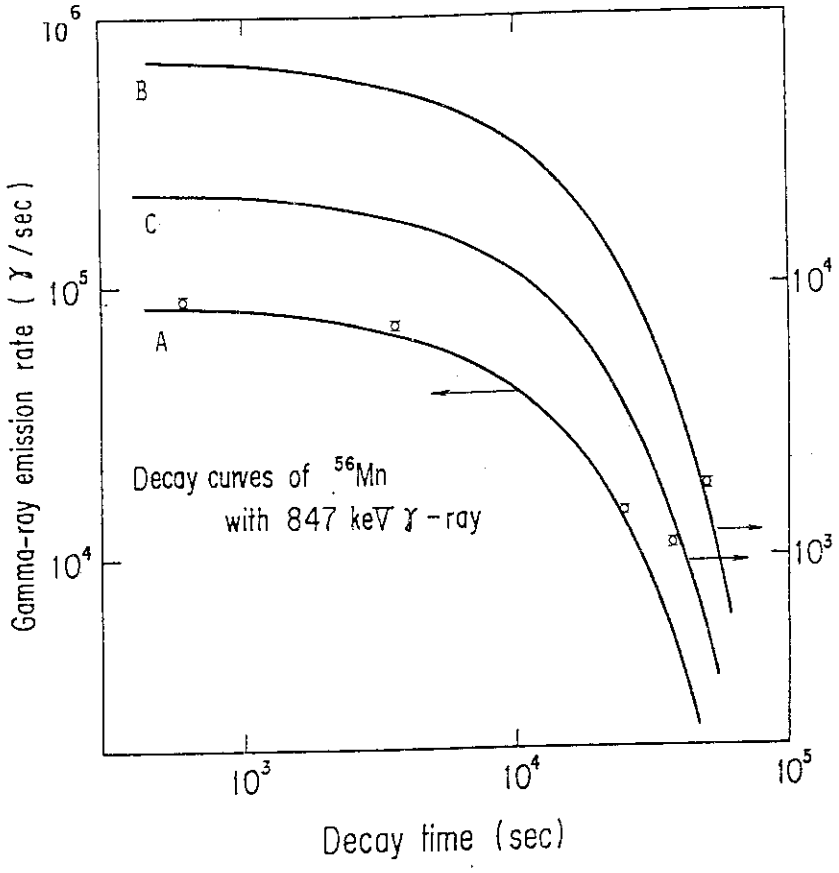

Fig. 11.1 Decay curves of ^{56}Mn with 847 keV gamma-ray

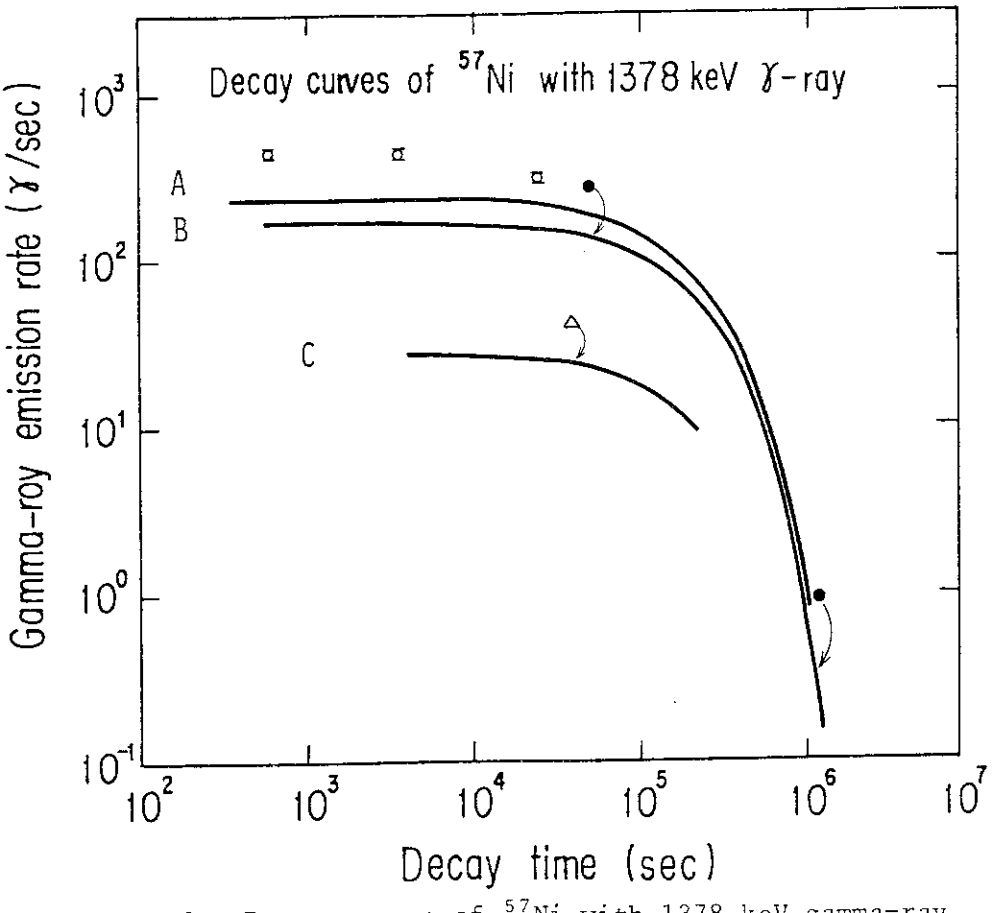

Fig. 11.2 Decay curves of ^{57}Ni with 1378 keV gamma-ray

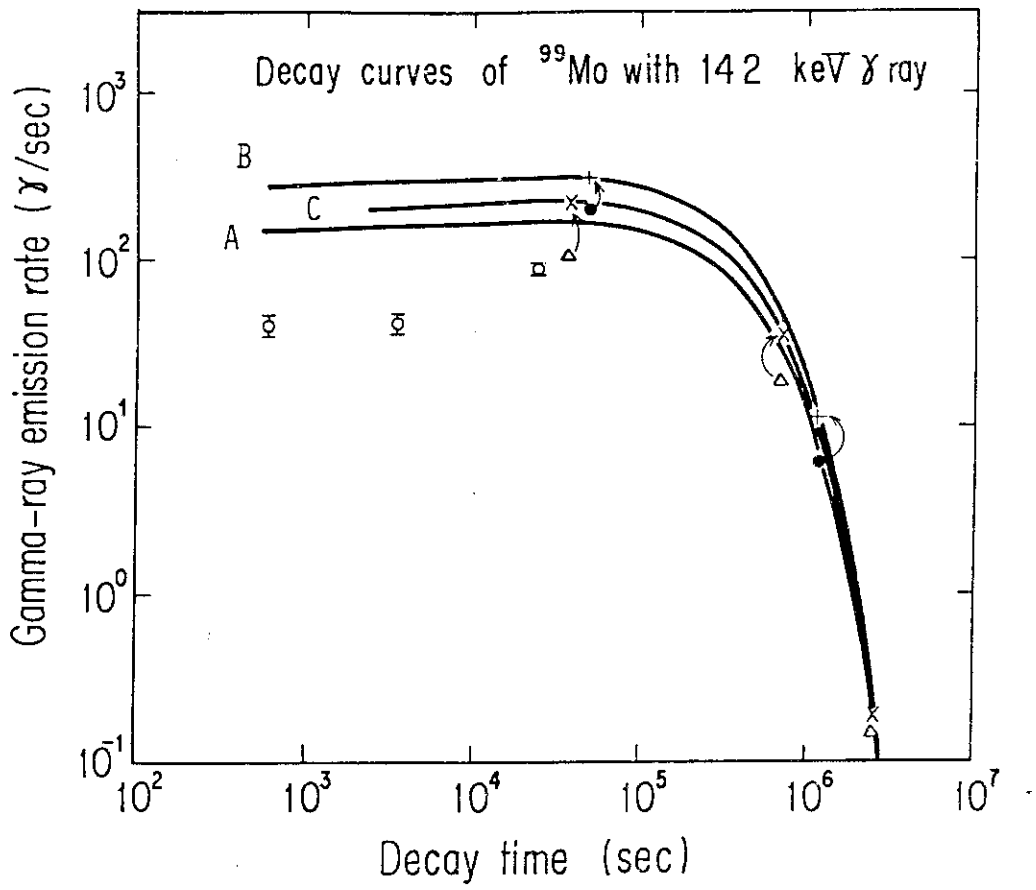

Fig. 11.3 Decay curves of ^{99}Mo with 141 keV gamma-ray

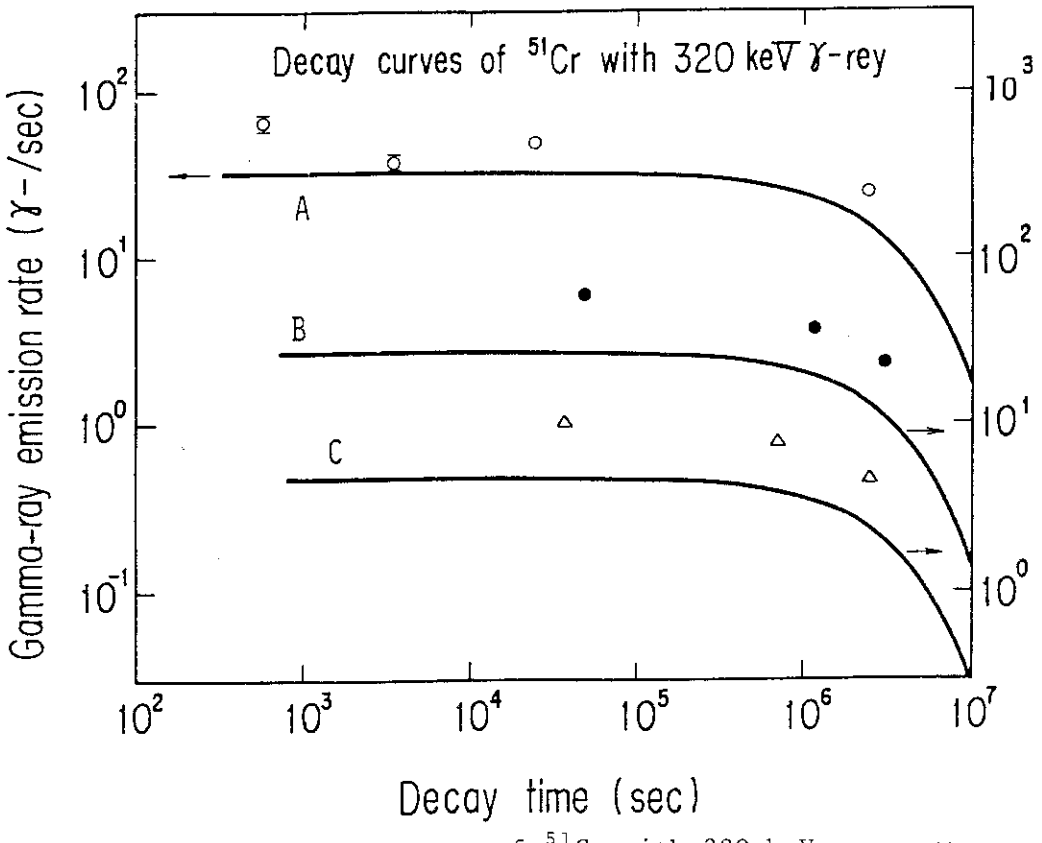

Fig. 11.4 Decay curves of ^{51}Cr with 320 keV gamma-ray

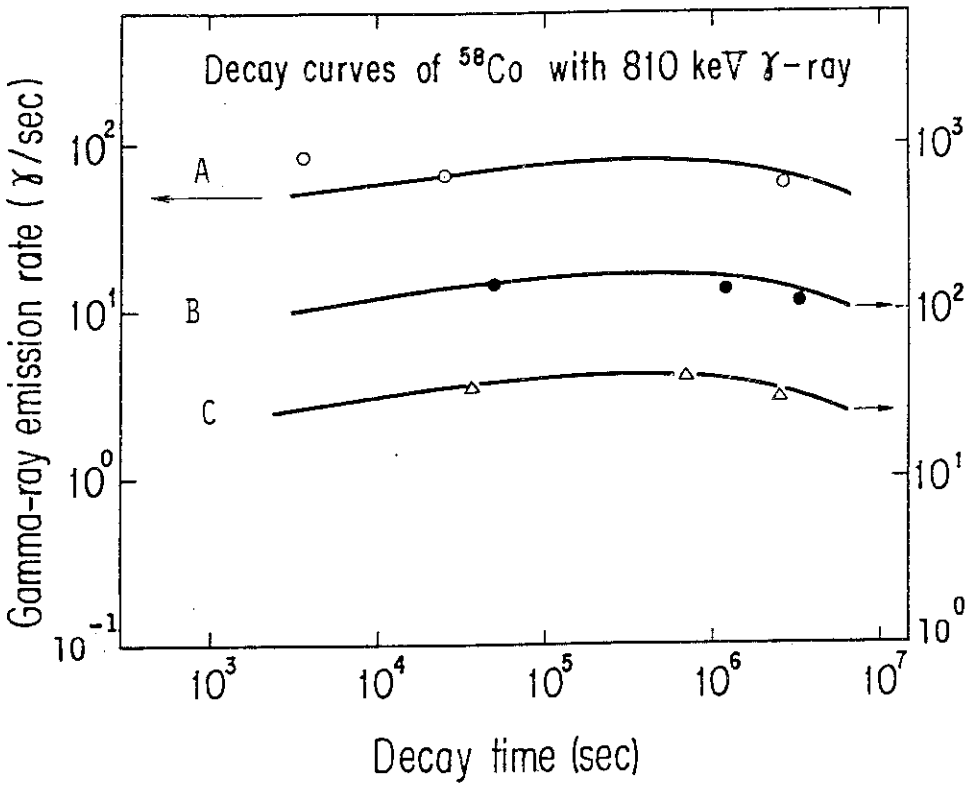

Fig. 11.5 Decay curves of ^{58}Co with 811 keV gamma-ray

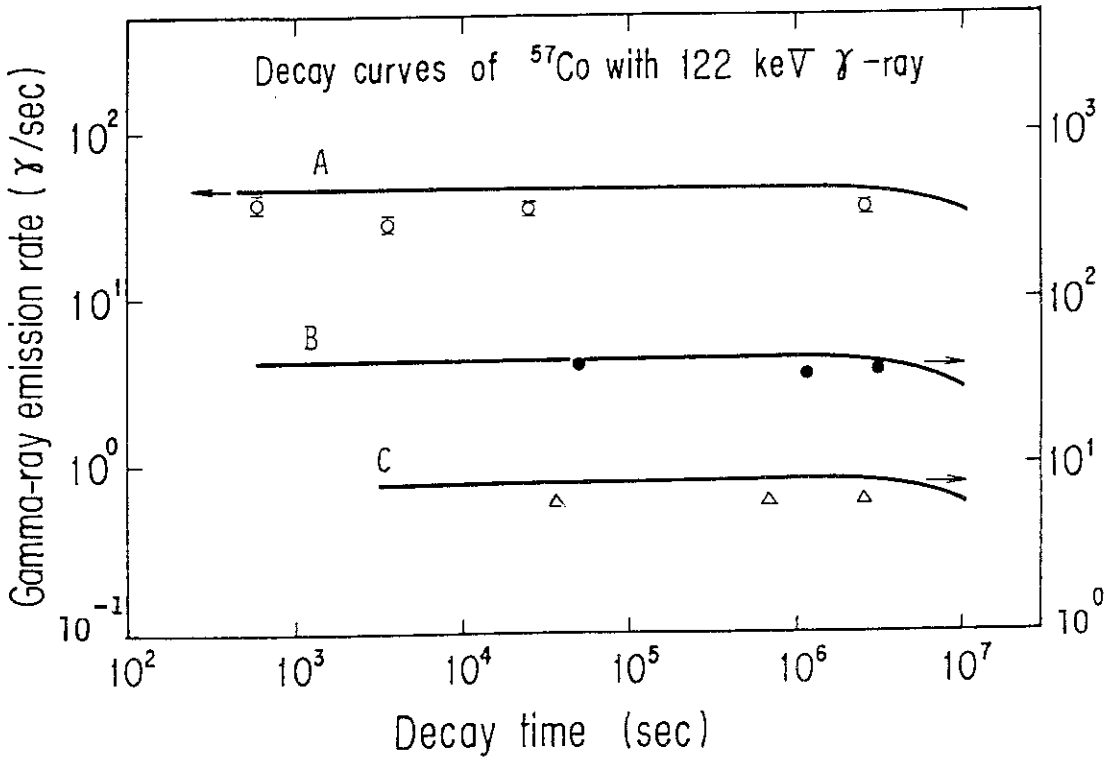

Fig. 11.6 Decay curves of ^{57}Co with 122 keV gamma-ray

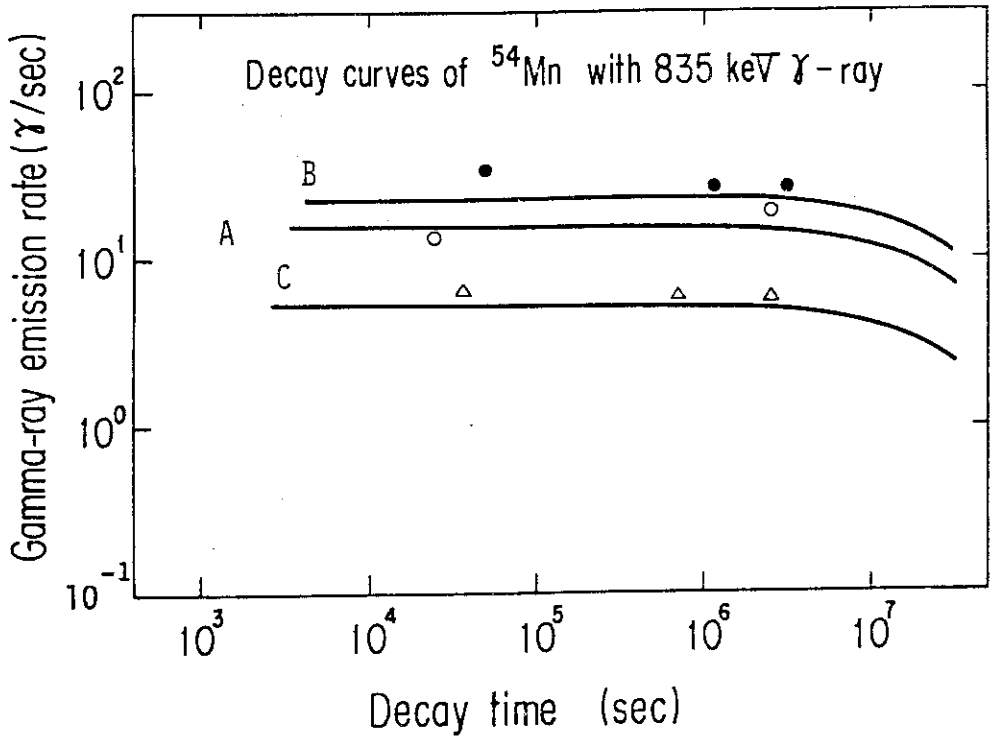

Fig. 11.7 Decay curves of ^{54}Mn with 835 keV gamma-ray

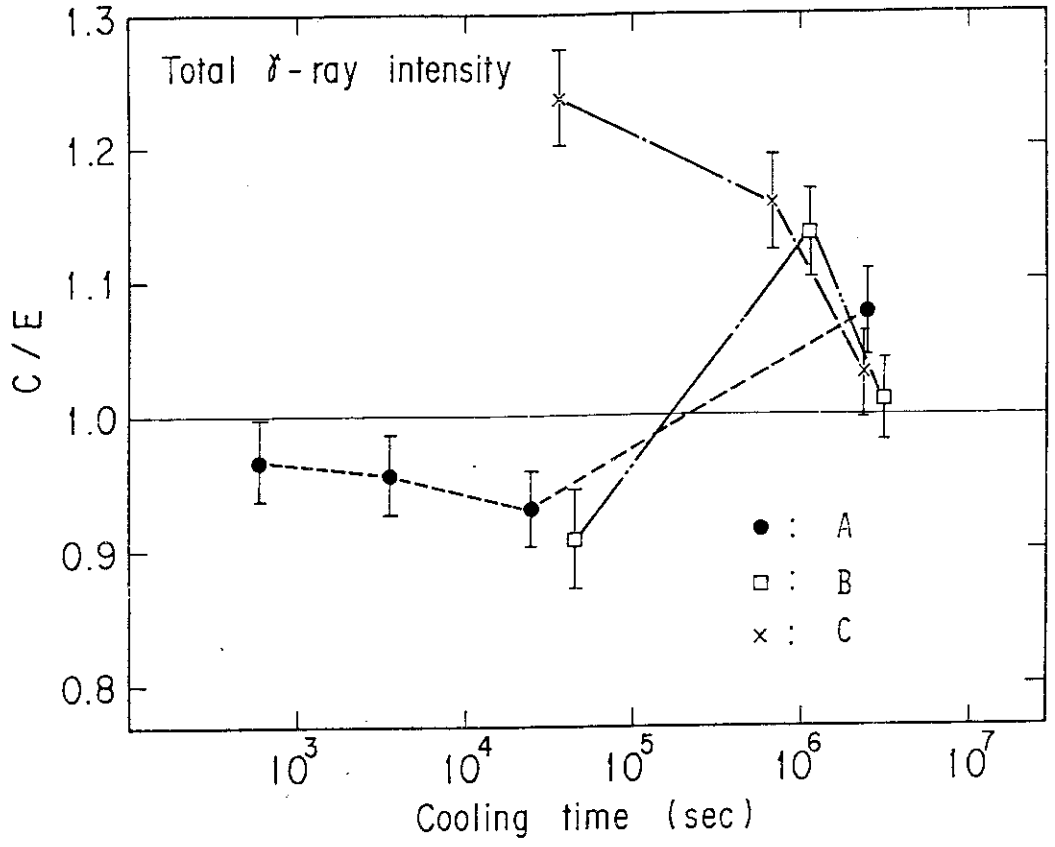

Fig. 12.1 Change of C/E for total gamma-ray intensities versus cooling times

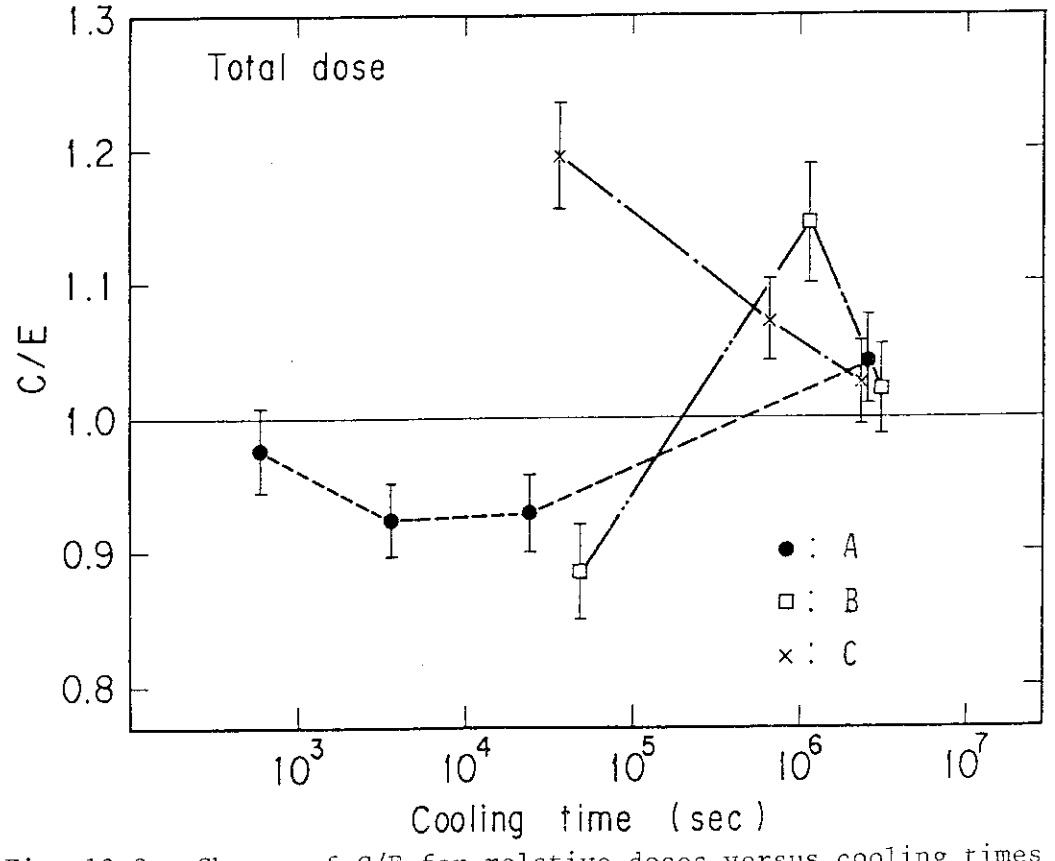

Fig. 12.2 Change of C/E for relative doses versus cooling times

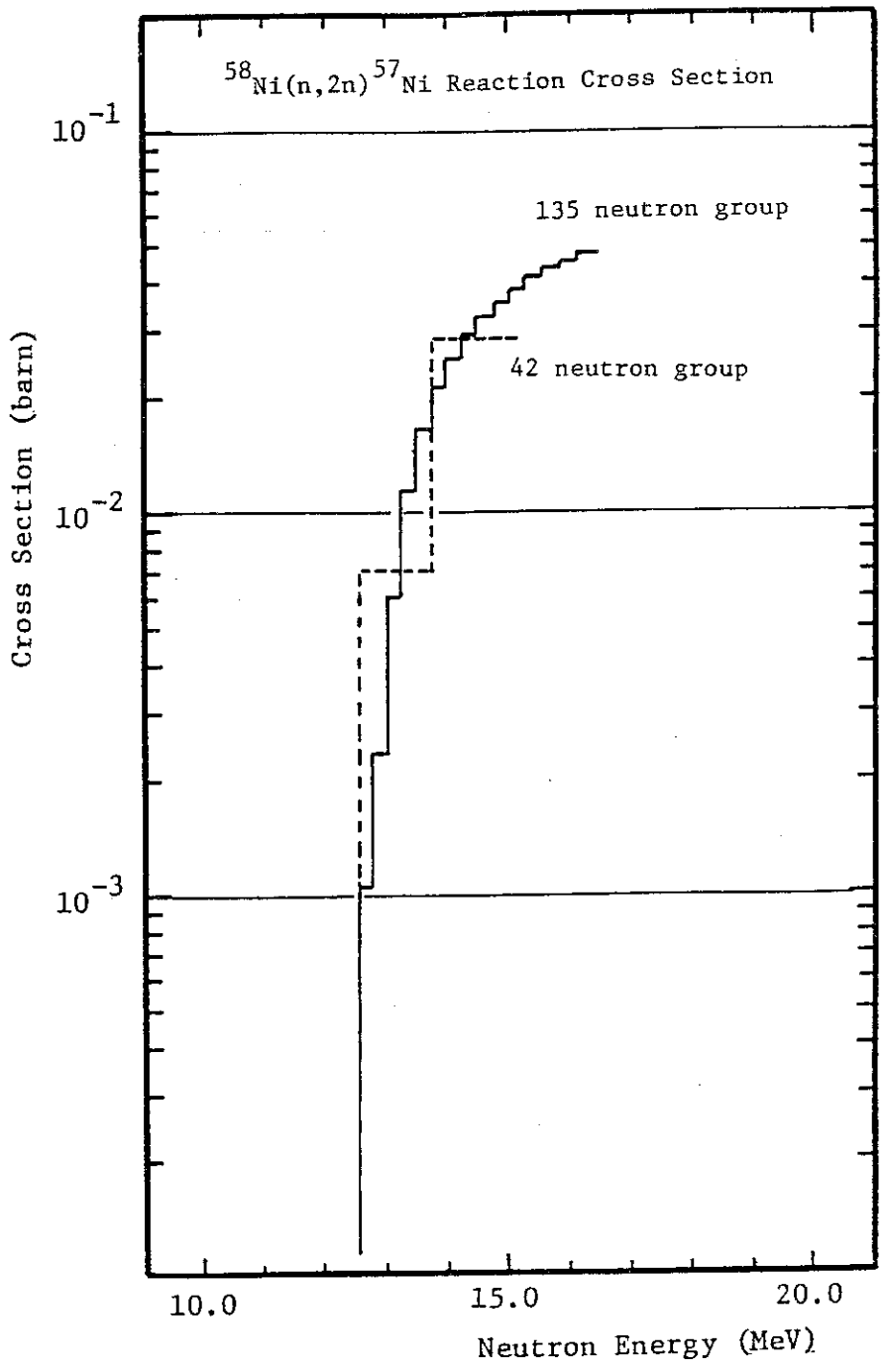

Fig. 13 Cross Section of ^{58}Ni(n,2n)^{57}Ni reaction
Dashed line and real line represent the cross section in 42 and 135 neutron group structures, respectively.

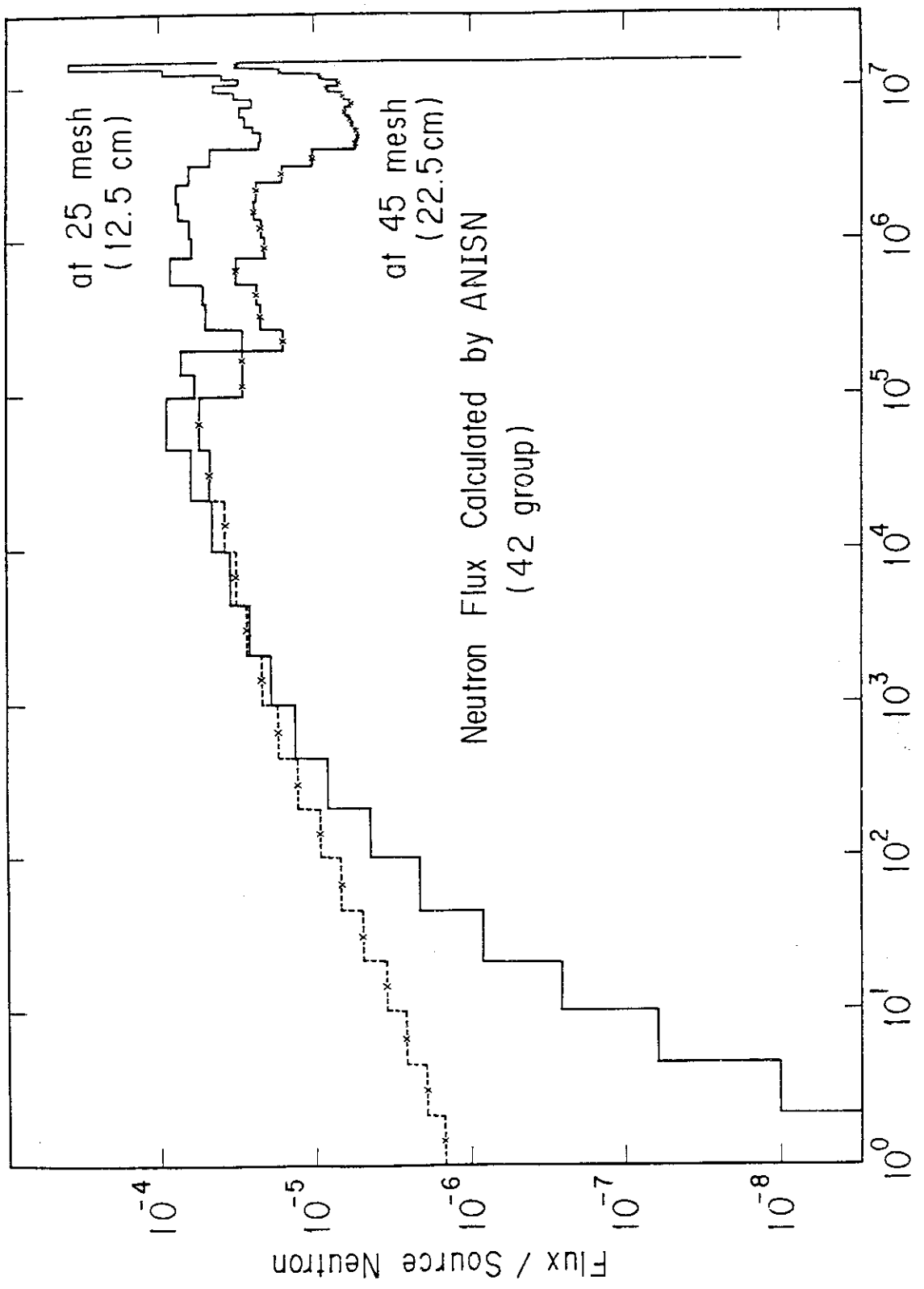

Fig. 14 Neutron spectra at 12.5 cm and 22.5 cm in the Li_2O-C assembly calculated by ANISN

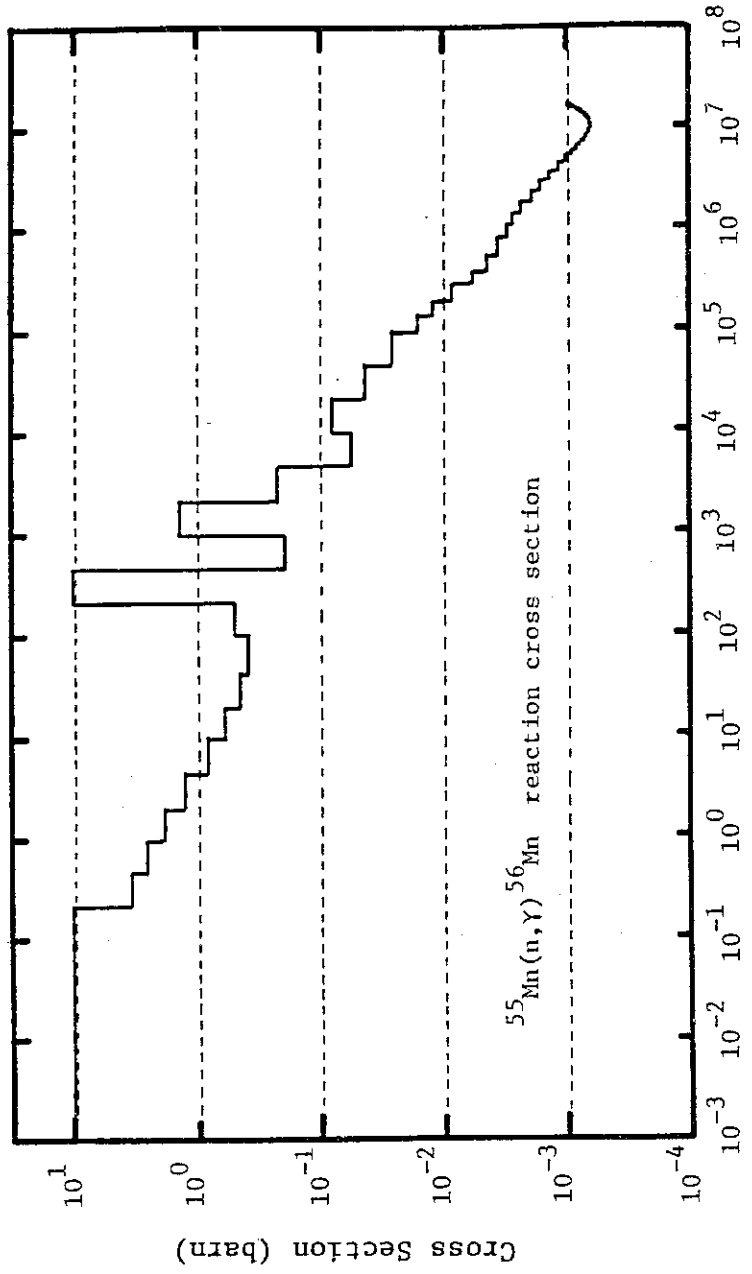

Fig. 15.1 Cross section of ^{55}Mn(n,γ)^{56}Mn reaction in the CROSSLIB library

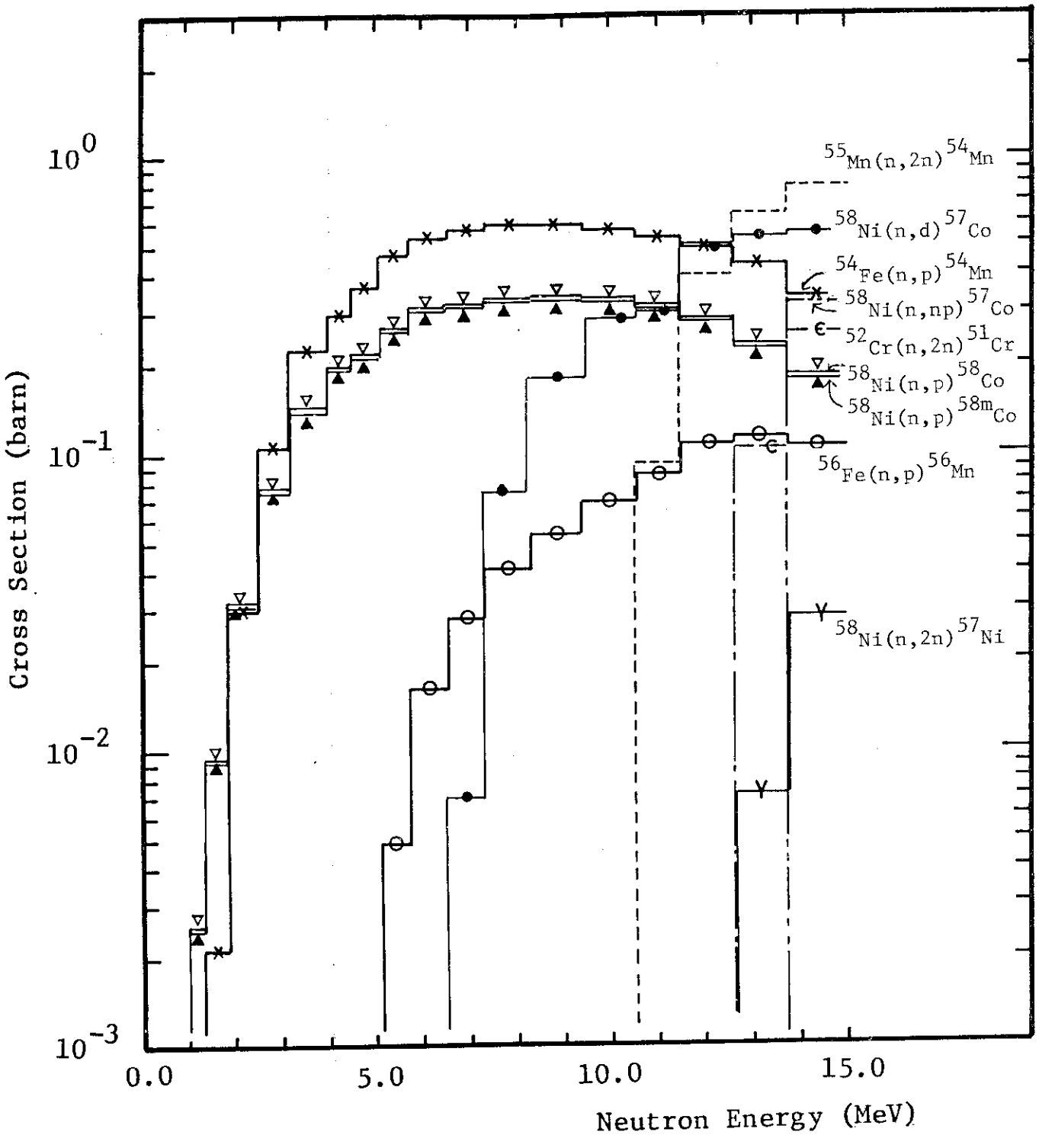

Fig. 15.2 Some activation reaction cross sections in the CROSSLIB library